UNIVERSITY OF CALIFORNIA
RIVERSIDE

Magnetic Assembly Route to Colloidal Responsive Photonic Nanostructures

A Dissertation submitted in partial satisfaction
of the requirements for the degree of

Doctor of Philosophy

in

Chemistry

by

Le He

December 2013

Dissertation Committee:
Dr. Yadong Yin, Chairperson
Dr. Christopher Bardeen
Dr. David Bocian

The Dissertation of Le He is approved:

_____

_____

_____

Committee Chairperson

University of California, Riverside

Acknowledgements

The completion of my dissertation for a Ph.D. degree has been a long journey. Undertaking this PhD has been a truly life-changing experience for me and it would not have been possible without the support and guidance that I received from many people. The biggest joy of completion is to look over the journey past and remember all the friends and family who have helped and supported me along this long but fulfilling road.

First, I would like to express my deepest gratitude to my mentor Dr. Yadong Yin for his careful guidance and invaluable help. Yadong is greater than other mentors because his role is far beyond lenders of intellectual loans. He has invested a huge amount of time and efforts since I ever started my first project. His enthusiasm in research set an excellent example which I hope I will be able to follow in the future. The most important thing I have learned from him is the positive attitude in dealing with any problems in life, which helped me overcome many crisis situations.

I am also very thankful to my other committee members Professor Bocian and Professor Bardeen for their valuable help and comments on my dissertation. Without the contribution from the committee, this dissertation can be little more than a set of technical exercises. I would acknowledge the substantial influence on this dissertation by many past and current members in Yin group: Dr. Tierui Zhang, Dr. Xiaogang Han, Dr. Wenshou Wang, Dr. Yan Wang, Dr, Miaomiao Ye, Dr. Suqing Wang, Dr. Diana Q. Lima,

Dr. Gaoren Li, Dr. Chuanbo Gao, Dr. Jie Han, Dr. Shengyang Tao, Dr. Fangquan Xia, Dr. Minfen Gu, Dr. Fengyan Ge, Dr. Jibong Joo, Dr. Geondae Moon, James Gobel, Michael Dahl, Yiding Liu, Yaocai Bai, Wenjing Xu, Junxiang Fu, Dr. Lei Sun, Qipeng Lu, Jiemei Lei, Na Li, Hongxia Yu, Xin Wang, Jingzhong Zhang, Hongyan Liu, Lishun Fu.

I have received valuable help in both academic research and daily life from Dr. Yu Lu, Dr. Jianping Ge and Dr. Yongxing Hu, Dr. Qiao Zhang and Dr. Zhenda Lu. I also would like to give special thanks to those who have worked with me closely in the lab: Mingsheng Wang, high school student Michael Jenner, and undergraduate student Francesca Anson.

I would like to take this opportunity to thank Prof. Bardeen, Prof. Jing Shi, Professor Wenwan Zhong, Dr. Ni Li, Dr. Deqi Wang and Dr. Zhong Yan for their great help in the collaboration of many projects at UCR.

I would like to thank my parents Guosheng He and Fengping He, my parents-in –law Jianquan Li and Caiping Wu and other family members for their infinite support throughout everything; and most of all, my loving, supportive, encouraging and patient wife Mingming Li whose faithful support during my Ph.D. stage is so appreciated. There are no words to express the gratitude I feel in my heart that you came into my life and how you make everyday so colorful. I would like to express my love to my little princess Jiaxiao He, who has brough, is and will always be bringing so much happiness.

Dedication

To my darling Mingming and little princess Xiaoxiao

ABSTRACT OF THIS DISSERTATION

Magnetic Assembly Route to Colloidal Responsive Photonic Nanostructures

by

Le He

Doctor of Philosophy, Graduate Program in Chemistry
University of California, Riverside, December 2013
Dr. Yadong Yin, Chairperson

Responsive photonic bandgap materials, more commonly known as responsive photonic crystals, which can remotely change their structural colors in response to the external stimuli, have important applications in areas such as color displays, biological and chemical sensors, inks and paints, or many optically active components. Despite the development of different types of colloidal responsive photonic systems, wide use of these systems in practical applications is hampered by low fabrication efficiency, limited tunability of the band gap, a slow response to the external stimuli, and difficulty of integration into existing photonic systems.

Through the magnetic assembly route, we attempted to develop new types of responsive photonic nanostructures with improved fabrication efficiency, rapid response, and wide tunability of the band gap. We have demonstrated the rapid assembly of superparamagnetic colloidal particles into various photonic nanostructures. We have

also demonstrated that an external magnetic field can be used as an effective stimulus to manipulate the photonic properties of the self-assembled nanostructures by affecting the lattice constant, the orientation, or the crystal structures.

As there are many more choices for nonmagnetic colloidal particles with uniform size and optimal refractive index, it would be advantageous to extend this magnetic assembly strategy to nonmagnetic particles. We have demonstrated the use of nanocrystal-based ferrofluids to direct the assembly of nonmagnetic colloidal particles into photonic crystal structures. The process is general, efficient, convenient, and scalable and thus represents a new and practical platform for the fabrication of colloidal crystal-based photonic devices.

We have also developed a universal strategy that allows convenient magnetically-driven assembly of general objects in defined locations with high spatial resolution. The process involves immersing a polymer relief pattern in a uniformly magnetized ferrofluid, which modulates the local magnetic fields around the pattern. Nonmagnetic target objects dispersed in the same ferrofluid can then be magnetically assembled at positions defined by the polymer pattern. As the nonmagnetic polymer patterns can be conveniently fabricated at low cost, our method provides a general yet very effective means to assemble a wide range of nanoscale objects, paving the way towards patterning functional microstructures.

Table of Contents

List of Figures

List of Schemes

Chapter 1

Introduction to Magnetically Responsive Photonic Crystals

1.1 Colloidal Assembly

Owing to the structural similarities with atomic systems, the assembly of colloidal particles has been extensively studied to mimic the behavior of simple atomic liquids and solids, e. g. to investigate the thermodynamics and kinetics of crystallization and melting, as well as the glass transition.[1-4] Compared with atomic systems, it is more convenient to conduct the study of colloidal particles in more experimentally accessible length and time scales. During the last several decades, progress in the fundamental study of colloidal assembly has enabled deep understanding of atomic world. For example, the study of colloidal assembly in aqueous dispersion helped to clarify the early stage of crystallization in dilute solutions.[5, 6] The assembly of binary nanoparticles provided valuable insight for the construction of ionic crystals.[7]

On the other hand, self-assembly of colloidal building blocks represents a powerful bottom-up method for the fabrication of functional nanostructured materials, for example, nanoscale electronic, magnetic, optical, catalytic, and many energy-related devices.[8] Colloidal assembly can be simply categorized into two types, colloidal crystals and colloidal clusters (colloidal 'molecules'), depending on the length scales of structures

formed. A colloidal crystal typically consists of millions of particles, similar to the ionic crystals made of lots of ions. During the past several decades, studies in the self-assembly of periodical arrays of monodisperse colloidal particles, mainly isotropic spheres, were particularly boosted by the interest in the development of photonic crystals.[9-12] In other cases, people are also interested in the organization of colloidal particles into colloidal clusters with controlled size, shape, structures and, sometimes, positions.[13-17] The assembly of colloidal clusters is typically driven the directional interparticle interactions in a way similar to the formation of molecules through bonding between atoms. Colloidal clusters can also be achieved through confining the number of particles assembled within local areas. While monodisperse colloidal spheres have been extensively used in most studies of colloidal photonic crystals, recent processes in the synthesis of uniform anisotropic colloidal building blocks offer the possibility of assembling more diverse and complex structures.

Colloidal self-assembly occurs when the interactions between colloidal particles were sufficiently balanced.[18] Colloidal particles interact with each other through many types of short-range and long-range forces. For example, the short-range strong attractive van der Waals forces drive the aggregation of colloidal particles when they come close to each other. Therefore, repulsive interparticle interactions are necessary to maintain the stability of colloidal dispersions, which can be realized through the build-up

of surface charges on colloidal particles or the grafting of a polymer layer which provides a steric barrier against particle aggregation. Dipolar colloidal particles not only can interact with each other through additional magnetic or electric dipole-dipole forces, but also interact with external electric and magnetic fields.[19-21] Thanks to recent progresses in the preparation of colloidal particles with tailored size, shape, surface property and functions, a variety of assembly methods have been developed to organize colloidal building blocks into to colloidal clusters or colloidal crystals.[22]

1.2 Colloidal Responsive Photonic Nanostructures

Photonic crystals are periodical nanostructures of dielectric materials that can affect the propagation of photos in the same way as the periodic potential in a semiconductor crystal affects the electron motion by defining allowed and forbidden electronic energy bands. While the concept of photonic crystals was developed by John and Yablonovitch in 1987, photonic crystals are very common in nature.[23, 24] For example, the iridescent colors displayed in the wings of Morpho butterflyies and precious opals were found to result from a mechanism different from that of dyes or pigments.[25-27] The color produced by a dye or pigment originates from the absorption of light to excite an electron between the ground and excited state of the chromophore. In contrast, the color in photonic crystals has a more physical origin that stems from the modulation of photon motions when light travels through their periodic nanostructures. Such unique colors originating from the interaction of light with periodically arranged structures of dielectric materials are often called structural colors, which are iridescent and metallic, cannot be mimicked by chemical dyes or pigments, and free from photobleaching unlike traditional pigments or dyes. Therefore, structural-colored photonic materials with band gaps located in the visible regime, or artificial opals, are of special interest as important chromatic materials.[28]

Recently, there are immediate interests in the development of responsive photonic

bandgap materials, more commonly known as responsive photonic crystals, which can change their color in response to external stimuli.[29, 30] Responsive photonic materials have attracted much attention due to their important uses in areas such as color displays, biological and chemical sensors, inks and paints, and many active components in optical devices.[10, 12, 31, 32] Many interesting applications have been proposed for responsive photonic crystal structures. For example, they may be used as optical switches for full automation of optical circuits when significant improvements towards the quality of colloidal crystals and their response time are realized.[33] Military vehicles covered with such materials may be able to dynamically change their colors and patterns to match their surroundings. Such materials might also be embedded in banknotes or other security documents for anti-counterfeiting purposes. The hidden information cannot be revealed until an external stimulus such as a pressure or temperature change is applied. The photonic effect can also be used as a mechanism to develop chemical and biological sensors for detecting target analytes by outputting optical signals. These types of crystals may also find great use as active color units in the fabrication of flexible display media, including both active video displays and rewritable paper that can be reused many times.

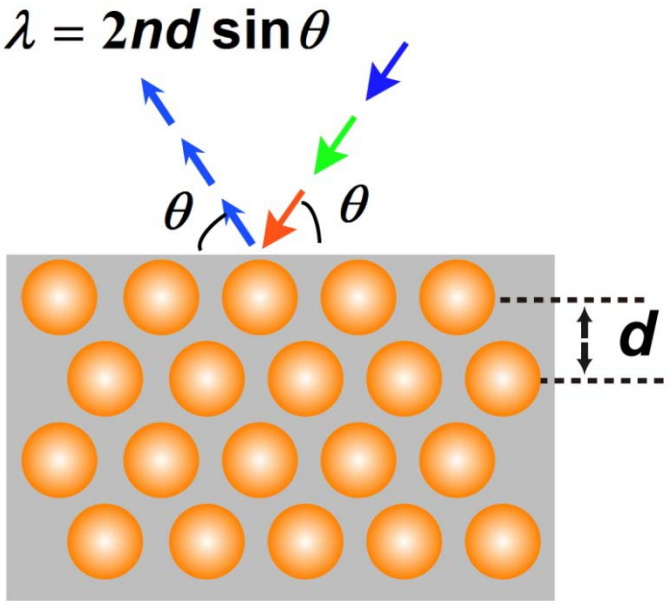

Scheme 1.1. Illustration of Bragg diffraction by a periodic photonic crystal. The transmission of light within certain frequencies is forbidden so that the crystal displays structural colors through diffraction.

The diffraction wavelength (or band gap position) of the colloidal arrays can be described by Bragg's law, $m\lambda = 2nd\sin\theta$, where m is the diffraction order, λ is the wavelength of incident light, n is the effective refractive index, d is the lattice spacing, and θ is the glancing angle between the incident light and diffraction crystal plane (Scheme 1.1). In order to develop responsive photonic nanostructures, it is necessary to tune at least one of the parameters related to the diffraction wavelength. In principle, the stimulus can be any means that can effectively induce changes in the refractive indices of the building blocks or the surrounding matrix, and changes in the lattice constants and/or spatial symmetry of the crystalline arrays.

The diffraction intensity gradually decreases as the diffraction order goes up. In order to fabricate photonic nanostructures with strong visible diffractions, the periodicity should be comparable to the wavelength of visible light, which becomes significantly challenging through conventional top-down strategies based on optical lithography. Unlike typical top-down approaches, colloidal assembly strategies for photonic crystal fabrication are technologically favorable due to mild processing conditions, low cost, and potential for scale-up.[34] It is also more convenient to modify the building blocks before or after the formation of crystal structures to enable responsiveness to a given stimulus. For example, oxide materials such as WO_3, VO_2 and $BaTiO_3$ have been used as matrix materials for producing tunable photonic crystals because the refractive indices of these

materials are sensitive to electric fields or temperature changes.[35-37] Colloidal arrays filtrated with liquid crystals also show tunable photonic properties upon the application of an external electric field or a change in temperature.[38-40] The majority of approaches to tunable photonic crystals, however, are focused on controlling the lattice constants or spatial symmetry of the crystals through the application of chemical stimuli, temperature variation, mechanical forces, electrical or magnetic fields, or light.[41-46] A notable example is a hydrogel/colloidal array composite in which the lattice spacing can be tuned by the swelling and deswelling of the hydrogel.[10]

Despite the development of different types of colloidal responsive photonic systems, wide use of these systems in practical applications is hampered by low fabrication efficiency, limited tunability of the band gap (with peak position changes typically in the range of tens of nanometers), a slow response to the external stimuli (typically several minutes to a few hours), and difficulty of integration into existing photonic systems. Typical self-assembly methods utilize gravitational force, centrifugal force, hydrodynamic flow, electrophoretic deposition, capillary force and electrostatic interaction to assemble colloidal crystals.[29] The formation of high quality colloidal crystals with large areas usually takes hours to days or even months to complete. The small tuning range is mainly due to the limited changes in the crystal structure that the

external stimuli can induce. The slow response is usually the result of retarded physical/chemical changes that the external stimuli can cause.

To this end, the magnetic field has been proposed as an effective stimulus to rapidly guide the assembly of magnetic particles into periodic colloidal arrays and tune the diffractions of photonic structures.[21] Strong magnetic interactions can be initiated instantly by the application of an external magnetic field, providing enough driving force for rapid assembly of colloidal particles even within one second.[47, 48] Magnetic forces, acting at a large distance, drive the formation of ordered colloidal arrays and provide convenient control over the photonic properties by changing the interparticle distance.[49] Magnetic fields can also induce phase transitions in pre-assembled 3D colloidal crystals, in which the static or dynamic structural changes in these systems are always accompanied by the switching of photonic properties.[50] Magnetic interactions, directional in nature, not only guide the formation of anisotropic photonic structures, but also enable additional control over the orientation of the magnetic assemblies so that one can conveniently tune their optical properties through rotational manipulation.[51, 52] The complexity achievable in the spatial distribution of magnetic fields also makes it possible to define patterns of photonic structures by controlling the local assembly behavior of dipolar particles.[53] In the following sections of this chapter, mechanisms of magnetic assembly and tuning will be detailed, starting from the introduction of the magnetic

interactions exerted on colloidal particles, followed by the discussion of magnetic assembly of colloidal particles into different ordered structures and magnetic tuning of optical properties of photonic nanostructures.

1.3 Magnetic Interactions

There are two types of magnetic interactions experienced by dipolar colloidal particles in external magnetic fields, which originate from their permanent or induced dipole moments.[54] The interparticle dipole-dipole force describes the interaction of a dipole with the magnetic field induced by another dipole, while the packing force results from the gradient of the external magnetic field. Among the many types of magnetic materials, superparamagnetic colloidal particles are presumably the most suitable building blocks for reversible assembly and manipulation as their strong and widely tunable dipolar interactions can be fully initiated and controlled by the external magnetic fields. Ferromagnetic particles have net magnetic dipole moments in the absence of a magnetic field so they tend to aggregate in colloidal dispersions due to the magnetic dipole-dipole attraction. Conversely, there is no effective magnetic attraction between paramagnetic particles in the absence of magnetic fields as their dipole moments are only initiated in the external magnetic fields. Compared with typical paramagnetic materials, superparamagnetic particles have much higher magnetic susceptibility, rendering them significantly more responsive to an external magnetic field. As an example, the magnetic interactions experienced by superparamagnetic particles in magnetic fields will be first discussed.

An external magnetic field induces a magnetic dipole moment in a superparamagnetic particle $\boldsymbol{m} = \chi \boldsymbol{H} V$, where χ is the volume susceptibility of the particle, $\boldsymbol{H}$ the local magnetic field, and V the volume of the particle. When the external magnetic field is adequately strong, the magnetic moment of the particle will reach a saturated value. For a spherical particle (particle 1) with a magnetic moment of $\boldsymbol{m}$, its induced magnetic field $\boldsymbol{H}_1$ felt by another particle (particle 2) can be described as $\boldsymbol{H}_1 = [3(\boldsymbol{m}\cdot\boldsymbol{r})\boldsymbol{r} - \boldsymbol{m}]/d^3$, where $\boldsymbol{r}$ is the unit vector parallel to the line pointed from the center of particle 1 to that of particle 2 and d is the center-center distance. The dipole-dipole interaction energy of particle 2 with the same magnetic moment m can be thus written as $U_2 = \boldsymbol{m}\cdot\boldsymbol{H}_1 = (3\cos^2\alpha - 1)m^2/d^3$, where α, ranging from 0^o to 90^o, is the angle between the external magnetic field and the line connecting the center of the two particles. The dipole force exerted on particle 2 induced by particle 1 can be expressed as:

$$\boldsymbol{F}_2 = \nabla(\boldsymbol{m}\cdot\boldsymbol{H}_1) = \frac{3(1-3\cos^2\alpha)m^2}{d^4}\boldsymbol{r}$$

The above equation clearly shows the dependence of the dipole-dipole force on the configuration of the two dipoles. At the critical angle of 54.09^o, the interaction approaches zero. The dipole-dipole interaction is attractive when $0^o \leq \alpha < 54.09^o$ and repulsive in cases where $54.09^o < \alpha \leq 90^o$ (**Figure 1.1**). When the magnetic interaction energy is enough to overcome thermal fluctuations, the dipole-dipole force drives the assembly of particles into 1D chain-like structures (**Figure 1.1d**).[49]

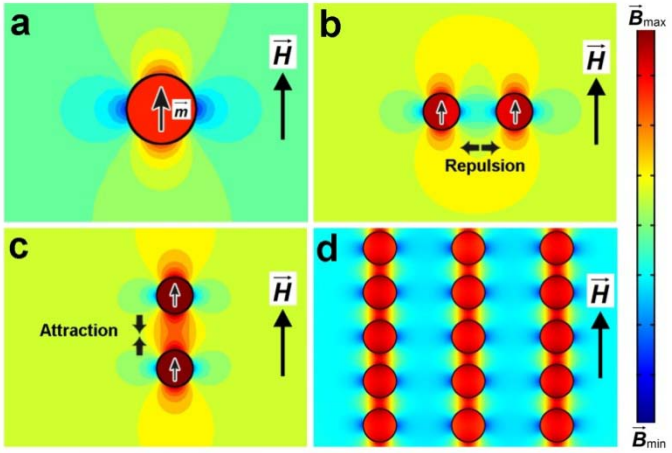

Figure 1.1. (a) Magnetic field distribution around a superparamagnetic particle with a dipole moment in the same direction as the external magnetic field. The repulsive (b) and attractive (c) dipole-dipole forces in different particle configurations drive the formation of particle chains along the magnetic field (d). The color bar on the right shows the relative strength of the local magnetic field. Reproduced with permission from Ref. 49 © 2012 American Chemical Society.

Similarly, the packing force can be understood as the interaction of a magnetic dipole with the external magnetic field. The interaction energy of a magnetic dipole $\boldsymbol{m}$ in an external magnetic field $\boldsymbol{H}$ is expressed by $U_m = \boldsymbol{m}\cdot\boldsymbol{H}$ so the packing force can be written as $\boldsymbol{F}_p = \nabla(\boldsymbol{m}\cdot\boldsymbol{H})$. The packing force drives the movement of magnetic particles towards regions with the maximum magnetic field strength and induces a particle concentration gradient or crystallization.[55] As discussed in the following sections, the particle concentration plays a critical role in their assembly behavior. More importantly, it allows state-of-the-art design of spatial magnetic field gradients to control the local assembly behavior which may eventually lead to high-resolution, for example, pixel-level manipulation in parallel.

Nonmagnetic particles typically have no effective response to normal external magnetic fields due to their negligible induced magnetic moments. However, when dispersed in a magnetized ferrofluid, a nonmagnetic particle behaves as a magnetic "hole" with an imaginary magnetic moment which can be approximately considered as equal to the total moment of the displaced ferrofluid but in the opposite direction of the magnetic field, $\boldsymbol{m} = -V\chi_{eff}\boldsymbol{H}$, where V is the volume of the particles, χ_{eff} is the effective volume susceptibility of the ferrofluid and $\boldsymbol{H}$ is the local magnetic field strength.[56] The dipole-dipole interaction between magnetic holes has the same directional nature as the real moments, and likewise drives the chaining of the nonmagnetic particles. However,

since nonmagnetic “dipolar” particles have positive magnetostatic energy, the gradient of the external magnetic field drives their movement towards regions with minimum magnetic field strengths. More interestingly, such negatively magnetized holes can form complex colloidal structures when assembled together with magnetic particles.[57]

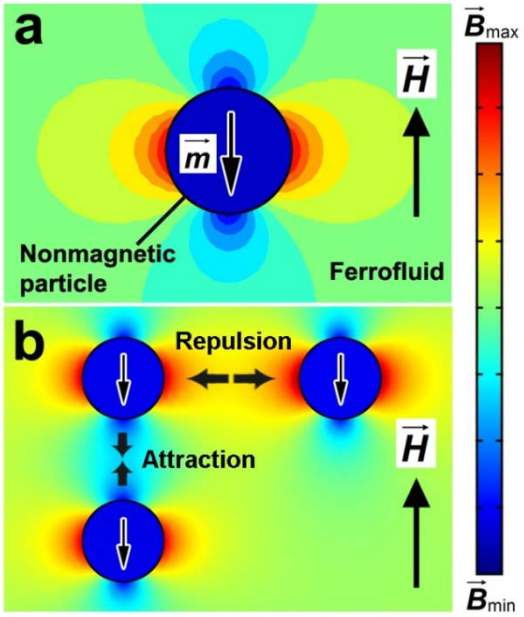

Figure 1.2. (a) Magnetic field distribution around a nonmagnetic particle with a dipole moment in the opposite direction of the external magnetic field. (b) The interparticle dipole-dipole force is repulsive or attractive depending on particle configurations. The color bar on the right shows the strength of the magnetic field. Reproduced with permission from Ref. 49 © 2012 American Chemical Society.

1.4 Magnetic Assembly of Colloidal Photonic Structures

Colloidal dipolar spheres can self-assemble into various crystal structures which allow exploration of the phase complexity in a single sample as their interparticle interactions can be conveniently tuned within an experimentally accessible timescale. The phase diagrams of dipolar hard and soft spheres were simulated by calculating the Helmholtz free energy.[58] The simulated phase diagram for dipolar hard spheres shows fluid, *fcc*, hexagonal-close-packed (*hcp*), and body-centered-tetragonal (*bct*) phases while in cases of dipolar soft spheres the phase diagram exhibits an additional body-centered-orthorhombic (*bco*) phase. The key factors that determine the thermodynamic equilibrium state of dipolar colloidal suspensions are the local particle concentration and the interparticle interaction potentials from both repulsive and attractive forces. Magnetic fields can affect both factors through magnetic forces, which not only induce the self-assembly of one-dimensional (1D), two-dimensional (2D) and three-dimensional (3D) structures, but also cause phase transitions between the different structures.[50, 59] For example, the magnetic field gradient can drive the redistribution of colloidal particles to change local particle concentrations through the magnetic packing force. On the other hand, the strength of the external magnetic field can determine the induced moment in superparamagnetic particles, which controls the interparticle dipole-dipole potentials. The mechanism of magnetic assembly can be simply

understood as magnetic control of local particle concentration and interparticle potential in colloidal suspensions.

The transition between Brownian fluids and 1D particle chains represents the simplest switch between random and ordered states. When the interparticle dipole-dipole potential is strong enough to overcome thermal fluctuations, the alignment of dipolar particles along the direction of their magnetic moments is the direct result of the directional dipole-dipole force. Recently, we successfully characterized the particle chain structures in different ways, providing direct evidence of the 1D structure (**Figure 1.3**).[60, 61] In cases of colloidal "soft" particles, where long-range interparticle repulsions exit, such as electrostatic force, the magnetic dipole-dipole attraction can be balanced by the repulsions. Therefore, a force equilibrium can be established, leading to a defined interparticle separation. If the force balance is altered, the interparticle separation will change accordingly, which allows dynamic control over the lattice constant of the particle chains. Most studies on 1D dipolar photonic chains utilize soft superparamagnetic particles so an external magnetic field can induce the formation of dynamic particle chains with long-range 1D order at a relatively large interparticle separation. The large interparticle separation also permits a broader choice of materials due to higher tolerance of the monodispersity of the building blocks.

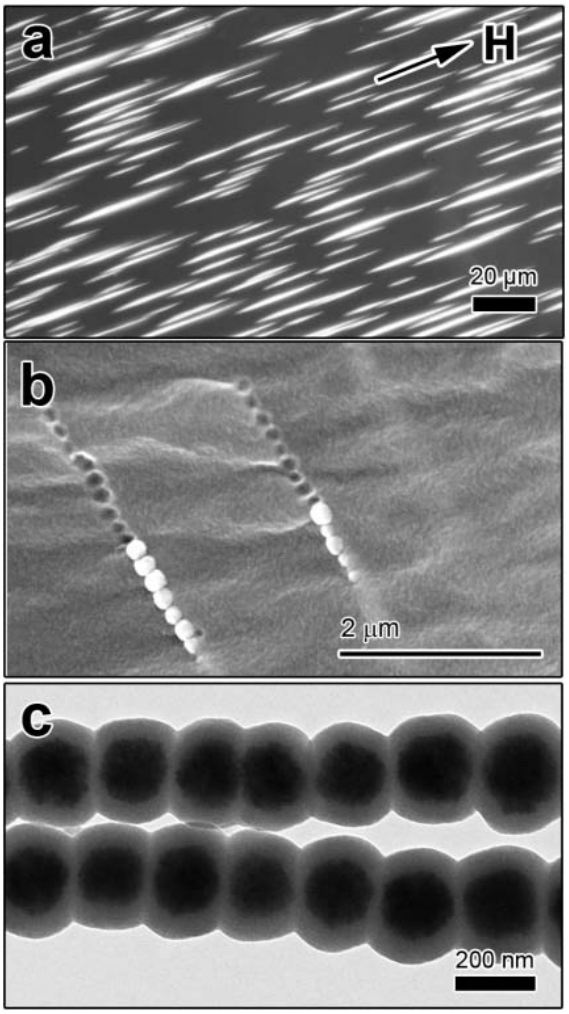

Figure 1.3. (a) Dark-field optical image showing 1D chain-like structures of CNCs along a magnetic field. (b) SEM image of Fe_3O_4@SiO_2 particle chains embedded in a PEGDA matrix showing the periodic arrangement of the particles inside each chain. (c) TEM image of nanochains of Fe_3O_4 CNCs fixed by wrapping in a layer of SiO_2 through a sol-gel process. Reproduced with permission from Ref. 49 © 2012 American Chemical Society.

In 1D dipolar particle chains, the interchain forces, such as magnetic dipole-dipole repulsion and other type of repulsive forces, keep the chains away from each other. However, when the concentration of the particle chains, as well as the interparticle dipole-dipole interactions, reaches an extent such that the interchain repulsive forces are sufficiently strong that they become thermodynamically unstable, the chains start to aggregate into zigzag multiple chains or 2D labyrinth structures.[20] As discussed above, the dipole-dipole force reaches its minimum at the critical angle of 54.09^{o}, which drives the formation of zigzag structures to minimize the interparticle magnetic dipole-dipole repulsion. However, the detailed study of the photonic properties of these 2D structures remained in its infancy owing to the difficulty in fabrications.[62] Very recently, we demonstrated the magnetic assembly of superparamagnetic particles into 2D dynamic labyrinth structures which can be solidified through a unique sol-gel process without disturbing its original ordering.[63] Thanks to the solidification by silica, the labyrinth structures can be well retained against capillary force during drying, making it possible to study their detailed structure using electron microscopy techniques (**Figure 1.4**). The direct observation of the zigzag arrangement between two neighboring chains suggests that the original chains shift their vertical position when they are pushed together during the 1D to 2D transition in order to minimize the repulsive dipole force, thus providing direct experimental proof of the 2D structures.

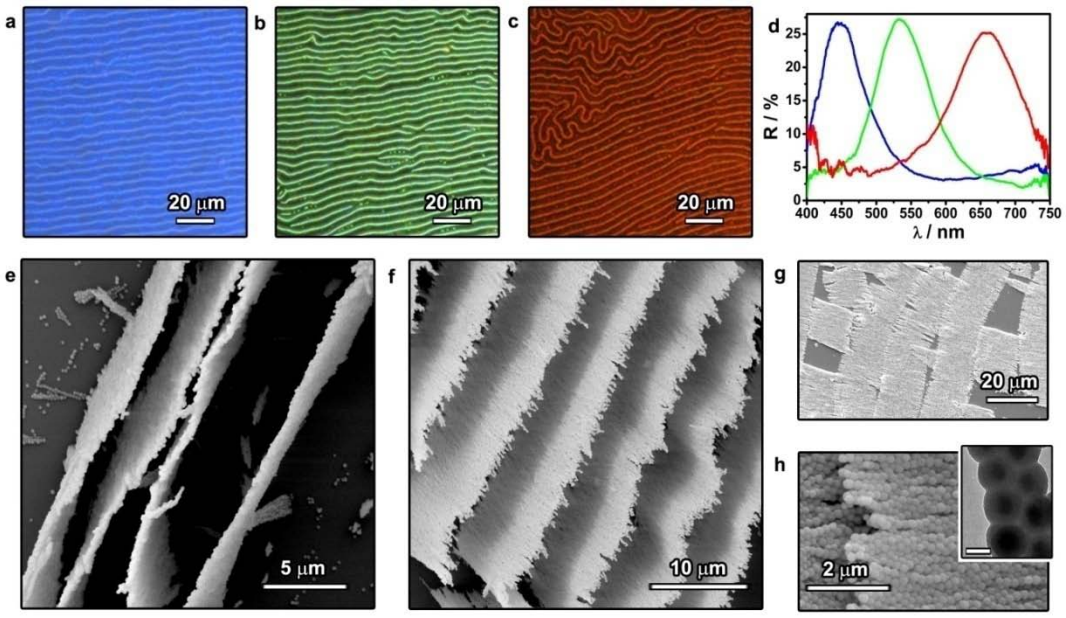

Figure 1.4. (a-c) Dark-field optical microscopy images of solidified photonic labyrinth structures with different diffraction colors made by using Fe_3O_4@SiO_2 CNCs of different sizes: (a), blue (d = ~ 120 nm), (b) green (d = ~ 150 nm), and (c) red (d = ~ 190 nm). The corresponding reflectance spectra are shown in (d). (e-h) Electron microscopy studies of the structure of photonic labyrinths, which comprise of sheet-like structures with a uniform width of ~ 20 μm. The TEM image in the inset in (h) clearly shows that the labyrinth structures adopt a zigzag arrangement. The scale bar in the inset is 100 nm. Reproduced with permission from Ref. 63 © 2013 American Chemical Society.

In some studies, 2D structures were considered as the intermediate state between 1D dipolar chains and 3D structures.[64] As the particle concentration and the interparticle potential were further increased, the 2D structures eventually evolved into highly crystalline 3D structures (**Scheme 1.2**). For example, Philipse et al. reported a magnetic field induced self-assembly of magnetic poly(methyl methacrylate) latex spheres, which were synthesized by a standard emulsion polymerization method using magnetite-stabilized emulsion droplets as seeds.[65] The slow crystallization process induced by the magnetic field gradients was realized through the local concentrating of particles driven by the magnetic packing forces. However, the assembly efficiency was very low due to weak magnetic response of the polymer beads. Moreover, the structure of the 3D crystals has not been identified. In other cases, the 3D structures were formed in the absence of interparticle magnetic interactions. For example, Asher et al. reported the formation of crystalline colloidal arrays with *fcc* structures from highly-charged monodisperse superparamagnetic colloidal spheres due to the minimization of interparticle electrostatic repulsive potentials.[66, 67] The introduction of magnetic interactions could then induce the compression of the preformed arrays along the magnetic field gradient. Besides *fcc* structures, theoretical studies predict a number of other potential 3D structures in the phase diagram of dipolar colloidal suspensions. Surprisingly, the phase diagrams of both dipolar soft and hard spheres predict a large

portion of the *hcp* phase, which is unstable in normal bulk suspensions.[58] Unfortunately, advancement in phase transitions of dipolar spheres has been limited by slow progress in the experimental observation of rich varieties of the computed phases. For example, the predicted transition between *fcc* and *hcp* for dipolar spheres has not yet been identified experimentally.

It is worth noting that the transitions between different structures usually require great changes of local particle concentrations and particle interaction potentials. Magnetic assembly of superparamagnetic particles is particularly suitable for this purpose. The induced magnetic moment can be controlled by manipulating the strength of the external magnetic field to tune the interparticle dipole-dipole interactions. The packing force owing to the magnetic field gradient can induce a local particle concentration gradient, which benefits the formation of different structures locally in a single sample. As discussed below, the ability to magnetically manipulate structures in suspensions of dipolar colloidal particles is of great importance for tuning their photonic properties.

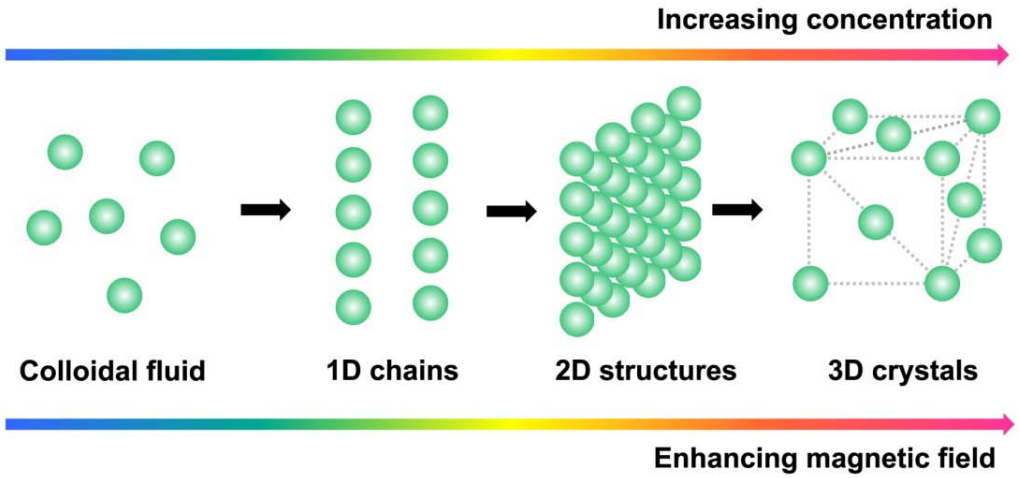

Scheme 1.2. Illustration of magnetically induced phase transitions between colloidal fluids, 1D particle chains, 2D sheets and 3D structures.

1.5 Magnetic Tuning of Photonic Properties

When the periodicity of and the dielectric contrast in the assemblies of dipolar particles match visible diffraction conditions, they may display iridescent structural colors. The diffraction wavelength (or band gap position) of the colloidal arrays can be described by Bragg's law, $m\lambda = 2nd\sin\theta$, where m is the diffraction order, λ is the wavelength of incident light, n is the effective refractive index, d is the lattice spacing, and θ is the glancing angle between the incident light and diffraction crystal plane. Accordingly, to magnetically tune the optical diffractions, the external magnetic field must be able to induce changes in either the refractive index of the components, or the symmetries, lattice parameters or orientations of the ordered arrays. Monodisperse superparamagnetic colloidal spheres are presumably the most suitable building blocks for magnetically responsive photonic nanostructures since their magnetic responses are much stronger than normal paramagnetic materials and their dipole-dipole interactions can be fully initiated and controlled by external magnetic fields.[21, 68] Tuning the photonic properties by the application of external magnetic fields is realized through the manipulation of the magnetic interaction potentials and the local particle concentrations, which eventually results in changes in the lattice constant d, the orientation θ, or the crystal structure (which changes the effective refractive index and/or the lattice constant).

Magnetically tuning the lattice constant (interparticle spacing) of colloidal photonic structures without causing significant disturbance of the ordering seems to be the simplest and most predictable way of controlling the optical properties. The interparticle spacing can be tuned by the manipulation of either the interparticle dipole-dipole interaction or the packing force. For example, Asher et al. developed magnetically controllable 3D crystalline colloidal arrays made of monodisperse polymer beads which exhibited a broad shift of the diffraction wavelength in response to non-uniform external magnetic fields.[66] Owing to the gradient of the external magnetic field, the packing force drives the movement of particles towards the field gradient maximum, resulting in the compression of the colloidal arrays and a blueshift of the diffraction wavelength. The effect of the magnetic dipole-dipole force is minor and only causes a minor distortion of the crystal structure in this case. As the magnetic content in the polymer beads is quite low, the response rate of the 3D arrays is relatively slow.

On the other hand, the interparticle distance can be more rapidly and conveniently tuned in 1D particle chains by controlling the interparticle dipole-dipole forces by using an external magnetic field. Bibette et al. pioneered the magnetic assembly of uniform emulsion droplets containing concentrated ferrofluids into 1D chains with optical diffractions tunable in a varying magnetic field.[69, 70] However, the thermodynamic instability of the emulsion droplets, their incompatibility with nonaqueous solvents, and

the complicated steps necessary for obtaining uniform droplets greatly limit the practical use of their system. Our group has previously developed 1D magnetically tunable photonic chain-like structures by assembling superparamagnetic Fe_3O_4 colloidal nanocrystal clusters (CNCs) with overall diameters in the range of 100-200 nm.[47, 71] Utilizing clusters of ~10-nm superparamagnetic Fe_3O_4 nanocrystals not only increases their magnetic responses and thereby magnetic interactions, but also avoids the superparamagnetic-ferromagnetic transition (at a domain size of ~ 30 nm for Fe_3O_4). As a result, we are able to instantly assemble them into ordered structures (less than 1 s) and rapidly tune the photonic properties across the whole visible region through the application of a relatively weak (typically 50 – 500 Oe) external magnetic field (**Figure 1.5**).[48, 49] The key to the assembly of CNCs and tuning of the optical diffraction is the coexistence of a highly tunable magnetic dipole-dipole force and comparable long-range electrostatic force, both of which are separation-dependent. Along the chain, the magnetic dipole-dipole attraction is balanced by the electrostatic force while the interchain magnetic repulsive force, as well as the electrostatic force, keep the chains away from each other. The rapid tuning of the diffraction is realized by controlling the interparticle separation *d* in response to the external magnetic fields. For example, enhancing the magnetic field strength induces a stronger magnetic attraction which brings the particles closer and consequently produces a blue-shift of the diffraction.

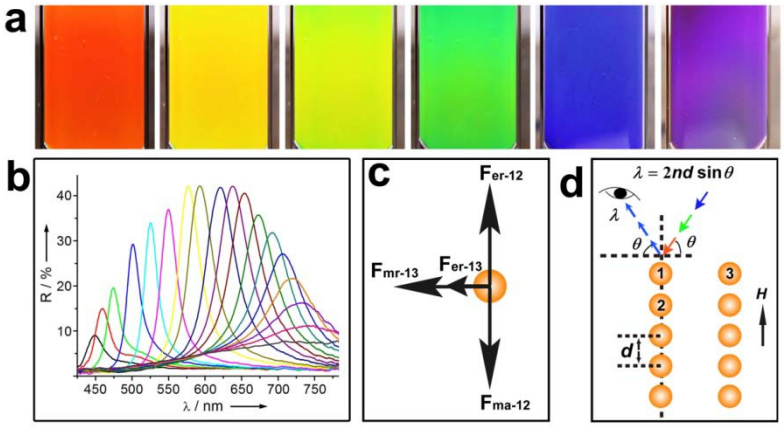

Figure 1.5. (a) Digital photos showing the diffraction color change in a typical CNC dispersion encapsulated in a capillary tube with a width of 1 cm in response to a magnetic field with increasing strengths from left to right. (b) Reflectance spectra of the same sample in different magnetic fields. (c) Illustration of interparticle force inside the chain and between different chains. (d) Scheme of Bragg diffraction from the chains of CNCs. Reproduced with permission from Ref. 49 © 2012 American Chemical Society.

The surface of the original CNCs is grafted with a layer of polyelectrolyte, polyacrylate, during the synthesis, which provides a strong interparticle electrostatic force in aqueous solution. Engineering the surface of Fe_3O_4 CNCs with a layer of silica through the sol-gel process increases their compatibility with nonaqueous solvents; further modifying the silica surface with a layer of hydrophobic silane enables the dispersion of the particles in nonpolar solvents. The charges carried by the silica coated Fe_3O_4 produce electrostatic interactions that can work with the magnetically induced attraction and enable successful assembly.[72] However, it is difficult to establish electrostatic repulsive interactions in nonpolar solvents due to the high energy barrier to forming surface charges. This challenge was addressed by introducing reverse micelles to reduce the energy barrier of charge separation in nonpolar solvents, thus creating electrostatic repulsive interactions that can counteract the magnetic attraction to allow ordering of the superparamagnetic colloids.[73] An important feature of the 1D tunable system is that one can achieve considerably strong diffraction intensity at a significantly low particle concentration (~ 0.1 % volume fraction vs. ~ 74 % for close-packed colloidal crystals). The low particle density, as well as the dynamic chaining structure with only one translational order, allows instant and reversible switching between the highly ordered and completely disordered states. Recent measurement suggested a switching rate of ~ 30 Hz for the aqueous system.

Besides controlling the interparticle spacing *d*, magnetic manipulation of the orientation (θ) of colloidal assemblies provides an alternative means of constructing magnetically responsive photonic structures. For example, Asher et al. developed a magnetically controllable photonic system using ferromagnetic 3D polymerized crystalline colloidal arrays (PCCAs).[52] The preformed 3D arrays were magnetized in a strong magnetic field to induce a permanent magnetic dipole inside each particle along the <111> direction. As the position and the arrangement of the particles relative to each other were locked inside the polymerized arrays, one was able to observe a net magnetization of the PCCAS. A weaker magnetic field can then induce the reorientation of the photonic crystals as the magnetic dipoles always tend to align along the external magnetic field to minimize the magnetic potential. Later, we demonstrated new types of 1D magnetically rotatable photonic units with reduced sizes by fixing photonic chains directly through a silica coating process or inside an emulsion droplet of UV-curable resins.[60, 61, 74] Due to the dipole-dipole interaction between neighboring particles, the superparamagnetic particle chains tend to align along the magnetic field to minimize their interaction energy so that the optical properties of the nanochains can be controlled by magnetically tuning their orientations relative to the incident light (**Figure 1.6**).

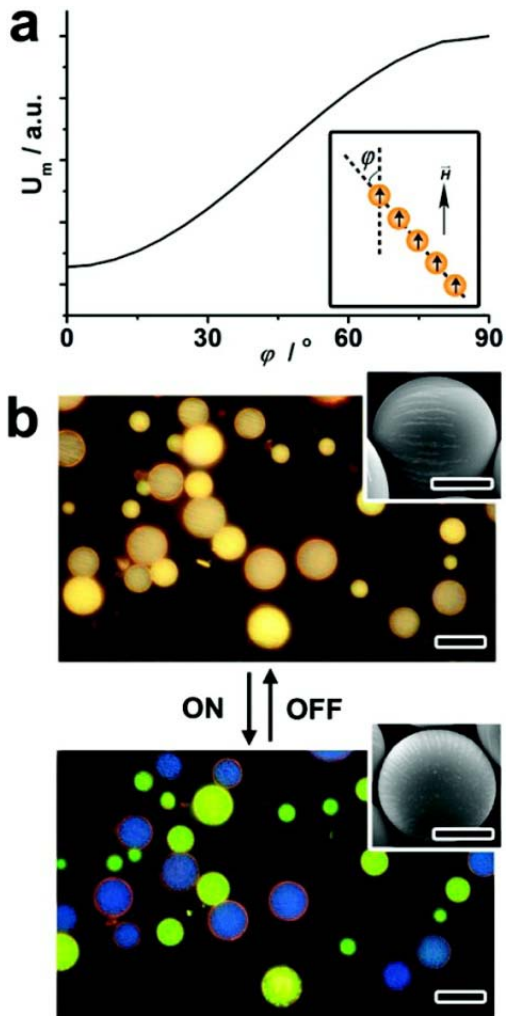

Figure 1.6. (a) Plot of magnetic dipole-dipole energy of a nanochain versus the orientation with respect to the external magnetic field. (b) "ON/OFF" switching of the color of a mixture of two types of microspheres, imaged by dark-field optical microscopy, from the native light brown of iron oxide to blue and green by tuning the magnetic field orientation from horizontal to vertical. Insets are SEM images of the microspheres in horizontal (off) and vertical (on) orientations. All scale bars are 20 μm. Reproduced with permission from Ref. 49 © 2012 American Chemical Society.

In the case of the 1D photonic chains, we also demonstrated that the lattice constant and the orientation can be controlled synergetically to realize magnetic control of the photonic properties. As can be seen from the Bragg equation, the diffraction color of the 1D dynamic photonic chains can be tuned through controlling the interparticle spacing d and/or their orientation θ. While d can be easily varied by adjusting the magnetic field strength, the orientation of the photonic chains follows the direction of the magnetic field. As an example, we have recently studied the assembly behavior of silica modified superparamagnetic CNCs (Fe_3O_4@SiO_2) in response to a complex magnetic field produced by a non-ideal linear Halbach array and found that a horizontal magnetic field sandwiched between two vertical fields could allow one to change the orientation of the particle chains, producing high contrast color patterns (**Figures 1.7a, 1.7b**). When subjected to a spatial magnetic field with large variance in field strength and direction, both the interparticle spacing and orientation of the photonic chains can be modulated to display multiple colors from different areas in a single sample. A rainbow-like color effect can be successfully created in the dispersion of magnetic particles near the edge of a cubic magnet (**Figures 1.7c, 1.7d**). The blueshift of diffraction color from left to right is due to both compression of the chains and the tilting of the chaining away from the viewing angle.

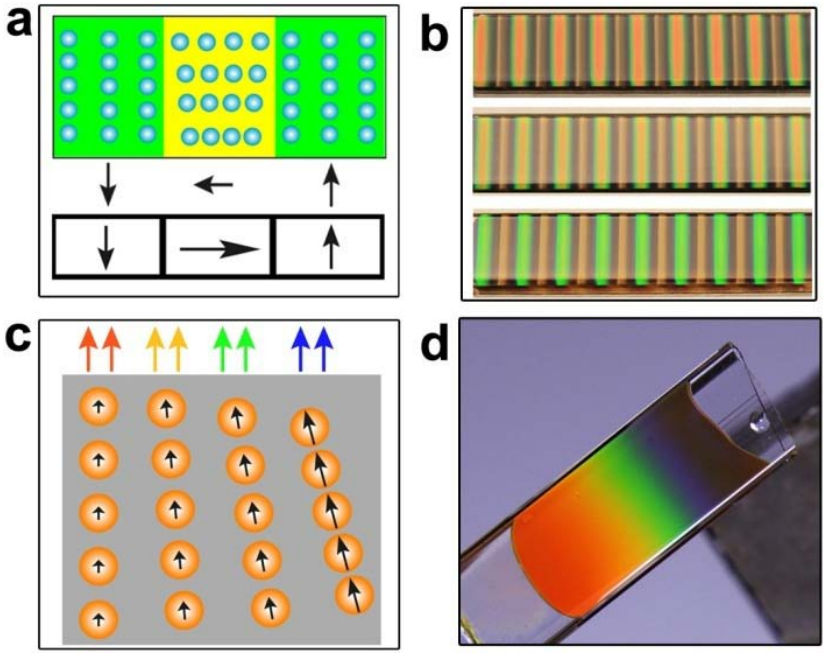

Figure 1.7. (a) Schematic illustration and (b) digital photo showing the assembly of Fe_3O_4@SiO_2 particles in a patterned magnetic field with alternating field orientation. (c) Schematic illustration and (d) digital photo showing a suspension of CNCs displaying rainbow-like colors due to the variance in the interparticle spacing *d* and the orientation θ in different regions controlled by the magnetic field. Reproduced with permission from Ref. 49 © 2012 American Chemical Society.

1.6 Scope of this dissertation

The majority of research on colloidal responsive photonic nanostructures has been focused on constructing the photonic crystal structures and incorporating stimulus-responsive materials into the self-assembled photonic crystal structures. In principle, the stimulus can be any means that can effectively induce changes in the refractive indices of the building blocks or the surrounding matrix, and changes in the lattice constants and/or spatial symmetry of the crystalline arrays. While various responsive mechanisms have been developed, such as mechanical stretching, solvent swelling, and temperature-dependent phase change, many challenges still exist, including limited tunability of the photonic properties, a slow response to the external stimuli, incomplete reversibility, and difficulty of integration into existing photonic devices. To broaden the tuning range of diffraction color, the external stimulus must be able to induce large changes in either the refractive index of the components, or the symmetries, lattice parameters or orientations of the ordered arrays. New mechanisms need to be established to also significantly enhance the response rate of the active components to the external stimuli in order to offer dynamic optical modulation that can meet the demand of practical applications.

The earlier work in our lab demonstrated that structural colored photonic nanostructures can be created instantly through a magnetic assembly strategy whose

photonic properties can be widely, rapidly and reversibly tuned in the whole visible spectrum. The application of external magnetic fields can efficiently create strong and controllable interaction between superparamagnetic magnetite (Fe_3O_4) colloidal nanocrystal clusters which induces dynamically chaining of particles along the magnetic field when balanced by different repulsive forces related to the polarity of the solvents. Each chain, with periodical interparticle spacing in the range of 100 to 200 nm, acts as the smallest 1D photonic unit and strongly diffracts visible light. The instant tuning of the diffraction colors is realized by changing the interparticle distance controlled by the external magnetic fields. Engineering the surface of the magnetic colloids with a layer of silica improves the compatibility of the magnetically responsive photonic structures with UV curable resin, which allows the fixation of the dynamic chain in a polymer matrix through combining instant magnetic assembly with a rapid UV polymerization process. The successful fixation of the photonic chains in a polymer matrix not only allows us to confirm the chaining structures through observation of the cross-section of the film, but also renders new applications for security and sensing devices.

While the magnetically responsive photonic system provides a new platform for various chromatic applications, the potential of the magnetic assembly strategy has not been fully exploited. For example, the magnetic fields for the assembly are typically generated by using a simple permanent magnet or an electromagnetic magnet.

Therefore, the magnetic fields are close to be uniform without complex spatial distributions. However, the effects of the field gradient, which commonly exists in practical applications, have not been taken into account. It is necessary to better understand the assembly behavior and the optical response in complex magnetic fields before the wide practical applications.

On the other hand, the earlier work was focused on the assembly of 1D photonic chainlike structures. Nevertheless, the phase diagram of the magnetically dipolar particles predicts more diverse 2D and 3D structures that might also possess photonic properties. Magnetic field may also induce phase transitions in suspensions of colloidal dipolar spheres along with a shifting of their photonic properties, providing a new responsive mechanism through the change of crystal structures. Experimental demonstration of the complete phase diagram will be of fundamental significance in condensed physics. The unique optical response to the external field might also find applications in fundamental studies of colloidal systems, for example, in the colloidal force measurement.

As there are much more choices for nonmagnetic colloidal particles with high size uniformity and optimal refractive index, it would be promising to extend this magnetic assembly strategy to nonmagnetic particles to allow their rapid assembly into large-area photonic crystals with high quality. Conventionally, magnetic assembly of nonmagnetic

materials is achieved by modifying these building blocks with magnetic materials, which apparently limits the choices of materials and the applicability of the processes. It is necessary to develop of a new magnetic assembly strategy which can utilize normal nonmagnetic particles as building blocks.

It is generally accepted that magnetic assembly, conceptually, is suitable for high-resolution patterning of colloidal nanostructures. In principle, magnetic manipulation of nanoscale objects can provide precise control over their local arrangement and properties if the external magnetic field can be modulated. The ordered assembly is typically achieved by using magnetic micro-patterns, for which the downside is that they require advanced micro-fabrication techniques to produce. Multiple steps and sophisticated instruments have been used to pattern micromagnets on solid substrates, adding significant challenges for device fabrication and integration.

This dissertation summarizes our recent efforts toward magnetic assembly, manipulation and patterning of colloidal responsive photonic structures. In chapter 2, the magnetic assembly behavior of superparamagnetic Fe_3O_4@SiO_2 colloids in complex magnetic fields produced by a nonideal linear Halbach array is discussed. We demonstrate that a horizontal magnetic field sandwiched between two vertical fields would allow one to change the orientation of the particle chains, producing a high contrast in color patterns. A phase transition of Fe_3O_4@SiO_2 particles from linear

particle chains to three-dimensional crystals is found to be determined by the interplay of the magnetic dipole force and packing force, as well as the strong electrostatic force. While a color pattern with tunable structures and diffractions can be instantly created when the particles are assembled in the form of linear chains in the regions with vertical fields, the large field gradient in the horizontal orientation may destabilize the chain structures and produces a pattern of 3D crystals that compliments that of initial chain assemblies. Our study not only demonstrates the great potential of magnetically responsive photonic structures in the visual graphic applications such as signage and security documents but also points out the potential challenge in pattern stability when the particle assemblies are subjected to complex magnetic fields that often involve large field gradients.

In chapter 3, we demonstrate the self-assembly and magnetically induced phase transition of 3D photonic nanostructures of superparamagnetic colloidal particles. We experimentally observed the predicted reversible transition from polycrystalline *fcc* to single-crystalline-like hexagonal packing structure controlled by the strengths of the external magnetic field in suspensions of superparamagnetic soft spheres. Our study shows that the diffraction in the absence of the magnetic field results from the crystallization of the magnetic particles driven by the interparticle electrostatic repulsions, which is a conclusion different from that in an earlier report which claimed the formation

of quasi-amorphous structure. Different from the 1D magnetically responsive photonic structures, the 3D photonic crystals can easily reach higher diffraction intensity in the magnetic field due to much higher density of diffraction units. Our observation indicates the unstable bulk hexagonal packing state can be created by the application of the external magnetic fields, which might lead to important extensions of using colloids as condensed matter model systems and creation of advanced materials with unconventional structures.

In chapter 4, we take advantage of the optical response of the core-shell magnetic colloids in magnetic fields to study the thickness of solvation layers formed when the colloidal silica surface is covered by different solvents. The key to the successful measurement of the thickness of the solvation layer is the effective screening of the electrostatic force so that the neighboring particles interact with each other through the repulsion resulting from the overlap of solvation layers, which balances the magnetically induced attraction and forms ordered assemblies. The thickness of solvation layer can be then estimated by using Bragg's law. A relationship between the hydrogen-bonding ability of the solvents and the thickness of solvation layer on Fe3O4@SiO2 colloidal surface has been identified, which is consistent with the prior understanding of a hydrogen-bonding origin of the solvation force. We believe this magneto-photonic method represents a simple yet very effective tool for studying many types of short-range

colloidal interactions including not only the solvation forces between various surfaces but also the steric effects which are fundamentally critical to chemistry, biochemistry and pharmacology.

In chapter 5, we show the extension of the magnetic assembly strategy to nonmagnetic building blocks through the magnetic hole effect. Conventionally, magnetic assembly of nonmagnetic materials is achieved by modifying these building blocks with magnetic materials, which apparently limits the choices of materials and the applicability of the processes. In our work, we demonstrate the use of nanocrystal-based ferrofluids to direct the assembly of nonmagnetic colloidal particles into photonic crystal structures. The process is general, efficient, convenient, and scalable and thus represents a new and practical platform for the fabrication of colloidal crystal-based photonic devices.

In chapter 6, we present a general strategy that allows convenient magnetically-driven assembly of nonmagnetic objects in defined locations with high spatial resolution. The process involves immersing a polymer relief pattern in a uniformly magnetized ferrofluid, which modulates the local magnetic fields around the pattern. Nonmagnetic target objects dispersed in the same ferrofluid can then be magnetically assembled at positions defined by the polymer pattern. As the nonmagnetic polymer patterns can be conveniently fabricated at low cost through

photolithography and soft-lithography processes, our method provides a general yet very effective means to assemble a wide range of nonmagnetic objects with controlled spatial distribution, paving the way towards patterning functional microstructures.

1.7 References

(1) Pusey, P. N.; van Megen, W. *Nature* **1986**, *320*, 340.

(2) Van Blaaderen, A.; Wiltzius, P. *Science* **1995**, *270*, 1177.

(3) Thomas, P. *J. Phys.: Condens. Matter* **1999**, *11*, R323.

(4) Auer, S.; Frenkel, D. *Nature* **2001**, *413*, 711.

(5) Anderson, V. J.; Lekkerkerker, H. N. W. *Nature* **2002**, *416*, 811.

(6) Gasser, U. *J. Phys.: Condens. Matter* **2009**, *21*, 203101.

(7) Zhang, H.; Edwards, E. W.; Wang, D.; Mohwald, H. *PCCP* **2006**, *8*, 3288.

(8) Ozin, G. A.; Hou, K.; Lotsch, B. V.; Cademartiri, L.; Puzzo, D. P.; Scotognella, F.; Ghadimi, A.; Thomson, J. *Mater. Today* **2009**, *12*, 12.

(9) Weissman, J. M.; Sunkara, H. B.; Tse, A. S.; Asher, S. A. *Science* **1996**, *274*, 959.

(10) Holtz, J. H.; Asher, S. A. *Nature* **1997**, *389*, 829.

(11) Xia, Y. N.; Gates, B.; Yin, Y. D.; Lu, Y. *Adv. Mater.* **2000**, *12*, 693.

(12) Arsenault, A. C.; Puzzo, D. P.; Manners, I.; Ozin, G. A. *Nat. Photon.* **2007**, *1*, 468.

(13) Yin, Y.; Lu, Y.; Gates, B.; Xia, Y. *J. Am. Chem. Soc.* **2001**, *123*, 8718.

(14) Yin, Y.; Xia, Y. *Adv. Mater.* **2001**, *13*, 267.

(15) Lee, I.; Zheng, H.; Rubner, M. F.; Hammond, P. T. *Adv. Mater.* **2002**, *14*, 572.

(16) Xia, Y.; Yin, Y.; Lu, Y.; McLellan, J. *Adv. Funct. Mater.* **2003**, *13*, 907.

(17) Yin, Y.; Xia, Y. *J. Am. Chem. Soc.* **2003**, *125*, 2048.

(18) Whitesides, G. M.; Grzybowski, B. *Science* **2002**, *295*, 2418.

(19) Tao, R.; Jiang, Q. *Phys. Rev. Lett.* **1994**, *73*, 205.

(20) Islam, M. F.; Lin, K. H.; Lacoste, D.; Lubensky, T. C.; Yodh, A. G. *Phys. Rev. E* **2003**, *67*, 021402.

(21) Ge, J.; He, L.; Hu, Y.; Yin, Y. *Nanoscale* **2010**, *3*, 177.

(22) Li, F.; Josephson, D. P.; Stein, A. *Angew. Chem. Int. Ed.* **2011**, *50*, 360.

(23) John, S. *Phys. Rev. Lett.* **1987**, *58*, 2486.

(24) Yablonovitch, E *Phys. Rev. Lett.* **1987**, *58*, 2059.

(25) Anderson, T. F.; Richards, J. A. G. *J. Appl. Phys.* **1942**, *13*, 748.

(26) Welch, V. L.; Vigneron, J. P. *Optical and Quantum Electronics* **2007**, *39*, 295.

(27) Sanders, J. V. *Nature* **1964**, *204*, 1151.

(28) Aguirre, C. I.; Reguera, E.; Stein, A. *Adv. Funct. Mater.* **2010**, *20*, 2565.

(29) Ge, J.; Yin, Y. *Angew. Chem. Int. Ed.* **2011**, *50*, 1492.

(30) *Responsive Photonic Nanostructures: Smart Nanoscale Optical Materials*; Yin, Y., Ed.; Royal Soceity of Chemistry, 2013.

(31) Ge, J. P.; Goebl, J.; He, L.; Lu, Z. D.; Yin, Y. D. *Adv. Mater.* **2009**, *21*, 4259.

(32) Xuan, R.; Wu, Q.; Yin, Y.; Ge, J. *J. Mater. Chem.* **2011**, *21*, 3672.

(33) Tanabe, T.; Notomi, M.; Mitsugi, S.; Shinya, A.; Kuramochi, E. *Appl. Phys. Lett.* **2005**, *87*, 151112.

(34) von Freymann, G.; Kitaev, V.; Lotsch, B. V.; Ozin, G. A. *Chem. Soc. Rev.* **2013**, *42*, 2528.

(35) Kuai, S.-L.; Bader, G.; Ashrit, P. V. *Appl. Phys. Lett.* **2005**, *86*, 221110.

(36) Pevtsov, A. B.; Kurdyukov, D. A.; Golubev, V. G.; Akimov, A. V.; Meluchev, A. A.; Sel'kin, A. V.; Kaplyanskii, A. A.; Yakovlev, D. R.; Bayer, M. *Physical Review B* **2007**, *75*, 153101/1.

(37) Zhou, J.; Sun, C. Q.; Pita, K.; Lam, Y. L.; Zhou, Y.; Ng, S. L.; Kam, C. H.; Li, L. T.; Gui, Z. L. *Appl. Phys. Lett.* **2001**, *78*, 661.

(38) Kang, D.; Maclennan, J. E.; Clark, N. A.; Zakhidov, A. A.; Baughman, R. H. *Phys. Rev. Lett.* **2001**, *86*, 4052.

(39) Leonard, S. W.; Mondia, J. P.; van Driel, H. M.; Toader, O.; John, S.; Busch, K.; Birner, A.; Gösele, U.; Lehmann, V. *Phys. Rev. B* **2000**, *61*, R2389.

(40) Mach, P.; Wiltzius, P.; Megens, M.; Weitz, D. A.; Lin, K.-h.; Lubensky, T. C.; Yodh, A. G. *J. Europhys. Lett.* **2002**, *58* 679.

(41) Gu, Z. Z.; Fujishima, A.; Sato, O. *J. Am. Chem. Soc.* **2000**, *122*, 12387.

(42) Ozaki, M.; Shimoda, Y.; Kasano, M.; Yoshino, K. *Adv. Mater.* **2002**, *14*, 514.

(43) Sumioka, K.; Kayashima, H.; Tsutsui, T. *Adv. Mater.* **2002**, *14*, 1284.

(44) Fleischhaker, F.; Arsenault, A. C.; Kitaev, V.; Peiris, F. C.; von Freymann, G.; Manners, I.; Zentel, R.; Ozin, G. A. *J. Am. Chem. Soc.* **2005**, *127*, 9318.

(45) Fleischhaker, F.; Arsenault, A. C.; Wang, Z.; Kitaev, V.; Peiris, F. C.; von Freymann, G.; Manners, I.; Zentel, R.; Ozin, G. A. *Adv. Mater.* **2005**, *17*, 2455.

(46) Jeong, U.; Xia, Y. *Angew. Chem. Int. Ed.* **2005**, *44*, 3099.

(47) Ge, J.; Hu, Y.; Yin, Y. *Angew. Chem. Int. Ed.* **2007**, *119*, 7572.

(48) Ge, J.; Hu, Y.; Zhang, T.; Huynh, T.; Yin, Y. *Langmuir* **2008**, *24*, 3671.

(49) He, L.; Wang, M.; Ge, J.; Yin, Y. *Acc. Chem. Res.* **2012**, *45*, 1431.

(50) He, L.; Malik, V.; Wang, M.; Hu, Y.; Anson, F. E.; Yin, Y. *Nanoscale* **2012**, *4*, 4438.

(51) Gates, B.; Xia, Y. *Adv. Mater.* **2001**, *13*, 1605.

(52) Xu, X. L.; Majetich, S. A.; Asher, S. A. *J. Am. Chem. Soc.* **2002**, *124*, 13864.

(53) He, L.; Hu, Y.; Han, X.; Lu, Y.; Lu, Z.; Yin, Y. *Langmuir* **2011**, *27*, 13444.

(54) Kraftmakher, Y. *Eur. J. Phys.* **2007**, *28*, 409.

(55) Erb, R. M.; Sebba, D. S.; Lazarides, A. A.; Yellen, B. B. *J. Appl. Phys.* **2008**, *103*, 063916.

(56) Skjeltorp, A. T. *Phys. Rev. Lett.* **1983**, *51*, 2306.

(57) Erb, R. M.; Son, H. S.; Samanta, B.; Rotello, V. M.; Yellen, B. B. *Nature* **2009**, *457*, 999.

(58) Hynninen, A-P.; Dijkstra, M. *Phys. Rev. Lett.* **2005**, *94*, 138303.

(59) Malik, V.; Petukhov, A. V.; He, L.; Yin, Y.; Schmidt, M. *Langmuir* **2012**, *28*, 14777.

(60) Ge, J.; Lee, H.; He, L.; Kim, J.; Lu, Z.; Kim, H.; Goebl, J.; Kwon, S.; Yin, Y. *J. Am. Chem. Soc.* **2009**, *131*, 15687.

(61) Hu, Y.; He, L.; Yin, Y. *Angew. Chem. Int. Ed.* **2011**, *50*, 3747.

(62) Wang, M.; He, L.; Yin, Y. *Mater. Today* **2013**, *16*, 110.

(63) Zhang, Q.; Janner, M.; He, L.; Wang, M.; Hu, Y.; Lu, Y.; Yin, Y. *Nano Lett.* **2013**, *13*, 1770.

(64) He, L.; Hu, Y.; Kim, H.; Ge, J.; Kwon, S.; Yin, Y. *Nano Lett.* **2010**, *10*, 4708.

(65) Sacanna, S.; Philipse, A. P. *Langmuir* **2006**, *22*, 10209.

(66) Xu, X. L.; Friedman, G.; Humfeld, K. D.; Majetich, S. A.; Asher, S. A. *Adv. Mater.* **2001**, *13*, 1681.

(67) Xu, X. L.; Friedman, G.; Humfeld, K. D.; Majetich, S. A.; Asher, S. A. *Chem. Mater.* **2002**, *14*, 1249.

(68) Bishop, K. J. M.; Wilmer, C. E.; Soh, S.; Grzybowski, B. A. *Small* **2009**, *5*, 1600.

(69) Bibette, J *J. Magn. Magn. Mater.* **1993**, *122*, 37.

(70) Calderon, F. L.; Stora, T.; Mondain Monval, O.; Poulin, P.; Bibette, J. *Phys. Rev. Lett.* **1994**, *72*, 2959.

(71) Ge, J.; Hu, Y.; Biasini, M.; Beyermann, W. P.; Yin, Y. *Angew. Chem.* **2007**, *119*, 4420.

(72) Ge, J.; Yin, Y. *Adv. Mater.* **2008**, *20*, 3485.

(73) Ge, J. P.; He, L.; Goebl, J.; Yin, Y. D. *J. Am. Chem. Soc.* **2009**, *131*, 3484.

(74) Kim, J.; Song, Y.; He, L.; Kim, H.; Lee, H.; Park, W.; Yin, Y.; Kwon, S. *Small* **2011**, *7*, 1163.

Chapter 2

Assembly and Photonic Properties of Superparamagnetic Colloids in Complex Magnetic Fields

2.1 Introduction

The utilization of magnetic field in nanoscale assembly is of both fundamental and practical interests: it not only helps us to probe colloidal interactions, but also allows the creation of novel complex structures and the fabrication of advanced photonic devices.[1-7] Due to the contactless control of magnetic field and fast response, magnetic field-assisted assembly has been regarded as a convenient and efficient method to create ordered colloidal arrays and modulate their photonic properties.[8-11] It has been demonstrated that the challenge of low fabrication efficiency in typical self-assembly methods to colloidal crystals, which greatly limits their practical applications, may be overcome with the help of magnetic fields.[12, 13] Asher et al. pioneered the application of magnetic field to tune the optical properties on pre-assembled colloidal crystals arrays by incorporating magnetic content in the building blocks.[14, 15] It was also shown that emulsion droplets containing iron oxide nanoparticles can organize into ordered structures in the presence of an external magnetic field.[16, 17] Recently, we have further developed magnetically

tunable photonic crystals by assembling superparamagnetic iron oxide nanocrystal clusters (CNCs) into one-dimensional (1D) chainlike structures driven by the balance of the magnetic dipole attractions along the magnetic field and various repulsions in different solvent media.[18-22] Due to the high magnetic content and controlled surface properties of CNCs, the optical diffraction can be tuned widely, rapidly, and reversibly. We have also demonstrated the fixation of dynamic photonic chains in a polymer matrix for applications such as rewritable photonic paper, humidity sensor, and structural color printing.[23-25] Fixing the periodical chains individually or inside polymer microspheres produces new types of photonic structures that allow convenient tuning of their photonic properties by magnetically controlling their orientations,[26, 27] thus promising for applications in high resolution color presentation.

Magnetic assembly generally originates from two types of magnetic interactions: the dipole force between magnetic colloidal particles and the packing force resulting from the magnetic field gradient.[28, 29] Although the advantages of magnetically tunable photonic structures have been demonstrated in terms of strong and fast response and tunable bandgap properties, common permanent magnets were used in most studies so that control of color at spatially patterned magnetic fields has not been systematically studied. For real applications such as field responsive color displays, a complex magnetic field with various spatial distributions is needed to control the localized ordering and

subsequent colors.[30, 31] In principle, the magnetic fields can be used to modulate the color of each pixel by controlling the assembly of colloidal particles locally. However, magnetic assembly of colloids is complex due to the fact that it is affected by the interplay of dipole and packing forces, the latter of which can cause dramatic change in local concentration of magnetic particles.[29, 32] It is of great importance to understand the assembly behavior of magnetic colloids under complex external fields. In this chapter, we study the assembly behavior of silica modified superparamagnetic CNCs (Fe_3O_4@SiO_2) in ethanol in response to a complex magnetic field produced by a nonideal linear Halbach array.[33] Thanks to the high magnetic content in CNCs, we were able to observe the phase transition of different structures formed in response to the Halbach array. Our study also clearly shows the possibility of instant creation of color patterns with tunable colors and structures by using spatially modulated magnetic fields.

2.2 Materials and Methods

Materials. Ethanol, anhydrous iron(III) chloride ($FeCl_3$), ammonium hydroxide solution, tetraethyl orthosilicate (TEOS) and sodium hydroxide (NaOH) were purchased from Fisher Scientific. Polyacrylic acid (PAA, MW = 1800) and Diethylene glycol (DEG) were obtained from Sigma-Aldrich. Distilled water was used in all experiments. All chemicals were directly used as received without further treatment. Capillary tubes with different thickness were obtained from Electron Microscopy Sciences. Refrigerator magnets were purchased from McMaster.

Synthesis of Fe_3O_4@SiO_2 . In a typical synthesis, a mixture of 4 mmol PAA, 0.4 mmol $FeCl_3$, and 17 mL DEG was heated at 220 ^oC under nitrogen protection for 1 hour. After injection of 1.75 mL of NaOH/DEG solution (2.5 mol/L), the solution was further heated for 1 hour at 220 ^oC, and then cooled down to room temperature. Upon cleaning with a mixture of water and ethanol for several times, Fe_3O_4 CNCs were dispersed in 3 mL of water, mixed sequentially with 1 mL of ammonium hydroxide solution, 20 mL ethanol, and 200 μL TEOS under mechanical stirring. After reacting for 40 min, the Fe_3O_4@SiO_2 particles were cleaned with ethanol for a few times and finally dispersed in 3 mL of ethanol. The CNC solution was sealed in glass capillary tubes using optical glue to maintain concentration and avoid contamination.

Characterization. The morphology of the Fe_3O_4@SiO_2 colloids was characterized using a Tecnai T12 transmission electron microscope (TEM). The UV-Vis spectra were measured by a probe-type Ocean Optics HR2000CG-UV-Vis spectrophotometer in reflection mode with an integration time of 700 ms. A Zeiss AXIO Imager optical microscope connected with a digital camera was used to observe the in-situ assembly of Fe_3O_4@SiO_2 colloids. Magnets were placed underneath the sample stage and could be manually moved vertically to change the magnet-sample distance.

2.3 Results and Discussions

A simple example of the linear Halbach array is a refrigerator magnet which allows augmentation of the magnetic field on one side while cancelling the field on the other side.[34, 35] **Figure 2.1** shows the simulated magnetic field distribution for a linear Halbach array generated from several discrete magnets. Compared with the field of a normal cubic magnet, the main characteristics of a Halbach array are: i) the poles of a Halbach array are on the same sides, which are different from common cubic magnet with south and north poles on opposite sides; ii) enhanced periodical magnetic field is generated on the top (strong) side while the field is mostly cancelled on the bottom (weak) side; iii) the direction of the magnetic field on the top side shows periodical change from vertical to horizontal with complex orientation in between; iv) the field gradient is large in regions with horizontal field near the array.

In this study we use a refrigerator magnet as a Halbach array to study the assembly of a colloidal dispersion of uniform superparamagnetic Fe_3O_4@SiO_2 particles in ethanol encapsulated in a flat glass capillary tube with thickness of 300 μm. Normally, a magnetic field of at least 50 Gauss is needed to initiate the assembly of Fe_3O_4@SiO_2 colloids containing ~130 nm superparamagnetic cores.[19] When the sample was placed at the weak side of the magnet, the field strength was not sufficient to induce effective ordering, thus, no obvious assembly behavior (**Figure 2.2a, 2.2d**). However, the field

on the other side of the magnet was strong enough to guide the magnetic particles to undergo transition from random state to ordered 1D chainlike arrays and 3D colloidal crystals depending on the distance between the sample and the magnet. **Figure 2.2b** illustrates the assembly behavior of Fe_3O_4@SiO_2 colloids at a relatively large sample-magnet distance (~1mm). Similar to the assembly by using a normal cubic magnet, 1D chains formed along the direction of the magnetic field, with the periodicity and diffraction wavelength determined by the balanced interaction between attractive dipole force and repulsive electrostatic force.[20] However, due to the complex nature of the magnetic field directions, the orientation of the photonic chains differed in different regions in accordance with the magnetic field. The diffraction color of the photonic chains can be observed in regions with vertical fields, leading to color patterns consistent with the periodical alternation of external magnetic field produced by the Halbach array (**Figure 2.2e**). Upon moving the sample closer to the magnet (< 0.5 mm), a phase separation of Fe_3O_4@SiO_2 colloids occurs due to the enhanced field gradient and consequently the stronger packing force, producing 3D colloidal crystals in regions with horizontal flux lines where the field gradient is the maximum (**Figure 2.2c, 2.2f**). The strong dipole-dipole repulsive force allows some of the horizontal chains remain stable above the 3D crystals assembled on the substrate surface. This assembly behavior makes the two sides of the glass capillary appear differently in color.

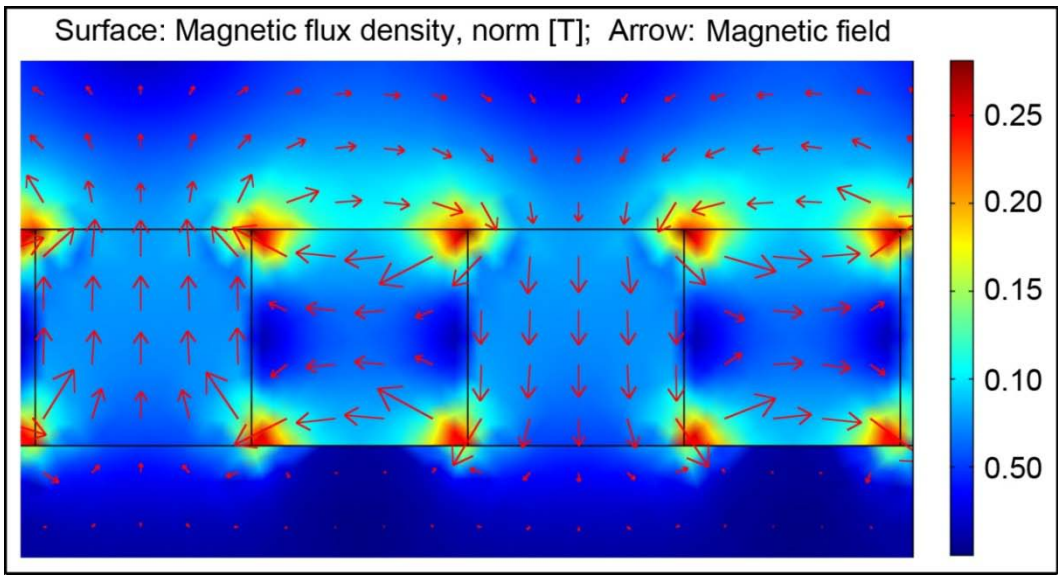

Figure 2.1. Simulated magnetic field of a nonideal linear Halbach array using discrete magnets in COMSOL Multiphysics. The arrow shows the direction of the magnetic field. The length of the arrow and the color shows the strengths of the H and B field, respectively. On top (strong) side, the direction of the magnetic field shows periodical change while the magnetic field was almost cancelled on bottom (weak) side. Reproduced with permission from Ref. 33 © 2012 American Chemical Society.

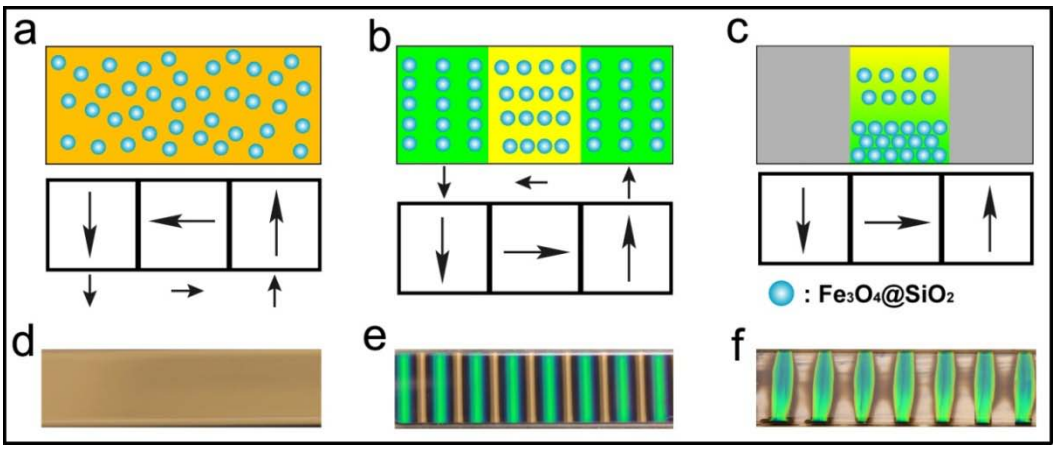

Figure 2.2. Schematic illustration of the general assembly behavior of magnetic colloids in the patterned magnetic field of a linear Halbach array. a) The field on the weak side of the array was insufficient to effectively induce the assembly of particles from random state. b, c)The field on strong side of the array induces the formation of periodical chains in regions with low field gradient (b) and 3D crystals in regions with high field gradient (c). d-f) Digital photos showing the assembly behavior of the magnetic colloids under the corresponding fields in (a-c). Photo (f) was taken immediately after removing the applied magnetic field. Reproduced with permission from Ref. 33 © 2012 American Chemical Society.

Although the field of the Halbach array can be treated as alternating regions with vertical and horizontal magnetic field, the orientation and the gradient of the local magnetic field direction and gradient are more complicated. The complex nature of the Halbach array makes the assembly behavior of $Fe_3O_4@SiO_2$ diverse in different regions. **Figure 2.3** shows the local assembly behavior from the center of regions with vertical magnetic field to that of horizontal field when the sample-magnet distance is ~1 mm. First, the orientation of the chains is vertical in **Figure 2.3a**, titled in **Figure 2.3b** and almost horizontal in **Figure 2.3c**, which is controlled by the direction of the external magnetic field. Second, both the length and thickness of chains increase from **Figure 2.3b** to **Figure 2.3e**, which can be explained by the increased field strength and thereby higher local particle concentration. The local density of chains in regions with vertical magnetic field decreases as time goes on, which also confirms the redistribution of $Fe_3O_4@SiO_2$ driven by the magnetic packing force (**Figure 2.4**). On the other hand, the particle chains gradually migrate to the positions with horizontal fields and accumulate at the side close to the magnet, where the field gradient is also higher. The particle chains eventually stack into 3D ordered structures, with the strong interparticle electrostatic repulsion being the counter packing force (**Figure 2.3f**). The timescale for forming 3D colloidal crystals is ~20 seconds to minutes. The formation of 3D crystals was found faster using larger particles with higher concentrations.

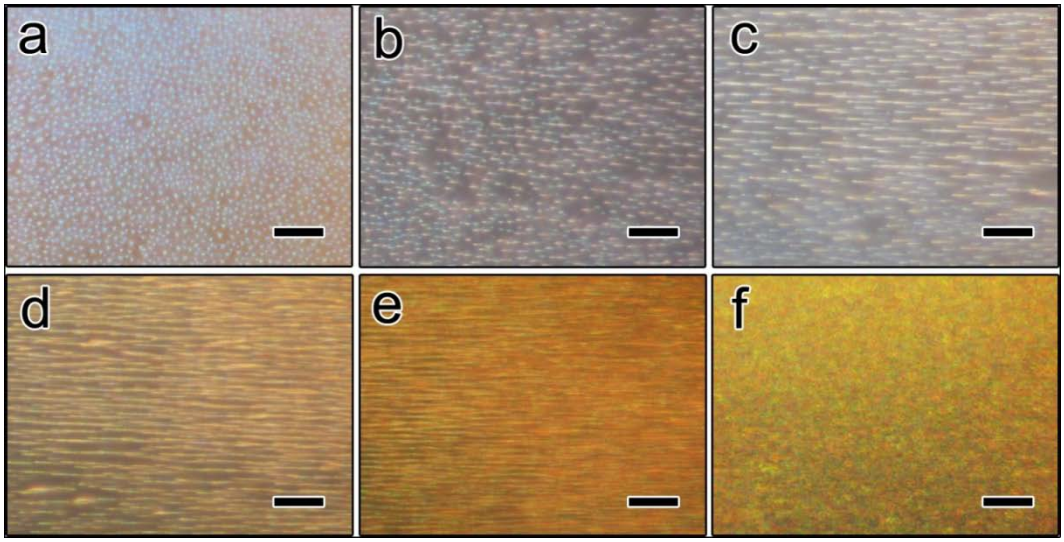

Figure 2.3. Dark-field optical microscope images showing the assembly of Fe_3O_4@SiO_2 particles at different regions. The direction of the magnetic field changes from vertical to horizontal gradually from a to f. The scale bars are 10 μm for all images. Reproduced with permission from Ref. 33 © 2012 American Chemical Society.

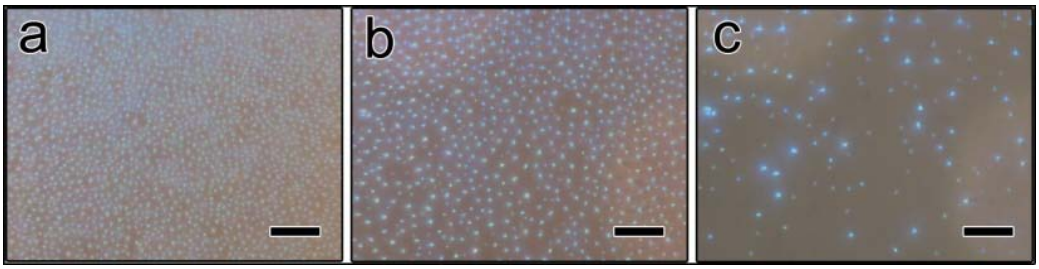

Figure 2.4. Dark-field optical microscopy images showing the local concentration change of Fe_3O_4@SiO_2 chains in the region as showed in figure 3a at different time: a) 0 min, b) 2 min and c) 10 min. Reproduced with permission from Ref. 33 © 2012 American Chemical Society.

To further characterize the local assembly behavior, the local reflectance spectra of Fe_3O_4@SiO_2 ethanol suspension were scanned (**Figure 2.5**). A strong diffraction peak appeared at 538 nm from the center of regions with vertical magnetic fields, which was chosen as the starting point (0 cm). In regions with vertical magnetic field, the diffraction intensity reached the maximum with the Bragg angle of 90^o ($\lambda = 2nd\sin\theta$). The orientation of the photonic chains was gradually tilted and the Bragg angle decreased so the diffraction wavelength gradually blueshifted and the diffraction intensity dropped as moving on to regions with horizontal fields (**Figure 2.5a**). When reaching the edge of the regions with horizontal magnetic fields, the diffraction peak disappeared and the measured reflectance mainly resulted from the scattering of Fe_3O_4@SiO_2 particles. The reflectance spectra kept almost unchanged in regions with horizontal fields. After passing the regions with horizontal fields and moving towards regions with vertical fields, the diffraction peak gradually redshifted with enhanced intensity until reaching the maximum as the Bragg angle went up to 90^o (**Figure 2.5b**). Both the diffraction wavelengths and intensities are almost identical in **Figure 2.5a** and **Figure 2.5b**, implying the periodical assembly behavior of Fe_3O_4@SiO_2 particles in accordance with the periodical change of magnetic fields. The periodical alternation of the assembly behavior and the resulting periodic optical modulation were further demonstrated by plotting the change of the reflectance at 538 nm from different regions (**Figure 2.5c**).

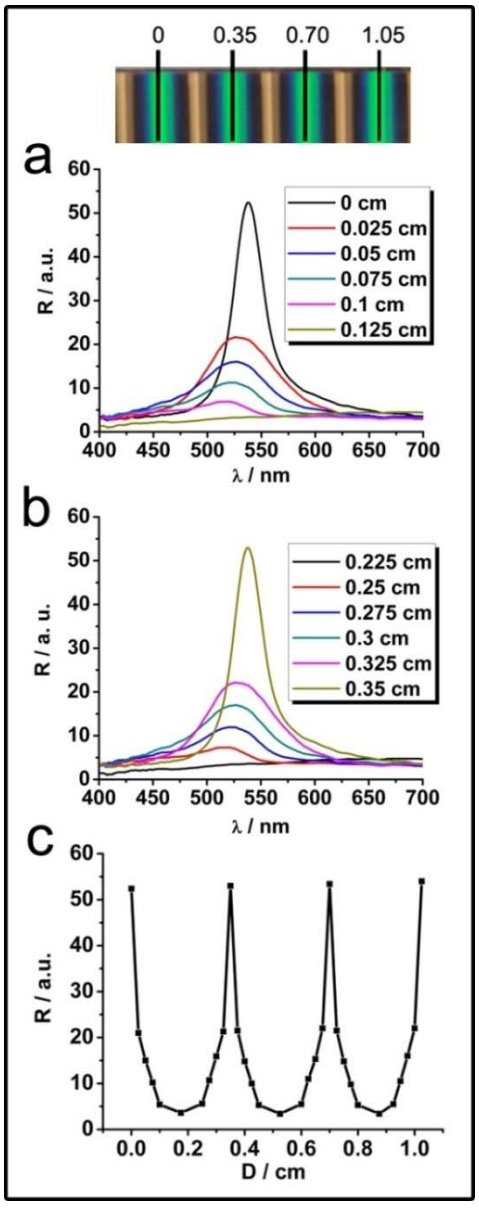

Figure 2.5. a-b) Typical local reflectance spectra of Fe_3O_4@SiO_2 ethanol suspension from different regions in the patterned magnetic field with a periodicity of 0.35 cm. The photo on the top shows the starting and ending points of regions tested. c) Summary of the reflectance at 538 nm mapped at different regions. Reproduced with permission from Ref. 33 © 2012 American Chemical Society.

The assembly of magnetic colloids in an alternating magnetic field of the linear Halbach array leads to the formation of color strips, as shown in **Figure 2.6**. We found that the diffraction color of 1D structures formed in regions with vertical magnetic field can be tuned rapidly and reversibly similar to the case using normal magnetic field.[9, 20] The color tuning is realized through changing the interparticle distance within individual chains in response to the change in the strength of external magnetic field. Dark-field optical microscope images clearly show that the color of the dynamic photonic chains, which appear as colorful dots when viewing from the top, changed from red to green as the sample-magnet distance decreased (**Figure 2.6a-c**). Unlike the case with vertical field, the 1D chains lie horizontally in the regions with horizontal magnetic field, and show the native brown color of Fe_3O_4@SiO_2 (**Figure 2.6d-f**) because no diffraction can be observed. No obvious color change can be observed upon changing the sample-magnet distance. Due to the difference in the orientation of the chains, color stripe patterns can be easily created which can be tuned from red to green (**Figures 2.6g-i**). **Figure 2.7** shows the reflectance spectra from the dynamic photonic chains in regions with vertical magnetic field. As the magnetic field increases, the diffraction peak blue-shifts and the intensity increases, similar to the case using normal cubic magnet, resulting from shorter interparticle distance and higher degrees of order.

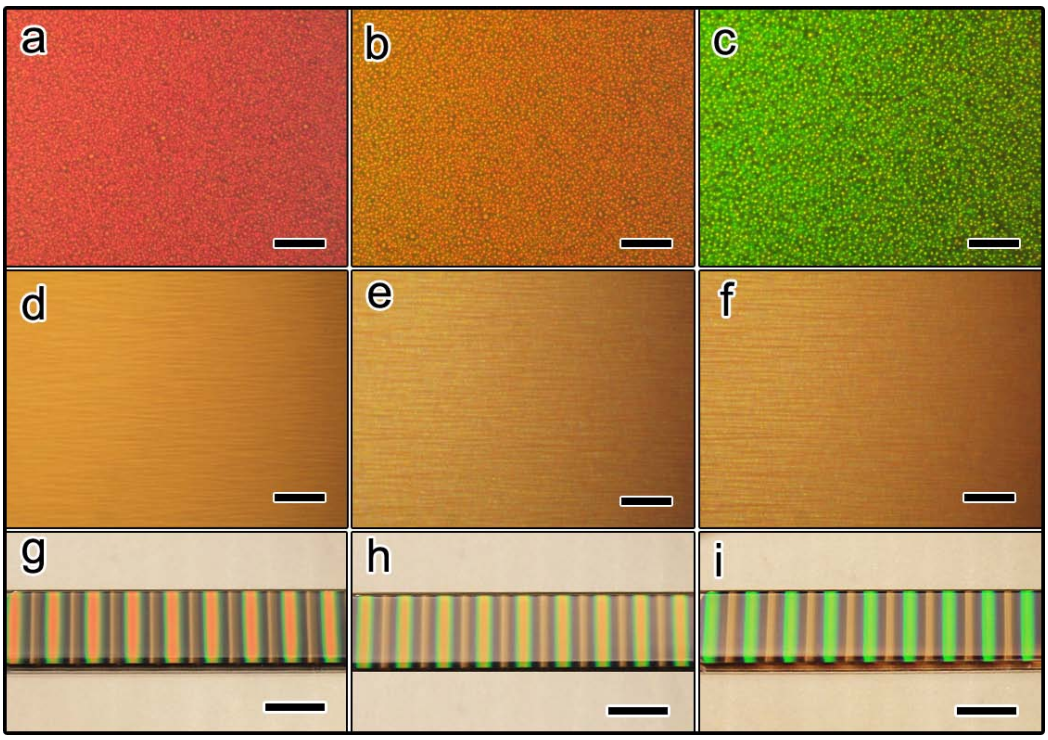

Figure 2.6. a-c) Dark-field optical microscope images showing the color change of dynamic photonic chains of Fe_3O_4@SiO_2 particles along the vertical magnetic field of 130G, 270 G and 390 G respectively. d-f) Optical microscopy images showing the assembly of Fe_3O_4@SiO_2 particles in horizontal magnetic field. g-i) Digital photos showing the pattern with different colors with increasing magnetic field. The scale bar is 10 μm in (a-f) and 5 mm in (g-i). Reproduced with permission from Ref. 33 © 2012 American Chemical Society.

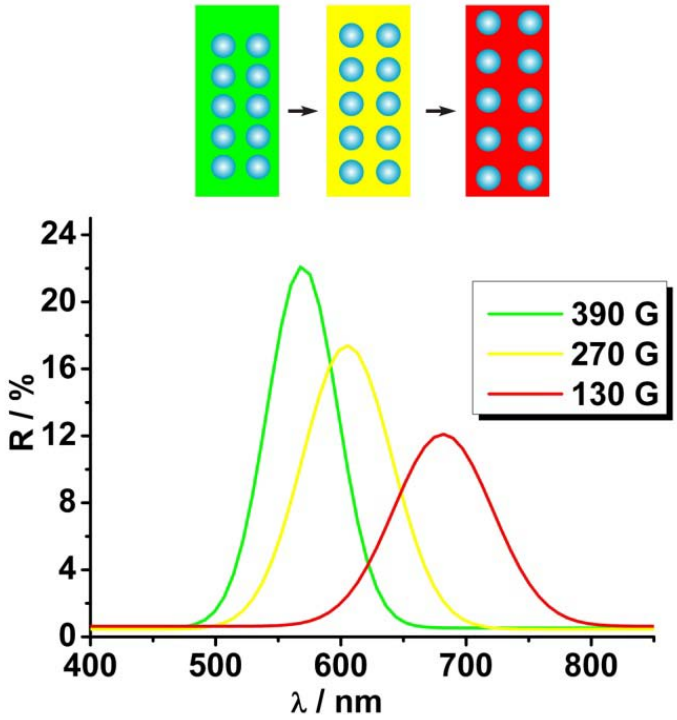

Figure 2.7. Reflectance spectra of photonic chains with orientation parallel to the incident light under different magnetic field strengths. The cartoon on the top shows the compression of the photonic chains in increased magnetic field. Reproduced with permission from Ref. 33 © 2012 American Chemical Society.

Since the 3D colloidal crystals form on the side of the capillary tube next to the magnet, we were unable to directly observe the structure formation through optical microscope. However, the disassembly process started from the edge and took longer time than the assembly which was driven by the strong magnetic forces (**Figure 2.8a**). After the formation of 3D colloidal crystals, we quickly removed the sample from the magnet and recorded the reflectance change. As shown in **Figure 2.8b** for a typical sample, a broad peak appears at 608 nm with an intensity of 43% upon the removal of the magnetic field. Similar to the case of crystallization of nonmagnetic particles in a ferrofluid,[10] the diffraction peak redshifted and the intensity first increased and then gradually dropped. Previously, Asher et al. demonstrated the use of the magnetic field to deform the lattice of colloidal crystal arrays, and found that the magnetic packing force and dipole force can only slightly disturb the pre-assembled crystals due to the weaker magnetic forces relative to the stronger electrostatic repulsive interactions. Owning to much higher content of magnetic materials, the magnetic forces exerted on Fe_3O_4@SiO_2 particles are comparable to the electrostatic interparticle repulsion so the degree of order inside the 3D crystals was greatly affected by the magnetic dipole force during their formation. Upon removal of the magnetic field, the magnetic forces disappeared so that Fe_3O_4@SiO_2 particles can adjust their positions and improve ordering. As a result, diffraction intensity increased. Meanwhile, the interparticle distance increased due to

the removal of the packing force and the consequent expansion of the 3D crystals, which explain the red shift of peak positions. As the 3D packing started to disassemble from the edges of the crystals (**Figure 2.8a**), the peak intensity decreased until it suddenly dropped dramatically when the disassembly was almost completed in the region under the optical probe.

As discussed above, the assembly of Fe_3O_4@SiO_2 is controlled by the magnetic dipole force and packing force. The complex nature of the magnetic field of Halbach array allows us to observe the phase transition driven by the interplay of the dipole and packing forces. In a low magnetic field, the dipole force induces chaining and the packing force drives the movement of particles locally to increase the density of chains and produce brighter colors. As the field strength and gradient increased, the increase of local concentration of magnetic particles causes the aggregation of chains so the ordering along the magnetic field might be disturbed. The packing force eventually induces the concentration gradient in different regions and the formation of the 3D structures while the dipole force controls the orientation of the photonic structures. The response of Fe_3O_4@SiO_2 to the magnetic dipole force, that is the formation of chains or the reorientation of photonic structures, is less than one second while the timescale to reach concentration equilibrium driven by packing force is normally 20 second to several minutes which involved much more movement of particles. Besides the magnetic

forces, the electrostatic force between Fe_3O_4@SiO_2 particles is also important to the formation of different photonic structures. It is worth noting that intentional addition of NaCl aqueous solution into the ethanol suspension of Fe_3O_4@SiO_2 screened the electrostatic force, resulting in disordered structures and loss of diffraction color under the same Halbach array.

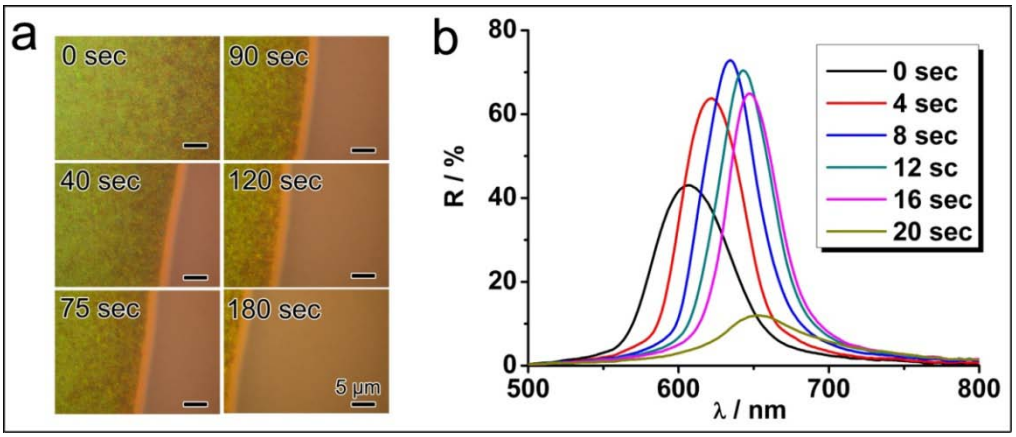

Figure 2.8. a) Optical microscope images showing the disassembly process of the 3D structures of Fe_3O_4@SiO_2 formed in the magnetic field of a patterned refrigerator magnet. b) Time-dependent reflectance spectra from a region in the 3D structures. Reproduced with permission from Ref. 33 © 2012 American Chemical Society.

2.4 Conclusion

In conclusion, we study the assembly of superparamagnetic Fe_3O_4@SiO_2 in patterned magnetic fields provided by a nonideal linear Halbach array. Thanks to the high magnetic content of the Fe_3O_4 particles, we were able to observe the phase transition of Fe_3O_4@SiO_2 in ethanol, which is driven by the magnetic dipole force and packing force. The difference in the direction of the magnetic field allows the creation of color patterns with tunable structures and diffractions driven by the dipole force. As the field strength and gradient increase, the increase in the local concentration of magnetic particles causes the aggregation of chains so the ordering along the magnetic field might be disturbed. The packing force eventually induces the concentration gradient in different regions and the formation of the 3D structures while the dipole force controls the orientation of the photonic structures. Apparently, the dipole force acts faster than the packing force due to less movement of particles involved. We hope that the current work can also improve the understanding of the assembly behavior of magnetic particles in nonuniform magnetic field, and sheds light on their applications in real color display or signage devices.

2.5 References

(1) Sacanna, S.; Philipse, A. P. *Langmuir* **2006**, *22*, 10209.

(2) Jeong, U.; Teng, X. W.; Wang, Y.; Yang, H.; Xia, Y. N. *Adv. Mater.* **2007**, *19*, 33.

(3) Nakata, K.; Hu, Y.; Uzun, O.; Bakr, O.; Stellacci, F. *Adv. Mater.* **2008**, *20*, 4294.

(4) Bishop, K. J. M.; Wilmer, C. E.; Soh, S.; Grzybowski, B. A. *Small* **2009**, *5*, 1600.

(5) Ding, T.; Song, K.; Clays, K.; Tung, C. H. *Adv. Mater.* **2009**, *21*, 1936.

(6) Erb, R. M.; Son, H. S.; Samanta, B.; Rotello, V. M.; Yellen, B. B. *Nature* **2009**, *457*, 999.

(7) Li, F.; Josephson, D. P.; Stein, A. *Angew. Chem. Int. Ed.*, *50*, 360.

(8) Xu, X. L.; Majetich, S. A.; Asher, S. A. *J. Am. Chem. Soc.* **2002**, *124*, 13864.

(9) Ge, J.; Hu, Y.; Yin, Y. *Angew. Chem. Int. Ed.* **2007**, *119*, 7572.

(10) He, L.; Hu, Y.; Kim, H.; Ge, J.; Kwon, S.; Yin, Y. *Nano Lett.* **2010**, *10*, 4708.

(11) Gates, B.; Xia, Y. *Adv. Mater.* **2001**, *13*, 1605.

(12) Xia, Y. N.; Gates, B.; Yin, Y. D.; Lu, Y. *Adv. Mater.* **2000**, *12*, 693.

(13) Ge, J.; Yin, Y. *Angew. Chem. Int. Ed.* **2011**, *50*, 1492.

(14) Xu, X. L.; Friedman, G.; Humfeld, K. D.; Majetich, S. A.; Asher, S. A. *Adv. Mater.* **2001**, *13*, 1681.

(15) Xu, X. L.; Friedman, G.; Humfeld, K. D.; Majetich, S. A.; Asher, S. A. *Chem. Mater.* **2002**, *14*, 1249.

(16) Bibette, J *J. Magn. Magn. Mater.* **1993**, *122*, 37.

(17) Leal Calderon, F.; Stora, T.; Mondain Monval, O.; Poulin, P.; Bibette, J. *Phys. Rev. Lett.* **1994**, *72*, 2959.

(18) Ge, J.; Hu, Y.; Biasini, M.; Beyermann, W. P.; Yin, Y. *Angew. Chem. Int. Ed.* **2007**, *119*, 4420.

(19) Ge, J.; Hu, Y.; Zhang, T.; Huynh, T.; Yin, Y. *Langmuir* **2008**, *24*, 3671.

(20) Ge, J.; Yin, Y. *Adv. Mater.* **2008**, *20*, 3485.

(21) Ge, J.; Yin, Y. *J. Mater. Chem.* **2008**, *18*, 5041.

(22) Ge, J.; He, L.; Goebl, J.; Yin, Y. *J. Am. Chem. Soc.* **2009**, *131*, 3484.

(23) Ge, J.; Goebl, J.; He, L.; Lu, Z.; Yin, Y. *Adv. Mater.* **2009**, *21*, 4259.

(24) Xuan, R.; Wu, Q.; Yin, Y.; Ge, J. *J. Mater. Chem.* **2011**, *21*, 3672.

(25) Kim, H.; Ge, J.; Kim, J.; Choi, S.-e.; Lee, H.; Lee, H.; Park, W.; Yin, Y.; Kwon, S. *Nature Photonics* **2009**, *3*, 534.

(26) Ge, J.; Lee, H.; He, L.; Kim, J.; Lu, Z.; Kim, H.; Goebl, J.; Kwon, S.; Yin, Y. *J. Am. Chem. Soc.* **2009**, *131*, 15687.

(27) Hu, Y.; He, L.; Yin, Y. *Angew. Chem. Int. Ed.* **2011**, *50*, 3747.

(28) Kraftmakher, Y. *European Journal of Physics* **2007**, *28*, 409.

(29) Ge, J.; He, L.; Hu, Y.; Yin, Y. *Nanoscale* **2010**, *3*, 177.

(30) Kim, J.; Song, Y.; He, L.; Kim, H.; Lee, H.; Park, W.; Yin, Y.; Kwon, S. *Small* **2011**,

7, 1163.

(31) Zhu, C.; Chen, L. S.; Xu, H.; Gu, Z. Z. *Macromol. Rapid Commun.* **2009**, *30*, 1945.

(32) Erb, R. M.; Sebba, D. S.; Lazarides, A. A.; Yellen, B. B. *J. Appl. Phys.* **2008**, *103*, 063916.

(33) He, L.; Hu, Y.; Han, X.; Lu, Y.; Lu, Z.; Yin, Y. *Langmuir* **2011**, *27*, 13444.

(34) Mallinson, J *Magnetics, IEEE Transactions on* **1973**, *9*, 678.

(35) Han, Q.; Ham, C.; Phillips, R. *IEE Proceedings - Electric Power Applications* **2005**, *152*, 535.

Chapter 3

Self-Assembly and Magnetically Induced Phase Transition of Three-Dimensional Colloidal Photonic Structures

3.1 Introduction

Colloidal dipolar spheres are interesting model systems in condensed matter physics. They can self-assemble into various crystals structures which allow exploration of the phase complexity in a single sample as their interparticle interactions can be conveniently tuned within an experimentally accessible timescale.[1-6] For example, electric dipolar interaction induced by an AC electric field was found to be able to initiate the structure evolution from hard-sphere fluids to strings, then sheets and finally 3D crystallites in electro-rheological fluids.[7, 8] A colloidal model system with an interaction tunable from hard sphere to soft and dipolar was pioneered by Yethiraj and Blaaderen, where the competition between the soft electrostatic force and anisotropic dipolar force between micrometer colloidal particles allows the creation of new crystal structures.[4] Later, the phase diagram of dipolar hard and soft spheres were simulated by calculating the Helmholtz free energy. The simulated phase diagram of dipolar hard spheres shows fluid, *fcc*, hexagonal-close-packed (*hcp*), and body-centered-tetragonal (*bct*) phases while

in cases of dipolar soft spheres phase diagram exhibits an additional body-centered-orthorhombic (*bco*) phase.[5] More surprisingly, phase diagrams of both dipolar soft and hard spheres predict a large portion of *hcp* phase, which is unstable in normal bulk suspensions. Unfortunately, advancement in phase transitions of dipolar spheres is still limited by the slow progress in the experimental observation of rich variety of the computed phases. For example, the predicted transition between *fcc* and *hcp* in dipolar spheres has not yet been identified experimentally.[5] While Various types of structures have been observed, including chains, columns, and labyrinth patterns, the direct structural confirmation has not been possible.

Recently, the interest in colloidal assembly has also been driven by the development of functional colloidal nanostructures, mainly photonic crystals.[9] Suspensions of monodisperse colloidal particles have shown great potential as building blocks for studying phase transitions and fabricating field-responsive colloidal photonic structures, where the static or dynamic structural changes in these systems are always accompanied by switching of photonic properties.[10-13] Asher group reported that the application of the external magnetic fields induces shifting of Bragg diffraction of preassembled *fcc* colloidal crystals made from a concentrated suspension of highly charged superparamagnetic polystyrene nanospheres. This occurs due to the compression of crystalline colloidal arrays along the magnetic field gradient.[14, 15] We previously

reported different phase transitions of submicrometer nonmagnetic colloidal particles in a ferrofluid which is exposed to external magnetic fields.[16] However, there have been rare experimental studies on crystal phase transition of magnetically dipolar soft spheres in suspension mainly due to the difficulty to build strong, comparable and widely tunable dipolar forces and electrostatic repulsion between colloidal particles.

Suspensions of highly charged superparamagnetic (SPM) colloidal spheres are presumably the most suitable dipolar soft building blocks for studying reversible phase transitions as their dipolar interactions can be fully initiated and controlled by the external magnetic fields.[17] We have previously exploited diluted suspensions (volume fraction $\varphi \sim 0.001$) of superparamagnetic magnetite particles to study simplest transition from soft-sphere fluid to magnetically dipolar chains, where dynamic tuning of interparticle distance inside the dipolar chains allows the shifting of diffraction color across the whole visible spectrum.[18-20] The key to the successful assembly and structural color tuning is the coexistence of highly tunable magnetically dipolar force and comparative long-range electrostatic force, both of which depend on the interparticle distance.[21] As mentioned above, the coexistence of these widely tunable forces makes our superparamagnetic particles good candidates for studying field-induced phase transitions. In the present work, we first exploit concentrated suspensions of highly charged superparamagnetic silica coated magnetite (Fe_3O_4@SiO_2) particles to study their

crystallization driven by electrostatic force and magnetically induced phase transition.[22] We further underwent a more detailed in-situ study of the phase transition of the Fe_3O_4@SiO_2 suspensions using Microradian X-ray Scattering technique.[23] Particle self-assembly ranging from 1D chainlike structures to 2D sheets, and finally to 3D semi-crystalline structures is observed as a function of the sedimentation-induced variation of the local particle concentration and the applied magnetic field. Our studies clearly demonstrate that the suspensions of superparamagnetic colloids are not only suitable model systems for study the fundamental aspects of colloidal assembly but also can be used to fabricate various types of colloidal photonic nanostructures.

3.2 Materials and Methods

Synthesis of Fe_3O_4@SiO_2. The superparamagnetic Fe_3O_4 colloidal nanocrystal clusters (CNCs) were prepared using the same procedure we previously reported.[25] The surface of the CNCs was modified with a layer of silica through a sol-gel coating process.[19] The Fe_3O_4@SiO_2 solutions were sealed in capillary tubes with different thickness using optical glue for optical observation and measurement to avoid contamination.

Characterization. The morphology of the Fe_3O_4@SiO_2 colloids was characterized using a Tecnai T12 transmission electron microscope (TEM). The TEM samples were prepared by transferring one drop of sample dispersion onto a carbon-coated copper grid and then drying in air. A Philips FEI XL30 scanning electron microscope (SEM) was used to investigate the morphology of the labyrinth structure. The UV-Vis spectra were measured by a probe-type Ocean Optics HR2000CG-UV-Vis spectrophotometer in reflection mode. The integration time was 700 ms. A Zeiss AXIO Imager optical microscope connected with a camera was used to observe the in-situ assembly of Fe_3O_4@SiO_2 colloids. A permanent magnet was placed underneath the sample stage and could be manually moved vertically to change the magnet-sample distance. Small Angle X-ray scattering experiments (SAXS) were performed at beamline X27c at the National Synchrotron Light Source (NSLS) of Brookhaven National Laboratory.

Cylindrical capillaries (0.5 mm in diameter) were filled with a concentrated suspension of core shell nanoparticles. The longer dimension (z-axis) of the capillary was always perpendicular to the direction of the X-ray beam as well as the direction of the magnetic field. A disk shaped permanent magnetic of known magnetic field strength was used to create a magnetic field on the capillary. The strength of magnetic field was varied by adjusting the position of the permanent magnetic on an aluminum bar. The magnetic was calibrated for fields at different spatial positions. The direction of magnetic field was perpendicular to the direction of the X-ray beam.

3.3 Results and Discussion

Fe_3O_4@SiO_2 particles were prepared using the same method we previously reported.[19, 25] In the present studies, the typical diameter of the superparamagnetic magnetite core is 100 to 120 nm and the thickness of silica shell is 20 to 30 nm. **Figure 3.1a** shows the TEM image of one typical Fe_3O_4@SiO_2 sample with the size polydispersity of approximately 11.5%. The particles are nearly spherical with concentric core-shell structures. The outer silica shell layer not only improves the uniformity in shape and size, but also allows the dispersity of particles in different polar solvents, such as water, alcohols, acetonitrile, dimethyl formide, and dimethyl sulfoxide. More importantly, the silica layer provides the negative surface charges necessary for soft interparticle repulsions in different solvents. At low concentration, the Fe_3O_4@SiO_2 suspension behaves as a Brownian fluid with no translational order and shows the native brown color of iron oxide. However, when the volume fraction is above a critical value φ_c, crystallization occurs driven by the electrostatic interaction and the suspension displays brilliant structural colors in the absence of external field, due to the high refractive index contrast between Fe_3O_4 (2.42) and the solvents, e. g. 1.33 for water (**Figure 3.1b**). Previously, Joo et al observed the similar phenomenon and attributed the structural color to the formation of quasi-amorphous colloidal structures.[26] However, in this study we show that the structural color rather results from the Bragg diffraction of

crystalline colloidal arrays similar to the case of monodisperse silica or polymer particles.[27] It is worth noting that the crystallization happens even the polydispersity of the particles is relatively large as the crystallization in hard sphere fluids was found to be suppressed thermodynamically when the polydispersity (e. g. nonuniformity in size) exceeds 7%.[28, 29] It is believed that the requirement of monodispersity for crystallization in soft systems might be lower due to the non-close-packed structures with relatively large interparticle separation. As the crystallization is driven by the minimization of the interparticle electrostatic force, the solvents play an important role by affecting the surface charge and the screening length. The ζ-potentials of our Fe_3O_4@SiO_2 particle were found to be -40 mV in ethanol, -50 mV in water and -64 mV in acetonitrile. As the ionic strength in aprotic polar solvents, such as acetonitrile, is typically lower than in protic polar solvents the particles experience stronger electrostatic repulsions in acetonitrile than in water and, consequently, crystallization happens with lower critical volume fraction. As a matter of fact, the acetonitrile suspension diffracts infrared light at lower volume fraction while no diffraction can be observed for the same sample in water with the same concentration.

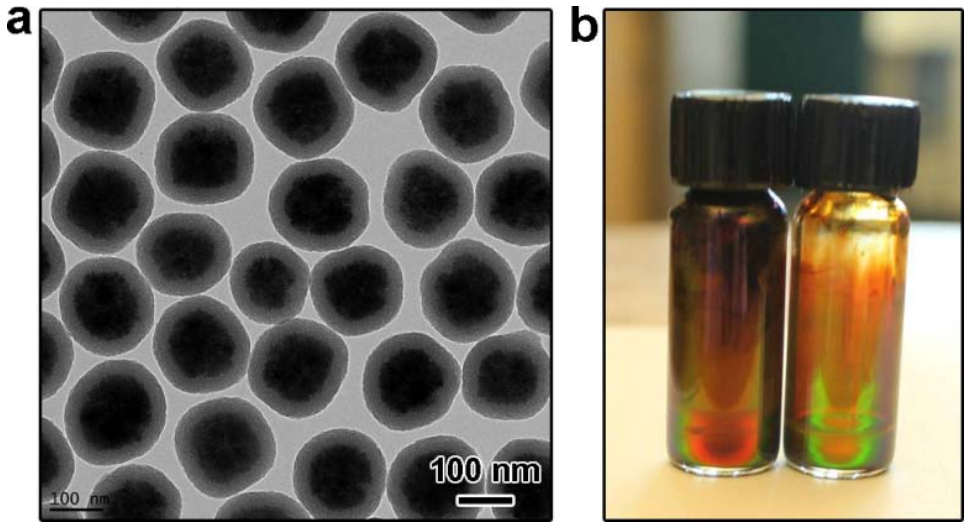

Figure 3.1. (a) TEM image of a typical sample of 180-nm (120-nm core @ 30-nm shell) Fe_3O_4@SiO_2 particles. (b) Digital photo showing two typical concentrated samples of Fe_3O_4@SiO_2 dispersed in acetonitrile (left) and water (right). Reproduced with permission from Ref. 22 @ 2012 Royal Society of Chemistry.

Optical microscope was first used to study the in-situ structural evolution of concentrated Fe_3O_4@SiO_2 suspensions in the magnetic field. A thin liquid film (~ 30 μm) was formed by sandwiching a drop of Fe_3O_4@SiO_2 aqueous dispersion (volume fraction φ ~ 0.1) between two cover glasses. As shown in **Figure 3.2a**, polycrystalline photonic crystals with reddish structural colors and domain size of around 10 μm were observed from the aqueous dispersion of a typical 180-nm (120-nm core @ 30-nm shell) Fe_3O_4@SiO_2 sample (volume fraction φ ~ 0.15) in the absence of the external magnetic field. Although the resolution in optical microscope is not high enough to identify the exact structure of each domain, the domain boundaries can be clearly observed. When a weak vertical magnetic field with strength ~ 120 Gauss was applied, the diffraction colors of the domains exhibit a blue-shift while the domain boundaries remain intact (**Figure 3.2b**). Careful inspection of the domain boundaries shows the formation of green "dots", which are believed to be vertically aligned photonic particle chains. When the magnetic field was further enhanced to 200 G, as shown in **Figure 3.2c**, the domain structures started to break and the boundaries became unobvious while the diffraction color continued to blue-shift. Further enhancing the magnetic field to 500 G resulted in a single-crystal-like structure with uniform diffraction color and the domain boundaries fully disappeared (**Figure 3.2d**). Upon removing the magnetic field, the diffraction color redshifts instantly.

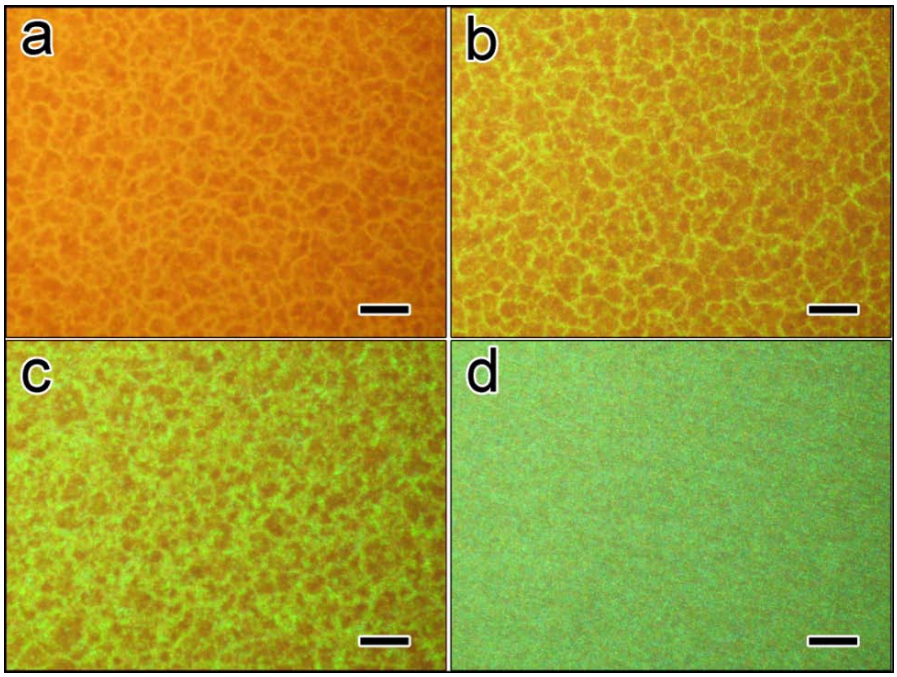

Figure 3.2. Dark-field optical microscope images of a thin liquid film of Fe_3O_4@SiO_2 aqueous dispersion with thickness of 30 μm showing the phase transition in the magnetic fields. The field strengths are (a) 0 G, (b) 120 G, (c) 200 G, and (d) 500 G. The scale bars are 20 μm. Reproduced with permission from Ref. 22 @ 2012 Royal Society of Chemistry.

Small angle X-ray scattering technique was used to further study the structural evolution. An acetonitrile suspension of 160-nm (100-nm Fe_3O_4 core @ 30-nm silica shell) magnetic particles with $\varphi \sim 0.12$ (in 0.5 mm glass capillary) is exposed to an external magnetic field produced by a permanent magnet. The direction of magnetic field was always perpendicular to the incident X-ray beam. The scattering pattern in the absence of the magnetic field exhibits Debye–Scherrer diffraction rings, indicating some polycrystalline structure formation by self-assembly of the core/shell nanoparticles (**Figure 3.3a**). Careful inspection of the scattering pattern indicates the formation of non-close-packed *fcc* structures similar to the crystalline colloidal arrays reported before.[30, 31] Due to the detection limitation in our measurement, the diffraction rings corresponding to (111) and (200) with expected q values of 0.026 and 0.030 nm^{-1} were shielded by the beam stopper and we were able to only observe the higher diffraction rings corresponding to other lattice planes of the *fcc* structure.[32, 33] The diffraction pattern shows three major rings with q ratio of $\sqrt{8}:\sqrt{24}:\sqrt{32}$, corresponding to (220), (422) and (440) lattice planes respectively (see arrows in **Figure 3.3a**) which matches with polycrystalline *fcc* structure with large translation order along the <111> direction, which can be explained by the preferred (111) symmetry of an *fcc* structure near the smooth wall of the cylindrical capillary tubes.[34] In other words, the incident angle is mainly along the <111> direction.

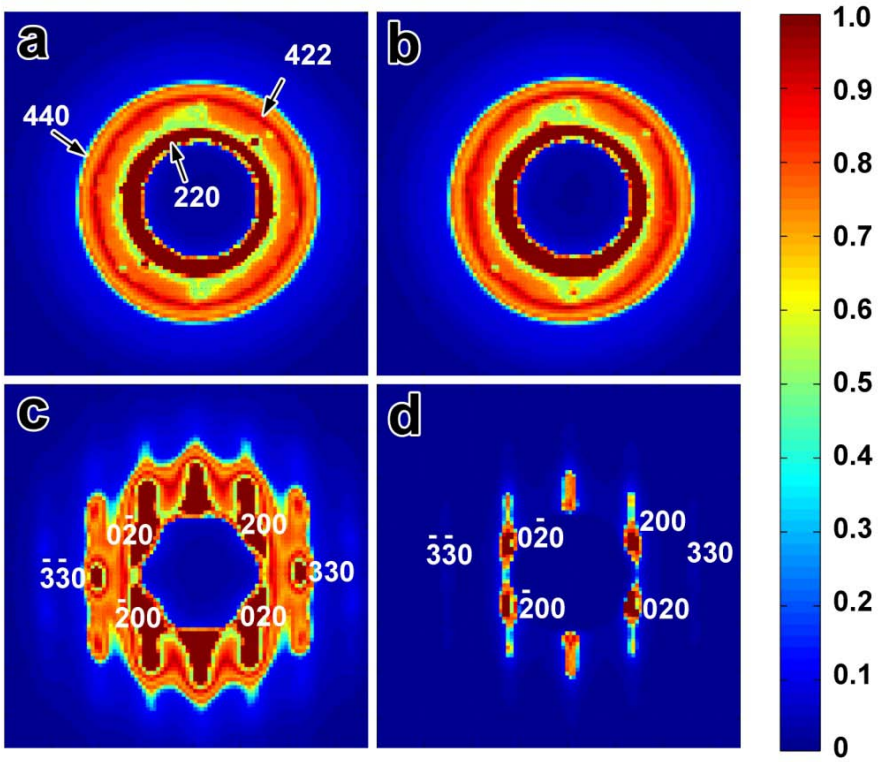

Figure 3.3. Small angle X-ray diffraction patterns of a 160-nm (100-nm Fe_3O_4 core @ 30-nm silica shell) Fe_3O_4@SiO_2 in acetonitrile sample (volume fraction $\varphi \sim 0.12$) in response to the external magnetic field. The magnetic field strengths are 0 G for (a), 100 G for (b), 900 G for (c) and 1600 G for (d). The colour bar on the right shows the relative diffraction intensity. Reproduced with permission from Ref. 22 @ 2012 Royal Society of Chemistry.

We hardly observe any change in the scattering pattern, when a small magnetic field of ~ 100 G is applied (**Figure 3.3b**), which indicates that colloidal ordering is not effectively disturbed by small magnetic field strength. However, further increasing the magnetic field to ~ 900 G, the Debye-Scherrer rings develop into three sets of six diffraction spots with notably elongation along the direction perpendicular to the applied magnetic field (**Figure 3.3c**). Consistent with the observation under optical microscope, the application of a strong magnetic field would induce the reconstruction of polycrystalline structure into well-oriented single-crystalline-like structure. The three sets of diffraction spots with q ratio of $\sqrt{3}:\sqrt{4}:\sqrt{7}$ can be indexed corresponding to (110), (200) and (210) planes respectively, which are the predicted allowed planes of single-crystalline *hexagonal-packed* structures with incident beam along <001> direction. The plane indexing the hexagonal structure was performed by drawing a comparison between the simulated hexagonal pattern (in reciprocal space) as reported previously and the observed X-ray scattering patterns.[35] Similarly, the diffraction patterns corresponding to (100) planes were not observed due to the detection limit. As the direction of magnetic field is perpendicular to the incident beam, the scattering pattern depicts the crystal has *hexagonal-packed* structures (ABAB arrangement). The diffraction spots in the scattering pattern get separated at higher magnetic field strength of 1600 G (**Figure 3.3d**), indicating the formation of the structure with improved

crystallinity. The scattering pattern again indicates a hexagonal symmetry of colloidal crystals. Here, colloidal crystal has ABAB arrangement of magnetic nanoparticles and translational disorder along the direction of the beam between the two hexagonal sheets makes it quasi 3D hexagonal structures.

The key factors that determine the thermodynamic equilibrium state of dipolar colloidal suspensions are the local particle concentration and the interparticle interaction potentials from both repulsive and attractive forces. Magnetic fields can affect both factors through magnetic forces, which not only induce the self-assembly of one-dimensional (1D), two-dimensional (2D) and three-dimensional (3D) structures, but also cause phase transitions between the different structures. For example, the magnetic field gradient can drive the redistribution of colloidal particles to change local particle concentrations through the magnetic packing force. On the other hand, the strength of the external magnetic field can determine the induced moment in superparamagnetic particles, which controls the interparticle dipole-dipole potentials. To better understand the phase behaviors of the superparamagnetic particle suspensions in the magnetic fields, we further performed in-situ Microradian X-ray Scattering studies.[23] More complicated transitions from colloidal fluids to 1D dipolar chain structures, 2D hexagonal sheets, and finally 3D structures was also confirmed. Our findings are in a good agreement with theoretical results on the assembly of these particles.[5] This study allows us to determine a colloidal

phase diagram where one can manipulate the crystalline phase and the lattice parameters of the colloidal crystal by externally tuning stimuli such as magnetic field and concentration gradient.

As seen from the optical observations, the photonic properties altered along with the phase transition. We studied the reflectance spectra of the aqueous dispersion in response to a changing magnetic field (**Figure 3.4**). In the absence of the magnetic field, a wide diffraction peak at ~ 620 nm appeared due to the Bragg diffraction from the polycrystalline structures. When a magnetic field of 160 G was applied, the diffraction peak slightly blue-shifted to 600 nm and another peak at ~540 nm appeared. The diffraction peak in shorter wavelength might result from the chaining of particles in the domain boundaries as shown in **Figure 3.2b**. When the magnetic field was enhanced to 222 G, only one peak remained, indicating the reconstruction of the crystal structures, which is consistent with the observation in optical microscope. When further enhancing the magnetic field to 1460 G, the peak position shifted to shorter wavelength while the diffraction intensity first increases and then decreases. While the shifting of the wavelengths is due to the compression of the crystal structures, the diffraction intensity drop indicates the disturbance of the ordering or the formation of new crystals structures. Previously, the same particles have been used to construct one-dimensional (1D) dynamic photonic chainlike structures. However, the Bragg diffraction intensity from 1D

photonic structures can rarely reach 60%.[18, 19, 36] In the 1D photonic chain case, each chain functions as the single diffraction unit so the structural color results from the collective diffraction of individual chains, as shown schematically in **Figure 3.5a**. As the separation between the chains is typically above 1 μm, the low density of diffraction unit limits the enhancement of overall diffraction intensity.[37] Dissimilarly, 3D photonic crystals usually possess stronger diffractions owning to much higher diffraction unit density (**Figure 3.5b**).[38] Although the diffraction spectra from polycrystalline crystals in the absence of the magnetic field show a broad peak, the scattering results imply that the application of strong external magnetic fields greatly improves both the structural and orientational ordering. Consequently, the diffraction intensity from the quasi 3D single-crystalline-like photonic crystals can easily reach 80%.

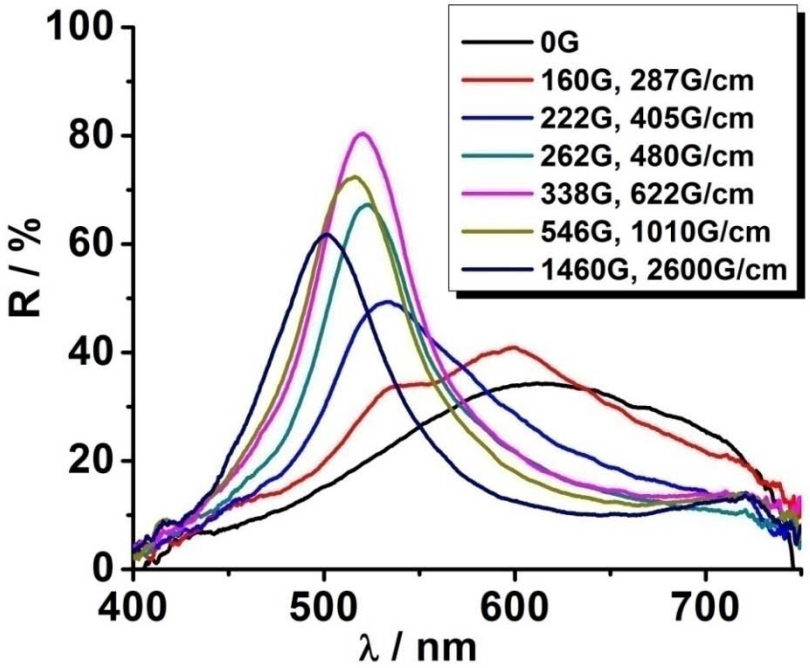

Figure 3.4. Reflectance spectra a 180-nm (120-nm core @ 30-nm shell) Fe_3O_4@SiO_2 aqueous sample (volume fraction $\varphi \sim 0.15$) in response to the external magnetic fields. Reproduced with permission from Ref. 22 @ 2012 Royal Society of Chemistry.

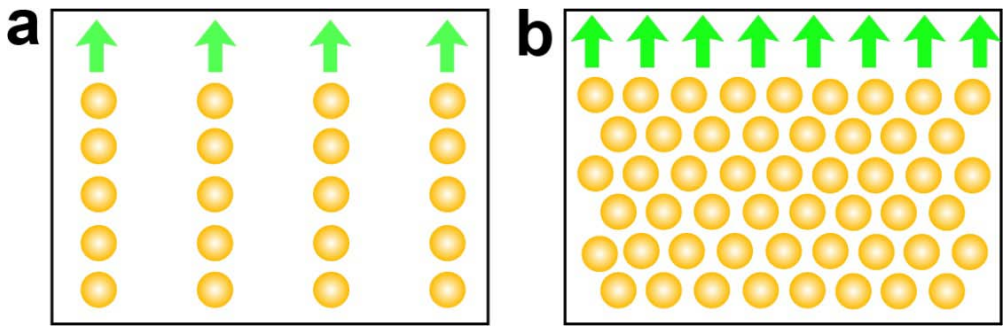

Figure 3.5. Schematic illustration of the difference in the Bragg diffraction mechanism for Fe_3O_4@SiO_2 suspensions at low and high concentrations in the magnetic field. (a) At low concentration, the structural colour results from the collective Bragg diffraction of individual chain assemblies. (b) The single-crystalline-like 3D structures diffract light as a whole unit. Reproduced with permission from Ref. 22 @ 2012 Royal Society of Chemistry.

3.4 Conclusion

In conclusion, we experimentally observed the predicted reversible transition from polycrystalline *fcc* to single-crystalline-like hexagonal packing structure controlled by the strengths of the external magnetic field in suspensions of superparamagnetic soft spheres. Our study shows that the diffraction in the absence of the magnetic field results from the crystallization of the magnetic particles driven by the interparticle electrostatic repulsions, which is a conclusion different from that in an earlier report which claimed the formation of quasi-amorphous structure.[26] It is found that the crystallization was not suppressed for colloidal soft spheres with a polydispersity of over 7% due to the non-close-packed structures. Since the size of spheres is comparable to the wavelength range of visible light, the periodicity in the colloidal crystals results in strong Bragg diffraction so the suspensions display iridescent structural colors. Different from the 1D magnetically responsive photonic structures we previously reported, the 3D photonic crystals can reach higher diffraction intensity in the magnetic field due to much higher density of diffraction units. Our observation indicates the unstable bulk hexagonal packing state can be created by the application of the external magnetic fields, which might lead to important extensions of using colloids as condensed matter model systems and creation of advanced materials with unconventional structures.

3.5 References

(1) Pusey, P. N.; van Megen, W. *Nature* **1986**, *320*, 340.

(2) Van Blaaderen, A.; Wiltzius, P. *Science* **1995**, *270*, 1177.

(3) Thomas, P. *J. Phys.: Condens. Matter* **1999**, *11*, R323.

(4) Yethiraj, A.; van Blaaderen, A. *Nature* **2003**, *421*, 513.

(5) Hynninen, A.-P.; Dijkstra, M. *Phys. Rev. Lett.* **2005**, *94*, 138303.

(6) Brandt, P. C. *J. Chem. Phys.* **2009**, *130*, 204513.

(7) Martin, J. E.; Odinek, J.; Halsey, T. C. *Phys. Rev. Lett.* **1992**, *69*, 1524.

(8) Tao, R.; Jiang, Q. *Phys. Rev. Lett.* **1994**, *73*, 205.

(9) Xia, Y. N.; Gates, B.; Yin, Y. D.; Lu, Y. *Adv. Mater.* **2000**, *12*, 693.

(10) Holtz, J. H.; Asher, S. A. *Nature* **1997**, *389*, 829.

(11) Pan, G. S.; Kesavamoorthy, R.; Asher, S. A. *Journal of the American Chemical Society* **1998**, *120*, 6525.

(12) Foulger, S. H.; Jiang, P.; Lattam, A.; Smith, D. W.; Ballato, J.; Dausch, D. E.; Grego, S.; Stoner, B. R. *Advanced Materials* **2003**, *15*, 685.

(13) Ge, J.; Yin, Y. *Angew. Chem. Int. Ed.* **2011**, *50*, 1492.

(14) Xu, X. L.; Friedman, G.; Humfeld, K. D.; Majetich, S. A.; Asher, S. A. *Adv. Mater.* **2001**, *13*, 1681.

(15) Xu, X. L.; Friedman, G.; Humfeld, K. D.; Majetich, S. A.; Asher, S. A. *Chem.*

Mater. **2002**, *14*, 1249.

(16) He, L.; Hu, Y.; Kim, H.; Ge, J.; Kwon, S.; Yin, Y. *Nano Lett.* **2010**, *10*, 4708.

(17) Sacanna, S.; Philipse, A. P. *Langmuir* **2006**, *22*, 10209.

(18) Ge, J.; Hu, Y.; Yin, Y. *Angew. Chem. Int. Ed.* **2007**, *119*, 7572.

(19) Ge, J.; Yin, Y. *Adv. Mater.* **2008**, *20*, 3485.

(20) Ge, J. P.; He, L.; Goebl, J.; Yin, Y. D. *J. Am. Chem. Soc.* **2009**, *131*, 3484.

(21) Ge, J.; Hu, Y.; Zhang, T.; Huynh, T.; Yin, Y. *Langmuir* **2008**, *24*, 3671.

(22) He, L.; Malik, V.; Wang, M.; Hu, Y.; Anson, F.; Yin, Y. *Nanoscale* **2012**, *4*, 4438.

(23) Malik, V.; Petukhov, A. V.; He, L.; Yin, Y.; Schmidt, M. *Langmuir* **2012**, *28*, 14777.

(24) Zhang, Q.; Janner, M.; He, L.; Wang, M.; Hu, Y.; Lu, Y.; Yin, Y. *Nano Lett.* **2013**, *13*, 1770.

(25) Ge, J.; Hu, Y.; Biasini, M.; Beyermann, W. P.; Yin, Y. *Angew. Chem. Int. Ed.* **2007**, *119*, 4420.

(26) Lee, I.; Kim, D.; Kal, J.; Baek, H.; Kwak, D.; Go, D.; Kim, E.; Kang, C.; Chung, J.; Jang, Y.et al *Adv. Mater.* **2010**, *22*, 4973.

(27) Rundquist, P. A.; Photinos, P.; Jagannathan, S.; Asher, S. A. *J. Chem. Phys.* **1989**, *91*, 4932.

(28) Auer, S.; Frenkel, D. *Nature* **2001**, *413*, 711.

(29) Pusey, P. N.; Zaccarelli, E.; Valeriani, C.; Sanz, E.; Poon, W. C. K.; Cates, M. E. *Philosophical Transactions of the Royal Society A: Mathematical, Physical and Engineering Sciences* **2009**, *367*, 4993.

(30) Carlson, R. J.; Asher, S. A. *Appl. Spectrosc.* **1984**, *38*, 297.

(31) Kesavamoorthy, R.; Tandon, S.; Xu, S.; Jagannathan, S.; Asher, S. A. *J. Colloid Interface Sci.* **1992**, *153*, 188.

(32) Hamley, I. W.; Castelletto, V.; Fundin, J.; Yang, Z.; Price, C.; Booth, C. *Langmuir* **2002**, *18*, 1051.

(33) Park, M. J.; Bang, J.; Harada, T.; Char, K.; Lodge, T. P. *Macromolecules* **2004**, *37*, 9064.

(34) Asher, S A.; Holtz, J.; Liu, L.; Wu, Z. *J. Am. Chem. Soc.* **1994**, *116*, 4997.

(35) Klokkenburg, M.; Erne, B. H.; Wiedenmann, A.; Petukhov, A. V.; Philipse, A. P. *Phys. Rev. E* **2007**, *75*, 051408.

(36) Ge, J. P.; Yin, Y. D. *J. Mater. Chem.* **2008**, *18*, 5041.

(37) Ge, J; Lee, H.; He, L.; Kim, J.; Lu, Z.; Kim, H.; Goebl, J.; Kwon, S.; Yin, Y. *J. Am. Chem. Soc.* **2009**, *131*, 15687.

(38) He, L.; Hu, Y.; Han, X.; Lu, Y.; Lu, Z.; Yin, Y. *Langmuir* **2011**, *27*, 13444.

Chapter 4

Determination of Solvation Layer Thickness by a Magneto-photonic Approach

4.1 Introduction

The forces between colloidal particles play important roles in determining the stability of colloidal suspensions. Derjaguin-Landau-Verwey-Overbeek (DLVO) theory, which considers the sum of the London-van der Waals attraction and the electrostatic repulsion between two particles, has been widely used to explain and predict the stability of colloids in liquid medium.[1-3] The electrostatic repulsive interaction between colloids is believed to provide an energy barrier against particle aggregation**.** However, the DLVO theory fails in explaining the superior stability of silica colloids in aqueous suspensions under conditions of high ionic strength where the electrostatic forces are effectively screened.[4, 5] Recent studies have shown that another repulsive force, the solvation force, may become dominant when the distance between silica surfaces drops in the range of several nanometers.[6-13] While the physical origin of this strong short-range force is still under debate,[10, 14, 15] it has been mostly attributed to the formation of a thin

rigid layer of solvent molecules in the vicinity of silica surfaces through hydrogen bonding.[9, 13, 16, 17] According to this theory, a thicker solvation layer and stronger interparticle solvation force should develop for silica colloids in solvents with stronger hydrogen-bonding abilities. Yoon and Vivek studied the effects of adding short-chain alcohols into aqueous silica suspensions on the solvation force between silica surfaces.[18] They attributed the decrease in solvation force to the dehydration of the silica surface with the addition of short-chain alcohols and claimed that the solvation force may even disappear in a 15% methanol aqueous solution. However, the argument that the replacement of water with methanol results in the complete disappearance of a solvation force contradicts the hydrogen-bonding theory as methanol may also participate in the hydrogen bonding network and contribute to the solvation repulsions. Indeed, the solvation force between silica surfaces was found to exist in many nonaqueous solvents with strong hydrogen-bonding ability.[19] Further systematic studies are apparently needed to clarify the apparent contradictions existing in literature.

While the fundamental understanding of the colloidal interactions has been advanced with the realization of many force measurement tools, most experiments were carried out using invovled techniques and instrumentation, such as atomic force microscopy (AFM) or a surface force apparatus (SFA).[9, 20] It would be a great advantage to study the solvation force between colloidal particles using simple techniques with easily accessible

setups. Bibette et al. developed a magnetic chaining technique to directly probe repulsive forces between colloidal particles in aqueous suspensions.[21-24] Upon the application of an external magnetic field, monodispersed emulsion droplets containing superparamagnetic iron oxide nanocrystals self-assemble into chain structures with periodic arrangement as driven by the force balance between magnetic dipole-dipole attraction and different interparticle repulsions. As the distance between neighboring particles can be derived from the wavelength of the optical diffraction of the periodic assemblies through Braggs' law, different long-range and short-range repulsive forces have been studied.[22, 23, 25] Compared to conventional techniques, this method allows simple control over the interparticle distance and thus the force-distance law can be conveniently derived. However, the apparent drawbacks of the approach include the lack of long-term stability of the structures from emulsion droplets, and the complicated and time-consuming steps needed for the fabrication of uniform emulsion droplets due to the involvement of multiple size-selection processes. More importantly, the surface property of the droplet is determined by the surfactants used, which complicates the application of the technique for the study of many other short range interactions such as the solvation force.

Recently, we have extended this magneto-photonic effect to the development of responsive photonic structures with widely, rapidly and reversibly magnetically tunable

structural colors in the visible and near-infrared spectrum by using nanostructured superparamagnetic magnetite (Fe_3O_4) colloidal nanocrystal clusters.[26] Engineering the surface of the magnetic colloids with a layer of silica ($Fe_3O_4@SiO_2$) through a simple sol-gel process improves their compatibility with many other nonaqueous solvents such as alkanol solutions[27] and UV curable resins.[28-30] In this work, we take advantage of the optical response of the core-shell magnetic colloids under magnetic fields to study the thickness of solvation layers formed when the colloidal silica surface is covered by different solvents.[31] The key to the successful measurement of the thickness of the solvation layer is the effective screening of the electrostatic force so that the neighboring particles interact with each other through the repulsion resulting from the overlap of solvation layers, which balances the magnetically induced attraction and forms ordered assemblies. The thickness of solvation layer can be then estimated by using Bragg's law. A relationship between the hydrogen-bonding ability of the solvents and the thickness of solvation layer on $Fe_3O_4@SiO_2$ colloidal surface has been identified, which is consistent with the prior understanding of a hydrogen-bonding origin of the solvation force. Compared to conventional complex techniques, our magneto-photonic strategy represents an easily accessible method with a simple and inexpensive setup that produces consistent results.

4.2 Materials and Methods

Materials. Ethanol, anhydrous ferric chloride ($FeCl_3$), ammonium hydroxide solution, tetraethyl orthosilicate (TEOS), glycerol, ethylene glycol, isopropanol, methanol and sodium hydroxide (NaOH) were purchased from Fisher Scientific. Polyacrylic acid (PAA, MW = 1800) and Diethylene glycol (DEG) were obtained from Sigma-Aldrich. Distilled water was used in all experiments. All chemicals were directly used as received without further treatment.

Synthesis of Fe_3O_4@SiO_2. In a typical synthesis, a mixture of 4 mmol PAA, 0.4 mmol $FeCl_3$, and 17 mL DEG was heated at 220 ^oC under nitrogen protection for 1 hour. After injection of 1.75 mL of NaOH/DEG solution (2.5 mol/L), the solution was further heated for 1 hour at 220 ^oC, and then cooled down to room temperature. Upon cleaning with a mixture of water and ethanol several times, Fe_3O_4 CNCs were dispersed in 3 mL of water, mixed sequentially with 1 mL of ammonium hydroxide solution 20 mL ethanol, and 200 μL TEOS under mechanical stirring. After reacting for 40 min, the Fe_3O_4@SiO_2 particles were cleaned with ethanol for a few times and finally dispersed in 3 mL of different solvents. The Fe_3O_4@SiO_2 particles were washed three times before being transferred to a different solvent.

Characterization. The morphology of the Fe_3O_4@SiO_2 colloids was characterized using a Tecnai T12 transmission electron microscope (TEM). The measurement of

refractive indices of the solvents at 589 nm was performed using an Abbe refractometer. The UV-Vis spectra were measured by a probe-type Ocean Optics HR2000CG-UV-Vis spectrophotometer in reflection mode with an integration time of 700 ms. A Zeiss AXIO Imager optical microscope connected to a digital camera was used to observe the in-situ assembly of Fe_3O_4@SiO_2 colloids. Magnets were placed underneath the sample stage and could be manually moved vertically to change the magnet-sample distance.

4.3 Results and Discussion

Monodisperse superparamagnetic Fe_3O_4 colloidal nanocrystal clusters were prepared through a one-pot high-temperature precipitation reaction,[32] then coated with a layer of silica with controlled thickness through a sol-gel process.[27] The Fe_3O_4@SiO_2 core-shell particles can be dispersed in water and many nonaqueous polar solvents such as alcohols. The silica coating process improves the monodispersity of the particles and yields more spherical particles, facilitating more accurate measurements (**Figure 4.1**).

Figure 4.2 illustrates the basic principle in determining the thickness of the solvation layer. The Fe_3O_4@SiO_2 particles self-assemble into dynamic photonic chains in the external magnetic field. When the electrostatic force is effectively screened, the solvation force between Fe_3O_4@SiO_2 surfaces dominates at the separation of a few nanometers, where the thin rigid solvation layer contacts, to balance the magnetically induced interparticle attraction. The diffraction of the photonic chains follows the Bragg's Law $\lambda = 2n(d+2s)\sin\theta$, where λ is the diffraction wavelength, n the refractive index of the suspension, d the overall diameter of Fe_3O_4@SiO_2 particles, s the thickness of solvation layer and the Bragg angle, $\theta = 90^o$.[33, 34] The diffraction wavelength (λ) can be measured using a spectrometer, and the diameter of Fe_3O_4@SiO_2 particles can be identified by TEM while the refractive index of the suspensions can be measured. Finally, the thickness of the solvation layer (s) can be calculated using Bragg's law.

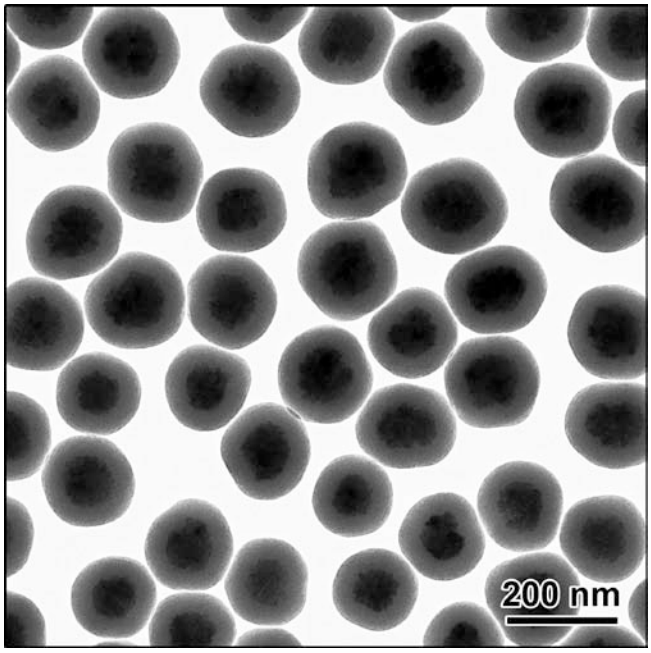

Figure 4.1. Typical TEM image of a Fe_3O_4@SiO_2 sample with an average diameter of 175 nm (115-nm core @ 30-nm shell). Reproduced with permission from Ref. 31 @ 2012 Royal Society of Chemistry.

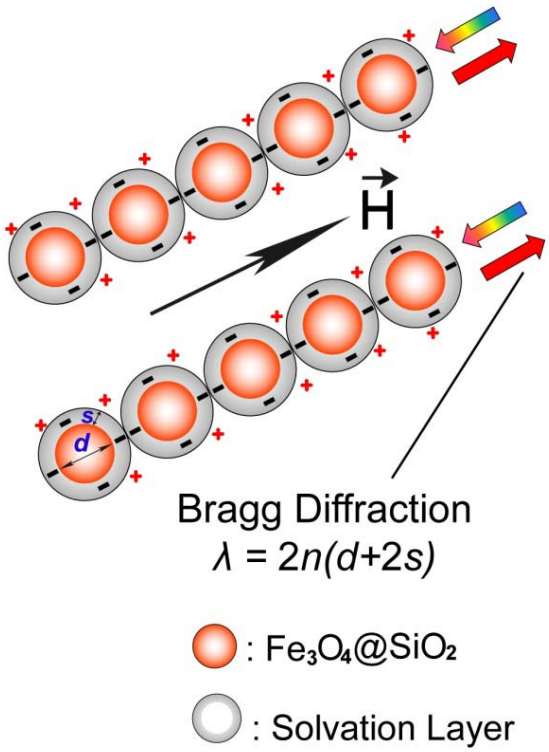

Figure 4.2. Schematic illustration of the magnetic assembly strategy to determine the thickness of the solvation layer (*s*) on the surface of Fe_3O_4@SiO_2 colloidal particles. In an external magnetic field, the Fe_3O_4@SiO_2 particles self-assemble into photonic chains along the magnetic field and Bragg diffract visible light. When the electrostatic force is effectively screened, the solvation layers contact and produce a repulsive force to balance the magnetic attraction between the colloids. The thickness of solvation layer (*s*) can be calculated using the Bragg Equation with the effective refractive index (*n*), the diameter of colloids (*d*), and the measured wavelength (λ) of diffraction of the chains. Reproduced with permission from Ref. 31 @ 2012 Royal Society of Chemistry.

In our earlier efforts to estimate solvation layer thickness,[27] we were not able to completely eliminate the electrostatic repulsion and our values were not consistent with those obtained using force measurement techniques, although they seem to fit estimations based on rheological arguments.[35, 36] It is well known that the interaction range of electrostatic forces can be characterized by the Debye length $\kappa^{-1}=(\epsilon k_B T/2000 N_A e^2 I)^{1/2}$, where ϵ is the dielectric constant, K_B the Boltzmann's constant, T the absolute temperature, N_A the Avogadro's number, e the elementary charge, and I the ionic strength.[37] When the ionic strength of the water solution reaches 0.05 M, the electrostatic force between silica surfaces could be effectively screened and the solvation force starts to dominate the interparticle repulsion.[5] On the other hand, as reported by Grabbe and Horn, a repulsive force, dominant at short ranges between silica surfaces in aqueous solutions, is independent of NaCl concentrations up to 0.1 M.[9] Utilizing the difference in sensitivity to ionic strength of the solution between the electrostatic force and the solvation force, it is possible to selectively screen the electrostatic force between silica surfaces while keeping the solvation force unaffected.

The Fe_3O_4@SiO_2 particle dispersion in a 50% water-ethanol (volume fraction) solution was chosen as a model system to test the effect of electrolyte concentration on the interparticle repulsive forces. **Figure 4.3** shows the reflectance spectra of a sample with a diameter of 208 nm (142 nm core diameter/33 nm shell thickness) in response to

different external magnetic fields. When the ionic strength is low, the long range electrostatic force dominates the repulsion between Fe_3O_4@SiO_2 particles so that the diffraction peak can be widely tuned by enhancing the strength of the magnetic field from 83 Gauss to 164 Gauss while the interparticle spacing decreases from ~90 nm to ~60 nm (**Figure 4.3a**). When the concentration of NaCl increases to 0.01 M, the diffraction blue-shifts relative to the above case in the same magnetic fields. The interparticle spacing only changed slightly from ~28 nm to ~24 nm (**Figure 4.3b**). The decrease of the long-range repulsion due to higher electrolyte concentration can be accounted for by the classical DLVO theory as the electrical double layers were compressed by the absorbed counterions. By further increasing the concentration of NaCl to 0.025 M, the diffraction peak moved to even shorter wavelengths (**Figure 4.3c**). Meanwhile, both the diffraction peak position and the interparticle separation remained constant even as the magnetic field changed from 83 Gauss to 164 Gauss. The interparticle spacing estimated using Bragg's equation was 6.6 nm, close to the range in which the solvation force became effective. The loss of tunability in diffraction wavelength also indicates the dominant repulsion came from the hard contact of the rigid solvation layer while the effectively screened double-layer repulsion became negligible. The diffraction peak finally disappeared due to the aggregation of chains when the magnetic field was further enhanced and the magnetic packing force became effective.

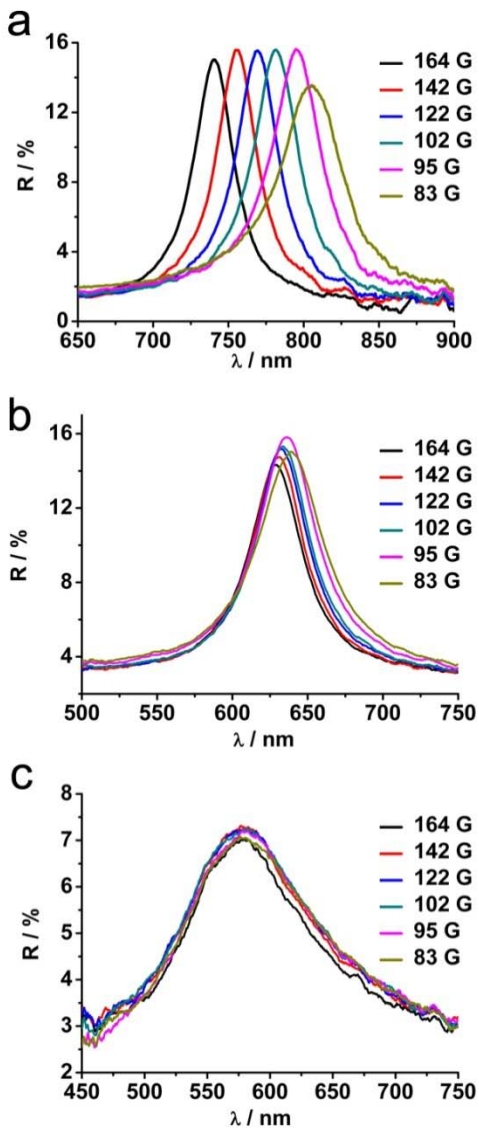

Figure 4.3. Reflection spectra from a 50% water-ethanol suspension of 208-nm (142-nm core @ 33-nm shell) Fe_3O_4@SiO_2 particles with the NaCl concentration of (a) 10^{-5} mol/L, (b) 0.01 mol/L, and (c) 0.025 mol/L in response to an external magnetic field with varying strengths. Reproduced with permission from Ref. 31 @ 2012 Royal Society of Chemistry.

To confirm the formation of chainlike structures from Fe_3O_4@SiO_2 particles under the condition of screened electrostatic forces, their assembly behavior in response to the magnetic field was studied using an optical microscope operated in dark-field mode. Fe_3O_4@SiO_2 particles were well-dispersed in the 50% water-ethanol mixture with 0.025 M NaCl and cannot be clearly imaged due to the Brownian motion (**Figure 4a**). When a magnetic field of c.a. 100 Gauss was applied, Fe_3O_4@SiO_2 particles self-assembled into chains along the magnetic field (**Figures 4b** and **4c**). The dynamic chains disappeared upon removal of the magnetic field with no obvious aggregation observed. When the field strength was increased to over 150 Gauss, the chains started to aggregate, consistent with the results from reflectance measurements. We also measured the solvation layer thickness on other Fe_3O_4@SiO_2 samples with diameters of 175 nm (115-nm core @ 30-nm shell), 186 nm (124-nm @ 32-nm shell), and 225 nm (149-nm core @ 38-nm shell) in 50% water-ethanol mixtures with 0.025 M NaCl. The reflectance spectra of all samples showed a similar profile with no change of diffraction wavelength in response to the variation of magnetic fields within a certain strength range. More importantly, the estimated thicknesses of the solvation layers were found to be essentially the same for all the samples (**Figure 4.5**), confirming the reliability of our method, as the thickness should be insensitive to the size of particles according to the hydrogen-bonding-origin theory.

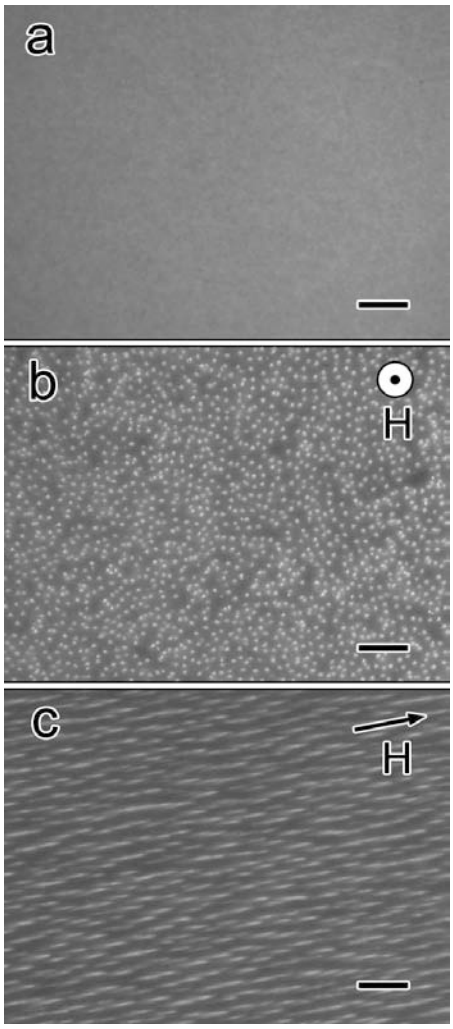

Figure 4.4. Optical microscope images showing the assembly of 208-nm (142-nm core @ 33-nm shell) Fe_3O_4@SiO_2 particles in 50% water-ethanol with NaCl concentration of 0.025 mol/L in a liquid film sandwiched between two glass slides under (a) no magnetic field, (b) magnetic field ~100 G parallel to the viewing angle, and (c) magnetic field ~100 G perpendicular to the viewing angle. Reproduced with permission from Ref. 31 @ 2012 Royal Society of Chemistry.

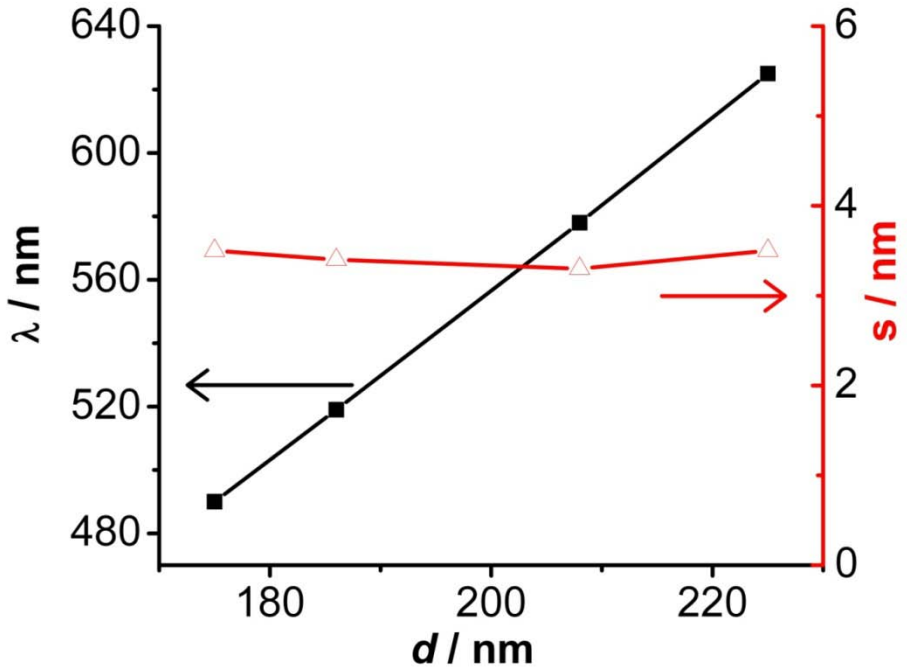

Figure 4.5. The diffraction wavelengths and the corresponding solvation layer thicknesses measured for different-sized Fe_3O_4@SiO_2 particles magnetically assembled in 50% water-ethanol mixtures containing 0.025 mol/L NaCl. Reproduced with permission from Ref. 31 @ 2012 Royal Society of Chemistry.

The above results demonstrate that our strategy of selectively screening the electrostatic force allows the estimation of solvation layer thickness on the surface of Fe_3O_4@SiO_2 particles. Since the screening of the electrostatic force in aqueous solutions has been previously studied, we demonstrate the application of the magneto-photonic method for the purpose of studying the effects of solvents on the solvation layer thickness. First, we studied how the solvation layer thickness changes upon the addition of ethanol. As shown in **Figure 4.6a**, the solvation layer on the surface of Fe_3O_4@SiO_2 particles was found to be thickest in pure water (~ 4.4 nm) and the addition of ethanol gradually contracted the solvation layer to a minimum of ~ 2 nm. Previously, Yoon and Vivek attributed the decrease in solvation layer to the dehydration of the silica surface with the addition of short-chain alcohols.[18] However, we believe the replacement of water with ethanol, which has relatively weaker hydrogen-bonding ability, might interfere with the hydrogen-bonding network so the overall rigid solvation layer would become thinner. Accordingly, increased replacement happens as the volume fraction of ethanol increases, further decreasing the solvation layer. Another phenomenon observed showed that the lowest concentration of NaCl required to effectively screen the electrostatic force follows a linear relationship with the volume fraction of water, but interestingly the effective concentration of NaCl in water was found to be the constant (**Figure 6b**).

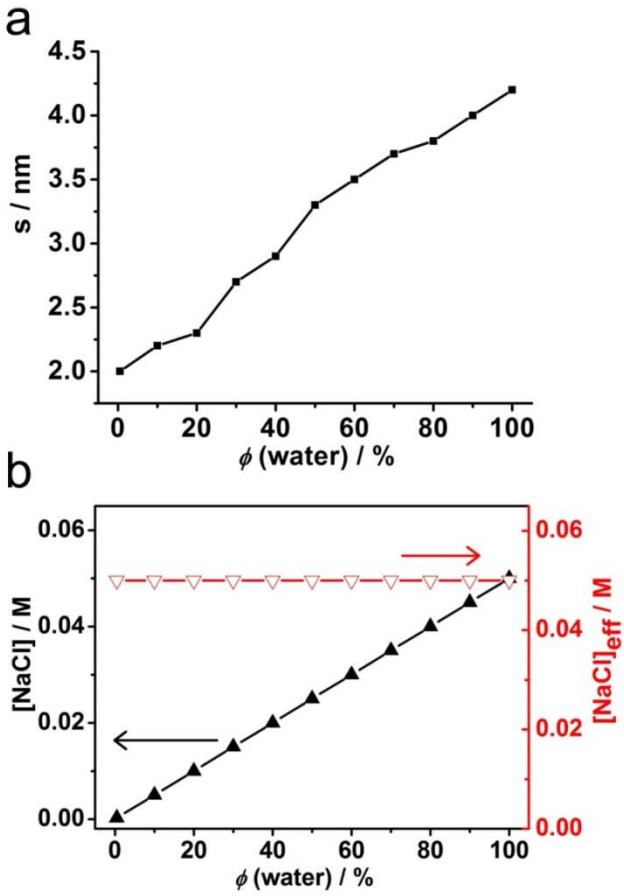

Figure 4.6. (a) The dependence of solvation layer thickness (*s*) on the volume fraction of water, determined by the magneto-photonic method using Fe_3O_4@SiO_2 particles. (b) The dependence on concentration of NaCl required to effectively screen the interparticle electrostatic force on the volume fraction of water in water-ethanol mixtures. The concentration of NaCl on the left side is defined as moles of NaCl per volume of water-ethanol mixture while the value on the right side is defined as moles of NaCl per volume of water. Reproduced with permission from Ref. 31 @ 2012 Royal Society of Chemistry.

Consistent with the hydrogen-bonding-origin theory, the addition of ethanol to Fe_3O_4@SiO_2 aqueous suspensions reduces the thickness of the solvation layer by replacing the water and interfering with the hydrogen-bonding network. With the expectation that the variation in hydrogen bonding abilities should result in changes in thickness of the solvation layer, we studied the thickness change in different aqueous ethylene glycol (EG) solutions and found, interestingly, that they exhibit a different profile from the case of ethanol/water mixtures, first shrinking and then expanding with increasing EG concentration (**Figure 4.7**). The initial drop below the 70% volume fraction can be explained by the disruption of the solvation layer by replacing water with EG, which has much weaker hydrogen-bonding ability similar to the case of ethanol. However, unlike the case of ethanol/water mixture, the thickness of solvation layer increases when EG concentration increases to above 70%. This concentration dependence is consistent with the solid-liquid phase equilibrium of the EG/water mixture which has been plotted in the same graph by using data from literature.[38-40] A minimum freezing point at ~70% EG concentration indicates the most severe disruption of the hydrogen-bonding network, which now also leads to the thinnest solvation layer in the same volume fraction. When the volume fraction of EG is beyond 70%, the formation of the solvation layer might be progressively dominated by increased hydrogen bonding between EG molecules resulting in a slight increase of the solvation layer thickness.

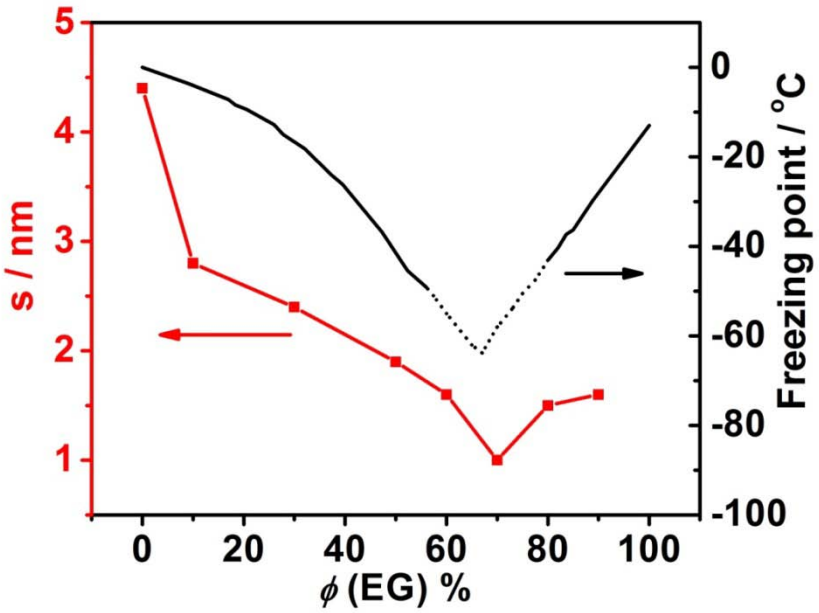

Figure 4.7. Red: Plots of solvation layer thickness of Fe_3O_4@SiO_2 particles in water/ EG mixtures. Black: The dependence of the freezing point of water/EG mixtures on the volume fraction EG, plotted using literature data. The dotted curve represents the metastable freezing temperatures. Reproduced with permission from Ref. 31 @ 2012 Royal Society of Chemistry.

Finally, we compared the dispersions of Fe_3O_4@SiO_2 particles in aqueous solutions of other nonaqueous solvents by keeping the volume fractions constant at 50%. **Table 1** summarizes the results from different mixtures. For simple alcohols with only one hydroxyl group (R-OH), the thickness of solvation layer decreases with the increase of the chain length of the R group. The thickness in a methanol-water mixture is ~4.1 nm, which is close to the value in pure water (~4.4 nm). When the methyl group (CH_3-) is replaced by an ethyl group (C_2H_5-) or isopropyl group ((CH_3)$_2$CH-), the solvation layer shrinks to 3.5 nm and 2.6 nm, respectively. Apparently, this trend is consistent with the decrease of hydrogen-bonding ability of alcohols as their carbon chain lengths increase.[19] Compared to simple alcohols with relatively strong hydrogen bonding abilities, the decrease in the thickness of solvation layer is more obvious when using weak hydrogen bonding solvents such as EG, diethylene glycol (DEG) or glycerol, which have been widely used as anti-freezing agents since tehy can severely disrupt hydrogen bonding of water and thus greatly depress the freezing point of the system. For example, the freezing point of 50% EG-water mixture is -39°C, which is lower than that of pure water (0°C) and pure EG (-13°C). As expected, a more severe disruption to the hydrogen bonding network by the addition of EG to the solution to reach a 70% volume fraction further reduces the freezing point to below -51 °C, which is consistent with the observation of the thinnest solvation layer at the same volume fraction.

Table 4.1. Summary of solvation layer thickness in water and various aqueous mixtures.

Reproduced with permission from Ref. 31 @ 2012 Royal Society of Chemistry.

Solvent	Molecular structure	Refractive Index	S / nm
Pure water	H_2O	1.3333	4.4
50% Methanol	CH_3OH	1.3425	4.1
50% Ethanol	C_2H_5OH	1.3578	3.5
50% 2-propanol	$(CH_3)_2CH\text{-}OH$	1.3658	2.6
50% EG	$HO\text{-}CH_2CH_2\text{-}OH$	1.3858	1.9
50% DEG	$(HO\text{-}CH_2CH_2)_2O$	1.3937	1.8
50% Glycerol	$(HO\text{-}CH_2)_2CH\text{-}OH$	1.4084	1.8

4.4 Conclusion

In conclusion, we report a simple and easily accessible magneto-photonic method to study the thickness of solvation layer on colloidal silica surfaces. By exposing uniform Fe_3O_4@SiO_2 colloidal particles dispersed in various solvents to a magnetic field, they are attracted to closely contact with one another and self-align into 1D periodically arranged photonic chains that diffract visible light consistent with Bragg's Law. By successfully screening the electrostatic force, the neighboring magnetic particles are separated by the rigid solvation layer immobilized on the silica surfaces, producing repulsive forces that balance the magnetically induced dipole interparticle attraction. The solvation layer thicknesses, as estimated by calculating the interparticle separation through the Bragg equation, were found to be consistent with literature values obtained by other force measurement methods.[9, 13] The hydrogen bonding ability of the solvents was found to be an important factor that determines the thickness of the solvation layer. When water was gradually replaced by alcohols with relatively weaker hydrogen bonding abilities, the hydrogen bonding network was interrupted, resulting in thinner solvation layers. We believe this magneto-photonic method represents a simple yet very effective tool for studying many types of short-range colloidal interactions including not only the solvation forces between various surfaces but also the steric effects which are fundamentally critical to chemistry, biochemistry and pharmacology.

4.5 References

(1) Derjaguin, B *Trans. Faraday Soc.* **1940**, *35*, 203.

(2) Derjaguin, B. V.; Landau, L. *USSR Acta Physicochim* **1941**, *14*, 633.

(3) Verwey, E. J.; Overbeek, J. T. G. *Theory of the stability of Lyophobic Colloids*; Elsiever: New York, 1947.

(4) Depasse, J; Watillon, A. *J. Colloid Interface Sci.* **1970**, *33*, 430.

(5) Yotsumoto, H.; Yoon, R.-H. *J. Colloid Interface Sci.* **1993**, *157*, 426.

(6) Derjaguin, B. V.; Churaev, N. V. *J. Colloid Interface Sci.* **1974**, *49*, 249.

(7) Churaev, N. V.; Derjaguin, B. V. *J. Colloid Interface Sci.* **1985**, *103*, 542.

(8) Horn, R. G.; Smith, D. T.; Haller, W. *Chem. Phys. Lett.* **1989**, *162*, 404.

(9) Grabbe, A.; Horn, R. G. *J. Colloid Interface Sci.* **1993**, *157*, 375.

(10) Vigil, G.; Xu, Z.; Steinberg, S.; Israelachvili, J. *J. Colloid Interface Sci.* **1994**, *165*, 367.

(11) Besseling, N. A. M. *Langmuir* **1997**, *13*, 2113.

(12) Manciu, M.; Ruckenstein, E. *Langmuir* **2001**, *17*, 7061.

(13) Valle-Delgado, J. J. *J. Chem. Phys.* **2005**, *123*, 034708.

(14) Tadros, T. F.; Lyklema, J. *J. Electroanal. Chem.* **1968**, *17*, 267.

(15) Van Megen, W.; Snook, I.; Overbeek, J. T. G.; Silberberg, A.; Levine, S.; White, J. W.; Verwey, E. J. W.; Israelachvili, J. N.; Lyklema, J.; Ottewill, R. H.et al *Faraday*

Discuss. Chem. Soc. **1978**, *65*, 43.

(16) Bailey, J. R.; McGuire, M. M. *Langmuir* **2007**, *23*, 10995.

(17) Eun, C.; Berkowitz, M. L. *J. Phys. Chem. B* **2009**, *113*, 13222.

(18) Yoon, R-H.; Vivek, S. *J. Colloid Interface Sci.* **1998**, *204*, 179.

(19) Raghavan, S R.; Walls, H. J.; Khan, S. A. *Langmuir* **2000**, *16*, 7920.

(20) Ducker, W. A.; Senden, T. J.; Pashley, R. M. *Nature* **1991**, *353*, 239.

(21) Bibette, J *J. Magn. Magn. Mater.* **1993**, *122*, 37.

(22) Calderon, F. L.; Stora, T.; Mondain Monval, O.; Poulin, P.; Bibette, J. *Phys. Rev. Lett.* **1994**, *72*, 2959.

(23) Dreyfus, R.; Lacoste, D.; Bibette, J.; Baudry, J. *Eur. Phys. J. E* **2009**, *28*, 113.

(24) Koenig, A.; Hebraud, P.; Gosse, C.; Dreyfus, R.; Baudry, J.; Bertrand, E.; Bibette, J. *Phys. Rev. Lett.* **2005**, *95*, 128301.

(25) Dimitrova, T. D.; Leal-Calderon, F. *Langmuir* **1999**, *15*, 8813.

(26) Ge, J.; Hu, Y.; Yin, Y. *Angew. Chem. Int. Ed.* **2007**, *119*, 7572.

(27) Ge, J.; Yin, Y. *Adv. Mater.* **2008**, *20*, 3485.

(28) Ge, J.; Lee, H.; He, L.; Kim, J.; Lu, Z.; Kim, H.; Goebl, J.; Kwon, S.; Yin, Y. *J. Am. Chem. Soc.* **2009**, *131*, 15687.

(29) Kim, H.; Ge, J.; Kim, J.; Choi, S.; Lee, H.; Lee, H.; Park, W.; Yin, Y.; Kwon, S. *Nature Photonics* **2009**, *3*, 534.

(30) Ge, J.; Yin, Y. *Angew. Chem. Int. Ed.* **2011**, *50*, 1492.

(31) He, L.; Hu, Y.; Wang, M.; Yin, Y. *ACS Nano* **2012**, *6*, 4196.

(32) Ge, J.; Hu, Y.; Biasini, M.; Beyermann, W. P.; Yin, Y. *Angew. Chem.* **2007**, *119*, 4420.

(33) Ge, J.; Hu, Y.; Zhang, T.; Huynh, T.; Yin, Y. *Langmuir* **2008**, *24*, 3671.

(34) Ge, J.; Yin, Y. *J. Mater. Chem.* **2008**, *18*, 5041.

(35) Ren, J.; Song, S.; Lopez-Valdivieso, A.; Shen, J.; Lu, S. *J. Colloid Interface Sci.* **2001**, *238*, 279.

(36) Song, S. X.; Song, S. X.; Peng, C. S. *J. Dispersion Sci. Technol.* **2005**, *26*, 197.

(37) Russel, W. B., Saville, D.A. and Schowalter, W.R. *Colloidal Dispersions*; Cambridge University Press, 1989.

(38) Ott, J. B.; Goates, J. R.; Lamb, J. D. *J. Chem. Thermodyn.* **1972**, *4*, 123.

(39) Cordray, D. R.; Kaplan, L. R.; Woyciesjes, P. M.; Kozak, T. F. *Fluid Phase Equilib.* **1996**, *117*, 146.

(40) Dean, J A. *Lange's Handbook of Chemistry (15th Edition)*; McGraw-Hill, 1999.

Chapter 5

Magnetic Assembly of Nonmagnetic Photonic Crystal Structures

5.1 Introduction

The practical application of photonic crystals, especially those with band gaps located in the visible regime, has been limited by the low efficiency and high cost involved in the conventional lithographic fabrication techniques.[1-6] The fabrication challenges have provided a major driving force for study of alternative approaches to photonic crystal preparation.[7] Indeed, many self-assembly processes have been successfully developed in the past two decades to organize uniform colloidal objects into ordered structures that show photonic response in the visible spectrum. Typical self-assembly methods include those utilizing gravitational force,[8] centrifugal force,[9] hydrodynamic flow,[10] electrophoretic deposition,[11] capillary force[12-15] and electrostatic interaction[16-18] to assemble colloidal crystals. However, there are still challenges that need to be addressed before the self-assembly approaches can be widely used for fabricating photonic materials in an effective manner. A major problem is in the fabrication efficiency: the formation of high-quality colloidal crystals over a large area

usually takes hours to days or even months to complete. The low production efficiency makes many applications impractical.

We have recently reported that nanostructured superparamagnetic magnetite (Fe_3O_4) particles can be conveniently assembled under the external magnetic field to instantly produce ordered one-dimensional (1D) photonic structures, as driven by the balanced interaction of the induced magnetic attraction and various repulsions among the magnetite particles.[19-23] Since there are many more choices for nonmagnetic colloidal particles with uniform size and optimal refractive index, it would be advantageous to extend this magnetic assembly strategy to nonmagnetic particles to allow their rapid assembly into large-area photonic crystals with high quality. Conventionally, magnetic assembly of nonmagnetic materials is achieved by modifying these building blocks with magnetic materials, which apparently limits the choices of materials and the applicability of the processes.[19, 21, 24, 25] In this chapter, we demonstrate the use of nanocrystal-based ferrofluids to direct the assembly of nonmagnetic colloidal particles into photonic crystal structures.[26] The process is general, efficient, convenient, and scalable and thus represents a new and practical platform for the fabrication of colloidal crystal-based photonic devices.[27, 28]

The key in the magnetic assembly strategy is to establish magnetic response for nonmagnetic particles. It is well known that nonmagnetic particles dispersed in

magnetized ferrofluid behave as magnetic "holes" with effective magnetic moments μ equal to the total moment of the displaced ferrofluid but in the opposite direction, $\mu = -V\chi_{eff}H$, where V is the volume of the particles, χ_{eff} the effective volume susceptibility of the ferrofluid, H local magnetic field strength.[29, 30] The application of a magnetic field induces a dipole-dipole interaction $F = 3\mu^2(1-3\cos^2\theta)/d^4$ between two particles, where θ is the angle between the line connecting the centers of the particles and the direction of the field and d is the center-center distance. The dipole-dipole interaction is attractive along the direction of magnetic field and repulsive perpendicular to the direction of magnetic field, which can drive the self-assembly of the magnetic holes into 1D chains, or form complex superstructures when particles with different effective magnetization relative to the ferrofluid are involved.[31] The gradient of the magnetic field also induces a packing force $F_m = \nabla(\mu B)$, where B is the strength of magnetic field. The packing force drives magnetic particles to move towards regions of maximum magnetic field and nonmagnetic particles towards regions of minimum magnetic field, resulting in concentration gradients in mixed magnetic and nonmagnetic colloid suspensions.[32]

Prior efforts in assembling magnetic holes have been limited to objects with sizes in the micrometer range because those of smaller dimensions do not possess high enough magnetic moment and the Brownian motion significantly interferes their assembly.[33, 34] Increasing the magnetic response of a magnetic hole requires either a stronger external

field or a higher concentration of magnetic nanoparticles, both of which can become problematic in practice due to the instability of the ferrofluid under these conditions. As a result, assembly based on magnetic hole effect has been difficult for nonmagnetic particles with size down to a few hundred nanometers, and has rarely been successfully applied to the fabrication of photonic crystals although the concept has been proposed previously.[7] In this work we address the issue by using highly surface-charged magnetic nanocrystals to produce ferrofluids that are stable against aggregation at high concentrations (volume fraction of 4 %) and under strong and high-gradient magnetic fields. The high stability of the ferrofluids allows the efficient assembly of ~ 185-nm nonmagnetic polymer beads into photonic structures under magnetic fields with a large variation in strength and field gradient. It is found that the interplay of magnetic dipole force and packing force determines the structure evolution of the assemblies from 1D periodic chains to 3D colloidal crystals. In particular, under a strong magnetic field with high field gradient, it is now possible to quickly produce 3D photonic crystals with high reflectance (83%) in the visible range within several minutes, making it a promising method for fast creation of large-area photonic crystals using nonmagnetic particles as building blocks.

5.2 Materials and Methods

Materials. Diethylene glycol (DEG, reagent grade), ethanol (denatured), and sodium hydroxide (NaOH, 98.8%) were purchased from Fisher Scientific. Anhydrous iron(III) chloride ($FeCl_3$, 98%) was purchased from Riedel-de Haën. Poly(acrylic acid) (PAA,MW = 1800) Styrene (Reagent Plus grade), Methyl Methacrylate (99%) and ammonium persulfate (A. C. S. reagent grade) were obtained from Sigma-Aldrich. P-styrene sulfonic acid sodium salt was supplied by TCI America. All chemicals were directly used as received without further treatment.

Synthesis of Superparamagnetic Fe_3O_4 CNCs. Highly water-soluble magnetite nanocrystals with average size of 11.5 nm were synthesized in solution at high temperature. In a typical synthesis, a mixture of 4 mmol of PAA, 2 mmol of $FeCl_3$, and 15 mL of DEG was heated to 220 °C in a nitrogen atmosphere with vigorous stirring. 4 mL of NaOH/DEG stock solution (2.5 mol/L) was then injected into the above solution which turned black immediately. After the temperature reached 220 °C again, another 5 mL of $FeCl_3$ stock solution (0.4 mol/L) was added into the reaction mixture. The temperature dropped to around 200 °C. Another 3 mL of NaOH/DEG stock solution (2.5 mol/L) was then injected at 220 °C. The resulting mixture was further heated for 10 min to yield 11.5 nm Fe_3O_4 nanocrystals. These colloids were first washed with a mixture of deionized (DI) water and ethanol several times to remove additional surfactant and salt,

and finally dispersed in 1 mL of DI water. The volume fraction of Fe_3O_4 in the final ferrofluid was about 5%.

Synthesis of Polystyrene spheres. Monodisperse Polystyrene spheres with size of 185 nm were synthesized through an emulsion polymerization method. 50 mL of deionized water was degassed with Nitrogen for 30 min. 3.3 mL of styrene and 0.5 mL of methyl methacrylate were injected into the above DI water. 0.05 g p-styrene sulfonic acid sodium salt in 1 mL DI water was then added. The mixture solution was further degassed with Nitrogen for 30 min and then heated to 70 °C. 0.5 g ammonium persulfate in 1 mL DI water was injected to initiate the polymerization. The reaction mixture was kept stirring at 70 °C for 7 h before cooled down to room temperature. The as-obtained polymer spheres were washed with DI water several times and dispersed in DI water. The volume fraction of polymer spheres was about 15%.

Characterization of Fe_3O_4 CNCs and polystyrene spheres. The morphology and size distribution of the Fe_3O_4 CNCs and polystyrene spheres were characterized under a Tecnai T12 transmission electron microscope (TEM). Colloids dispersed in water at an appropriate concentration were cast onto a carbon-coated copper grid, followed by evaporation under vacuum at room temperature.

5.3 Results and Discussion

Water-soluble superparamagnetic magnetite nanocrystals were synthesized using a one-step high-temperature polyol process that we reported previously.[35] The as-prepared Fe_3O_4 nanocrystals with average size of 11.5 nm have high surface charge and superior dispersability in water, making their aqueous solution a good candidate as the ferrofluidic media for magnetic hole assembly (**Figure 5.1a**). Monodisperse polystyrene (PS) beads with diameter of 185 nm were synthesized through emulsion polymerization of styrene and a small amount of methyl methacrylate (MMA) with sodium styrene sulfonate as the emulsifier (**Figure 5.1b**).[36]

The self-assembly behavior of the PS beads in the ferrofluid in response to an external magnetic fields was first studied in situ through optical microscopy. A thin liquid film (~30 μm) was formed by sandwiching a drop of mixed Fe_3O_4 nanocrystals and PS beads solution between two cover glasses. The assembly behavior was then observed from the top of the liquid film using an optical microscope operated in the dark field mode. **Figure 5.2** shows the structure evolution under the magnetic field with increasing field strengths. In the absence of the magnetic field, the colloids are well dispersed and the homogeneous solution shows the native brown color of iron oxide (**Figure 5.2a**). Brownian motion makes it difficult to capture a clear image of particles. When a 300-Gauss (300 G) magnetic field is vertically applied, PS beads instantaneously

line up along the field and appear as isolated green spots in the optical dark field (**Figure 5.2b**). The green color results from the diffraction of the PS chains with periodical interparticle distances comparable to the wavelength of visible light. A slight tilt (~30°) of the magnet from the vertical orientation confirms that each spot is actually a chain of particles (**Figure 5.2c**). The color shift from green to blue due to smaller diffraction angle is expected for 1D photonic structures. There chains are kept separated by both electrostatic and magnetic repulsions between them. Similar to the previous case of self-assembly of superparamagnetic colloidal particles,[22] these 1D photonic structures have fast and reversible response to external magnetic fields. When the field strength is increased to 500 G, these chains are gradually evolved into labyrinth-like structures.[37] **Figure 5.2d** shows the mixed state of chains and labyrinths. Careful inspection of the labyrinth structures through tilting the direction of the magnetic field to around 60^{o} indicates that they are in fact plate-like assemblies of PS beads (**Figure 5.2e**). Although it is difficult to observe uniform blue shift of diffraction due to the random crystal orientations of the plate-like assemblies, one can still clearly see the transition from green to blue-violet color when they are tilted away from the initial vertical orientation. After the magnetic field reaches 1500 G, only labyrinth structures can be observed, which do not change significantly upon further increasing the field strength.

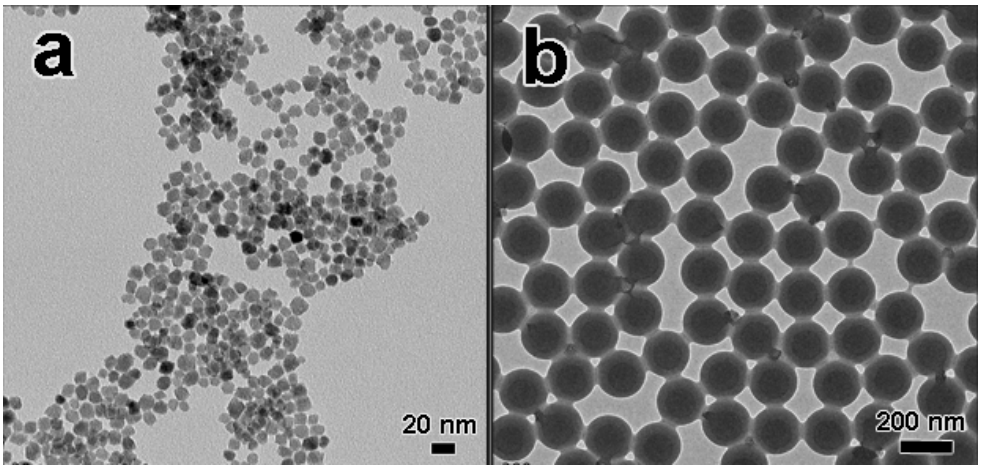

Figure 5.1. TEM images of (a) 11.5-nm magnetite (Fe_3O_4) nanocrystals and (b) 185-nm polystyrene (PS) spheres. Reproduced with permission from Ref. 26 @ 2010 American Chemical Society.

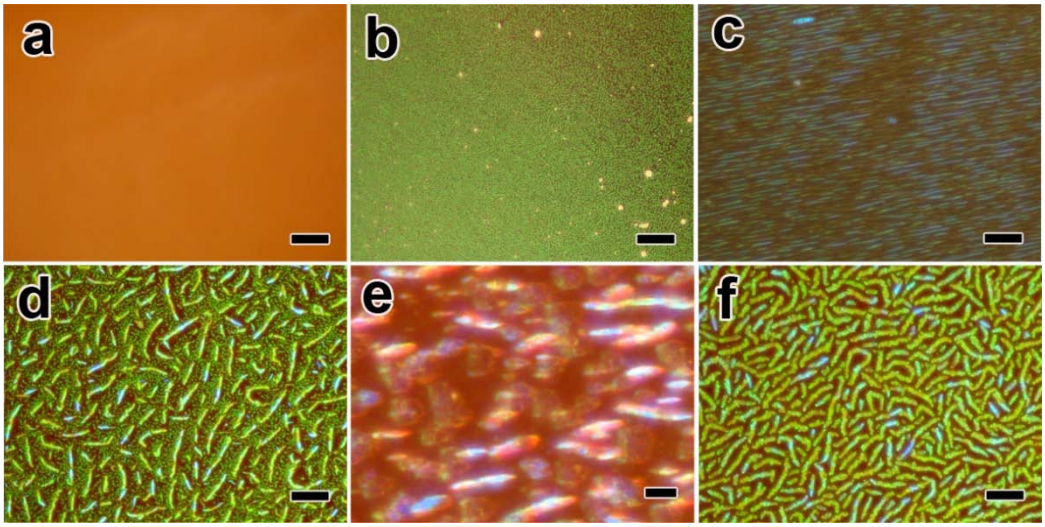

Figure 5.2. Optical microscope images showing the assembly of 185-nm PS (volume fraction of 3%) beads dispersed in the ferrofluid (volume fraction of 2%) in a 30-μm thick liquid film encapsulated between two glass slides under different magnetic fields: (a) 0 G and 0 G/cm; (b), (c) 300 G and 580 G/cm; (d), (e) 500 G and 982 G/cm; (f) 1500 G and 2670 G/cm. The direction of magnetic field is parallel to (a, b, d, f), 15^{o} (c) and 60^{o} (e) from the viewing angle. All scale bars are 20 μm except 50 μm for (e). Reproduced with permission from Ref. 26 @ 2010 American Chemical Society.

The transition from chains to labyrinths is mainly due to two reasons. Firstly, the magnetic moment of the Fe_3O_4 nanocrystals and consequently that of the holes (PS beads) are increased under stronger magnetic field. Secondly, the local concentration of PS particles goes up slightly as driven by the stronger packing force due to the increased magnetic field gradient. The inter-chain distance is thus reduced owing to the fact that more chains are formed on the top surface of the liquid film. Both the increased magnetic moment and decreased chain separation cause stronger repulsion between the chains, which eventually results in the aggregation of chains into labyrinth structures to minimize the free energy. The order along the direction of original chains is not significantly disrupted so that the labyrinths still diffract green light and appear very bright in the optical dark field. Interestingly, these labyrinth patterns are similar to those reported by Islam et al., even though their patterns are assemblies of magnetic nanocrystals, not nonmagnetic colloids.[37]

To further study the concentration gradient effect, we observed the self-assembly behavior in a liquid film with increased thickness (1 mm) and higher concentration of PS and ferrofluid (both at 4 % volume fraction). Unlike the thin film case, the large amount of PS in the background makes it difficult to image the 1D assemblies when the field strength is low, although their diffraction can be still collectively detected using a spectrometer as shown in later discussions. When the field is enhanced to 1050 G with

field gradient of 1900 G/cm, small green and large yellow domains can be observed although the overall contrast is still low. The small green domains are believed to be aggregates of a few chains while the large yellow domains are believed to be lamellar-like structures similar to the patterns resulted from the aggregation of magnetic nanocrystals.[37] The overall reflection of the liquid film decreases as lamellar structures grow larger, suggesting disturbed order along the field direction. As the magnet moves closer to the sample, the large domains can be further assembled into long-range ordered patterns (lamellar chains) with many small green domains sandwiched in between (**Figure 5.3b**). Interestingly, these small green domains can also connect to form continuous long chains upon increasing the field strength and gradient (Figure **5.3c**). Both the green and yellow chains expand in width when the field gradient is further strengthened (**Figure 5.3d**), after which only yellow lamellar chains exist with a slight increase in the magnetic field gradient (**Figure 5.3e**). The lamellar chains become unstable and break into domains with larger diameter under a field of 1300 G and 2320 G/cm (**Figure 5.3f**). These domains show irregular hexagonal arrangement from the top view, further aggregate into large ribbons (**Figure 5.3g**), and finally connect each other and form a uniform layer of 3D assemblies without contrast (**Figure 5.3h**) under even stronger magnetic field (1460 G and 2600 G/cm).

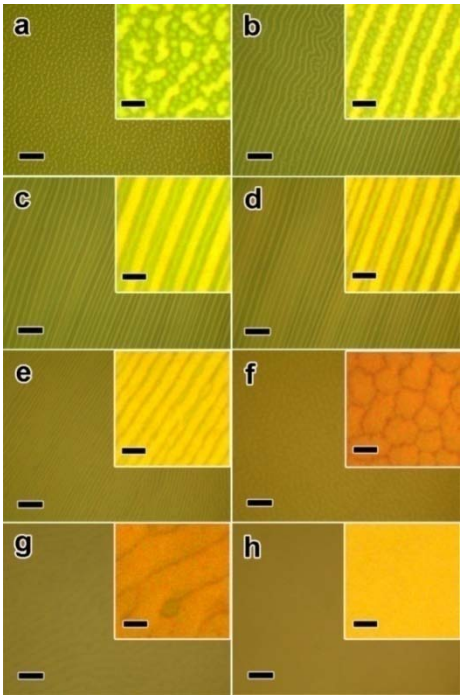

Figure 5.3. Optical microscope images showing the structure evolution of assembled 185-nm PS beads dispersed in the ferrofluid under increasing magnetic fields: (a) 1050 G and 1900 G/cm, (b) 1200 G and 2160 G/cm, (c) 1220 G and 2190 G/cm, (d) 1240 G and 2220 G/cm, (e) 1260 G and 2255 G/cm, (f) 1300 G and 2320 G/cm, (g) 1380 G and 2460 G/cm, (h) 1460 G and 2600 G/cm. The volume fractions are both 4% for PS and Fe_3O_4. The mixed solution is sealed in a glass cell with thickness of 1 mm. The direction of magnetic field is parallel to the viewing angle. The scale bars are 20 μm. Insets show the corresponding enlarged images. The lightness and contrast in the insets were adjusted to show the assembled patterns. The scale bars are 5 μm for all insets. Reproduced with permission from Ref. 26 @ 2010 American Chemical Society.

An important fact during the phase transition is that the free space without PS assemblies are gradually decreased (from **Figure 5.3a** to **5.3f**), which confirms the increasing local concentration of nonmagnetic beads. The growth of small domains into large lamellar ones is mainly owing to this concentration gradient effect driven by the packing force. The cause of the formation of these regularly arranged lamellar structures over a large area still requires further studies. Apparently, the electrostatic and magnetic repulsions play a role here by keeping the lamellar chains away from each other.

To monitor the local concentration distribution of nonmagnetic beads in ferrofluid under external magnetic fields, a mass transport model was developed to solve convection-diffusion equations with given boundary condition. We consider a mixture of PS beads and ferrofluid in a confined film, and the ferrofluid is assumed to be a continuum relative to the larger nonmagnetic beads. When an external magnetic field is applied to the mixture, magnetic packing force, $F_m = -\mu_0 V_{PS} M_f \nabla H$, is exerted to the nonmagnetic beads, where μ_0 is the permeability of free space, V_{PS} is the volume of the non-magnetic bead, M_f is the magnetization of the ferrofluid, and H is the magnetic field. Thus, nonmagnetic beads move towards the region of the lowest magnetic field gradient with terminal velocity, $v = -\frac{2R_p{}^2 \mu_0 M_p \nabla H}{9\eta}$ where R_p is the radius of nonmagnetic bead, and η is the viscosity of the medium. We assumed that the

relaxation time is short compared to the time span of interest. Total nonmagnetic bead flux can be stated as $J_{PS} = -D\nabla C + vC$ including magnetically induced drift flux and diffusion flux, where *D* is the diffusion constant, and *C* is the concentration of PS beads. Finally, local concentration of nonmagnetic beads can be evaluated by incorporating total flux into continuity equation, $\frac{\partial C}{\partial t} + \nabla \cdot J_{PS} = 0$, and one-dimensional calculation was performed to solve this equation. The calculation still clearly demonstrates that nonmagnetic beads dispersed in ferrofluids move toward the top region of the film, where the magnetic field is the minimum (**Figures 5.4** and **5.5**). Local concentration of polymer beads at the top region keeps increasing until reaching equilibrium, while nonmagnetic beads in other regions are depleted. The time to reach concentration equilibrium depends on the film thickness, ranging from 20 s for a 30-μm film to several minutes for a 1-mm film (**Figure 5.5**). Unlike the case of a 30-μm liquid film, a large concentration gradient of PS beads can build up in a 1-mm film.

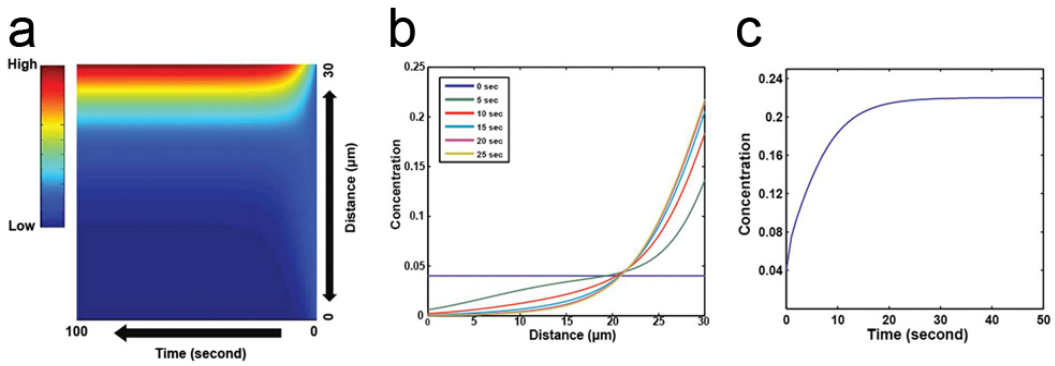

Figure 5.4. Local concentration of nonmagnetic beads in a 30-μm thick film under an external magnetic field. (a) Local concentration profile at time and location of interest. (b) Local concentration in different areas of the 30-μm cell at different time. (c) Local concentration evolution at the top region of the film. Reproduced with permission from Ref. 26 @ 2010 American Chemical Society.

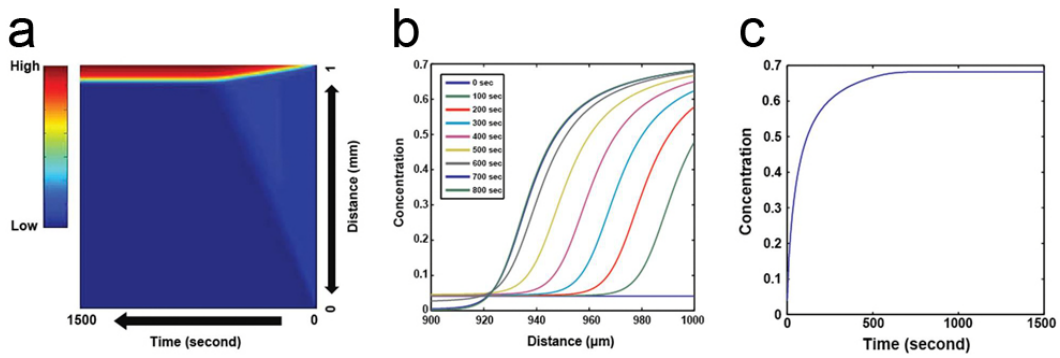

Figure 5.5. Local concentration of nonmagnetic beads in a 1-mm thick film under an external magnetic field. (a) Local concentration profile at time and location of interest. (b) Local concentration in different areas of the entire cell at different time. (c) Local concentration evolution at the top region of the film. Reproduced with permission from Ref. 26 @ 2010 American Chemical Society.

The ordering of PS beads leads to optical diffraction which can be measured by recording the reflectance using a spectrophotometer. As shown in **Figure 5.6a**, a diffraction peak appears at 595 nm in a field of 210 G, blue shifts to 578 nm at 260 G and to 567 nm at 311 G with gradual enhancement in intensity, as expected by the increased magnetic moment of PS beads and thereby stronger interparticle attraction and higher degree of order. Under weak magnetic fields, the diffraction is mainly contributed by the 1D chain-like assemblies. Further enhancing the field to 866 G does not significantly change the peak position, but only increases the peak intensity. This is very similar to the previous case of magnetic 1D assembly of Fe_3O_4@SiO_2 colloids in ethanol, where the diffraction does not shift in an enhancing field when the interparticle separation cannot be changed anymore.[21] Beyond 866 G, the magnetic packing force becomes significant and causes the aggregation of chains, forming larger domains of assemblies with slight red-shift in diffraction (**Figure 5.6b**). In consistent with the observation in optical microscopy, the aggregation of 1D chains into larger assemblies disturbs the original ordering along the field direction and, therefore, leads to the decreased diffraction intensity. Due to the relatively weak magnetic moment of PS, the reflectance of the assemblies is typically below 10%. However, a strong magnetic field with high gradient may drive the formation of 3D assemblies with much higher diffraction intensity as observed in optical microscopic studies.

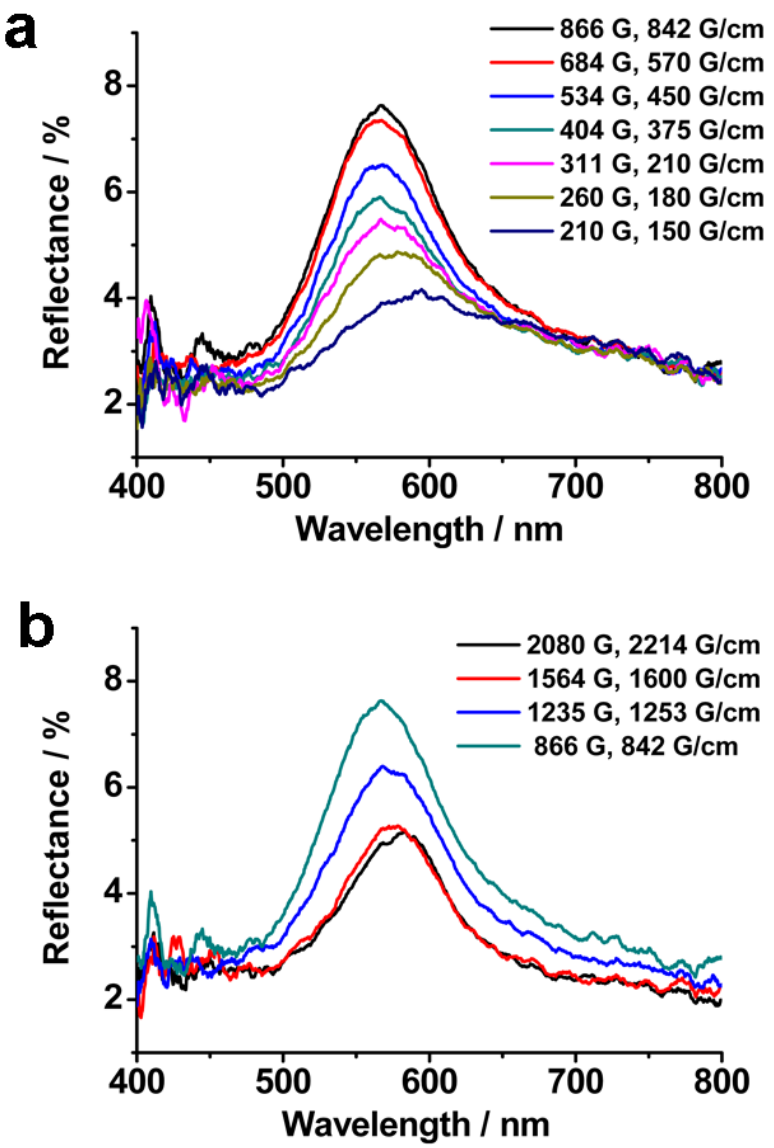

Figure 5.6 Reflection spectra of the 1-mm thick film of mixed PS beads and ferrofluid solution in response to an external magnetic field with varying strengths. The volume fractions are 4% for both PS and Fe_3O_4. Reproduced with permission from Ref. 26 @ 2010 American Chemical Society.

As shown in **Figure 5.7**, upon applying a magnetic field of 2530 G with gradient of 2500 G/cm, a weak diffraction peak at 563 nm appears immediately due to the chaining of the PS particles. After 1 min, the peak position moves to 533 nm and the intensity increases to 25%, indicating the structure evolution from 1D chains to 3D domains during which the lattice constant decreases. In the next 5 min, the peak position slightly red shifts while the intensity gradually increases and eventually reaches the maximum of ~ 83%, suggesting the formation of high quality 3D colloidal crystals. The enhancement of diffraction intensity can be attributed to the increase in the density, thickness, and long-range order of the 3D assemblies as the local concentration of PS spheres increases. The slight red shift during this period might result from the increased average refractive index as the volume fraction of PS spheres increases

To better understand the assembly process under a strong magnetic field, the magnet was removed at 3 min 30 s when the diffraction intensity reached over 50% and the diffraction spectra were recorded (**Figure 5.8**). Interestingly, the intensity continued to increase to 62% at 3 min 40 s, and reached ~ 80% at 5 min 30 s and the maximum of 83% at 9 min 30 s (**Figure 5.8a**). In the absence of an external magnetic field, the maximum reflectance can be maintained for ~ 8 min before starting to slowly drop. If the magnetic field is removed before 50% reflectance is obtained, the intensity would not increase but decrease immediately after removing the magnetic field. These observations

suggest that the assembly process may be divided into two steps. The first step involves the increase of local PS concentration due to the high magnetic field gradient. The movement of magnetic and nonmagnetic particles determines the duration of this step, which should be in the range of a few minutes. The concentration of PS beads increases dramatically upon applying the magnetic field so that they assemble into 3D structures near the top side of the cell (the side away from the magnet). Again, a quick transition from 1D chains to 3D domains occurs at the initial stage of this step, as suggested in **Figure 5.8a** by the apparent blue shift in the diffraction peak position. The second step is the repositioning of PS beads inside the 3D assemblies into more ordered arrangement as driven by the electrostatic interaction among the PS beads, thus further enhances the diffraction intensity. This step occurs relatively slower so that the diffraction can still increase even after the magnetic field is removed. However, if the external filed is only applied for a short period of time, the dense PS layer is not thick enough and will quickly disassemble upon removal of the external field. When the external field is always present, the PS beads experience the magnetic packing force which leads to slightly shorter interparticle distance (along the field direction) than that without the magnetic field. This explains the difference of peak position at maximum intensity in **Figures 5.7 and 5.8**. The “compression” effect by the magnetic field can also be observed in **Figure 5.8a**, where a distinctive red shift occurred in the diffraction peak immediately after the

magnetic field was removed. The disassembly of the 3D crystal is a slow process and proceeds from the bottom side. As shown in **Figure 5.8b**, after remaining at the maximum value for ~8 minutes, the diffraction intensity of the colloidal crystal gradually dropped and eventually disappeared after an additional 10 minutes. This disassembly process is not entirely the opposite operation of the assembly process; for example, the initial peak at 563 nm due to the 1D chains formed during the assembly process (**Figure 5.8a**) cannot be observed during the disassembly process (**Figure 5.8b**).

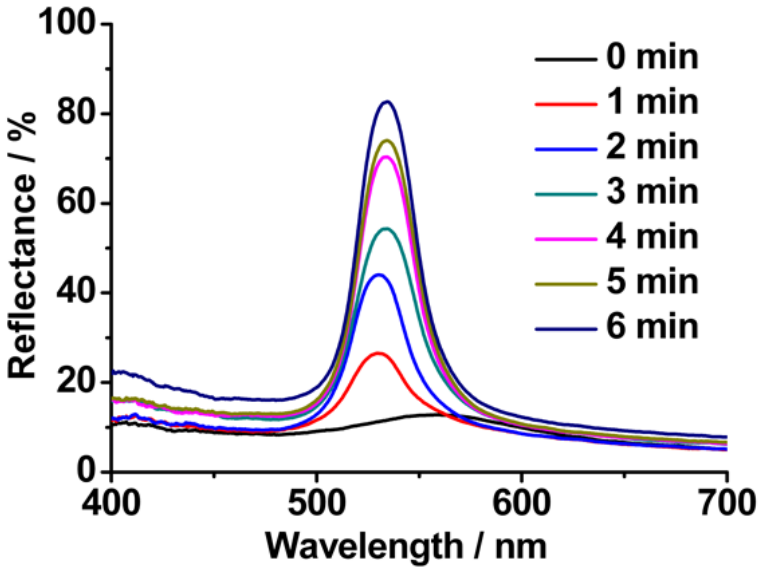

Figure 5.7. Time-dependent reflection spectra of the 1-mm thick film of mixed PS and ferrofluid solution in response to a fixed magnetic field of 2530 G with gradient of 2500 G/cm. The volume fractions are 4% for both PS and Fe_3O_4. Reproduced with permission from Ref. 26 @ 2010 American Chemical Society.

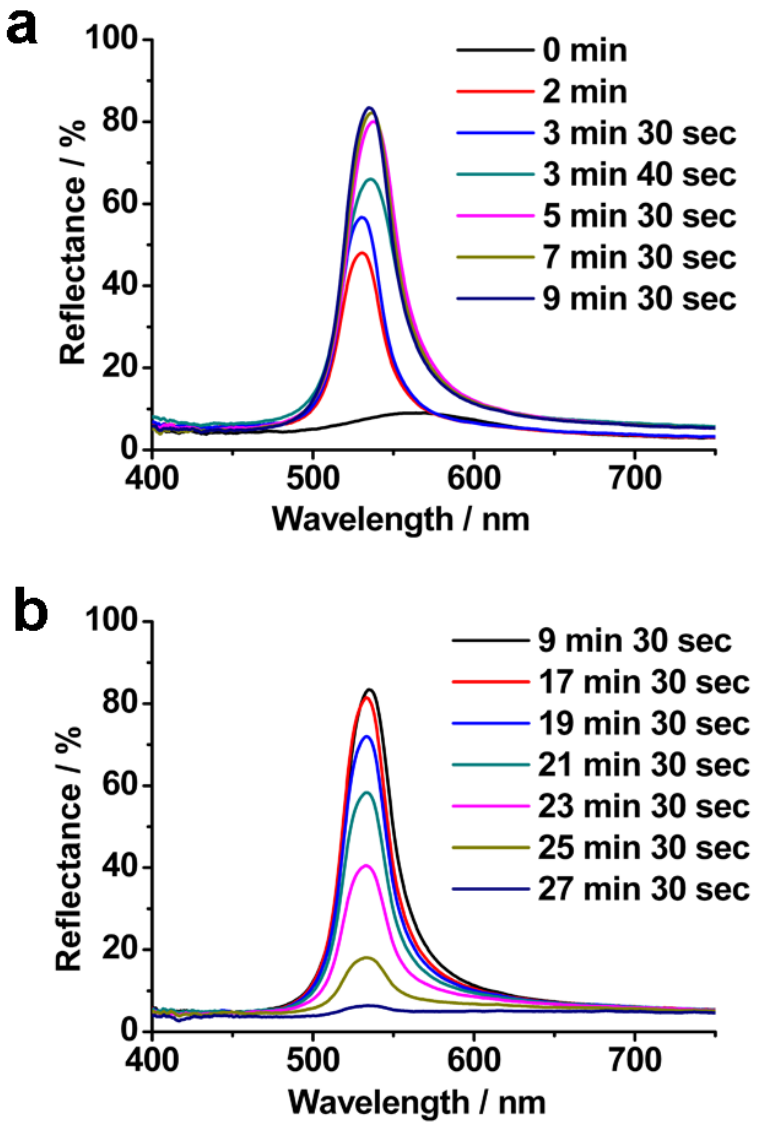

Figure 5.8. Time-dependent reflection spectra of the 1-mm thick film of mixed PS and ferrofluid solution in response to a magnetic field of 2530 G with gradient of 2500 G/cm. The magnetic field was removed at 3 min 30 sec. The volume fractions are 4% for both PS and Fe_3O_4. Reproduced with permission from Ref. 26 @ 2010 American Chemical Society.

It is worth noting that both Fe_3O_4 nanocrystals and PS beads have highly negative surface charge and we ignore the possibility of adsorption of Fe_3O_4 on PS beads to change the sign of their magnetostatic energy. The strong repulsive force resulted from highly charged surfaces provides the stability of both magnetic and nonmagnetic particles in the system. The stability of ferrofluid is crucial for manipulating the nonmagnetic particles while the high surface charge on PS beads contributes to the formation of high quality photonic crystals. Intentional addition of salts to the mixed solution causes the aggregation of particles even in the absence of the external magnetic field, and therefore colloidal crystals cannot be obtained. As indicated before, the structure evolution in current case is believed to result from the interplay of dipole force and packing force of the magnetic holes in ferrofluids. In a low magnetic field (also low field gradient), the ferrofluid can be treated as homogeneous and the dipole force dominates the assembly of PS beads and results in the formation of chain-like structures. In a high magnetic field (also with high field gradient), the packing force becomes dominant which creates a significant concentration gradient of PS beads and leads to their assembly into high quality 3D crystals. More rigorous numeric simulation might provide deep understanding of the assembly process and is under study.

5.4 Conclusion

In summary, a general magnetic assembly strategy based on magnetic hole effect has been developed to fabricate photonic crystals using nonmagnetic particles as building blocks. By tuning the magnetic field, it is possible to control the photonic structures from 1D particle chains to 3D colloidal crystals. The chain-like 1D photonic structures form in a weak magnetic field and show fast and reversible response to external magnetic fields. Increasing the strength and gradient of the magnetic field induces the evolution from 1D to 3D structures which involves complex phase changes and disrupts the photonic property. In a strong magnetic field with large field gradient, high quality 3D photonic structures with reflectance up to 83% can be produced in several minutes, which is very efficient comparing to other colloidal assembly methods. It is believed that this fabrication method can be easily scaled up using large area magnetic fields and extended to the assembly of building blocks with different compositions and morphologies. As an alternative to conventional methods, this new approach allows fast creation of high quality photonic crystal structures, thus providing a new platform for the fabrication of novel optical components for many practical applications.

3.5 References

(1) Wanke, M. C.; Lehmann, O.; Muller, K.; Wen, Q. Z.; Stuke, M. *Science* **1997**, *275*, 1284.

(2) Lin, S. Y.; Fleming, J. G.; Hetherington, D. L.; Smith, B. K.; Biswas, R.; Ho, K. M.; Sigalas, M. M.; Zubrzycki, W.; Kurtz, S. R.; Bur, J. *Nature* **1998**, *394*, 251.

(3) Fleming, J. G.; Lin, S. Y. *Optics Letters* **1999**, *24*, 49.

(4) Campbell, M.; Sharp, D. N.; Harrison, M. T.; Denning, R. G.; Turberfield, A. J. *Nature* **2000**, *404*, 53.

(5) Noda, S.; Tomoda, K.; Yamamoto, N.; Chutinan, A. *Science* **2000**, *289*, 604.

(6) Birner, A.; Wehrspohn, R. B.; Gosele, U. M.; Busch, K. *Advanced Materials* **2001**, *13*, 377.

(7) Xia, Y.; Gates, B.; Yin, Y.; Lu, Y. *Adv. Mater.* **2000**, *12*, 693.

(8) Braun, P. V.; Zehner, R. W.; White, C. A.; Weldon, M. K.; Kloc, C.; Patel, S. S.; Wiltzius, P. *Advanced Materials* **2001**, *13*, 721.

(9) Lee, S.; Yi, G.; Yang, S. *Lab on a Chip* **2006**, *6*, 1171.

(10) Lu, Y.; Yin, Y.; Gates, B.; Xia, Y. *Langmuir* **2001**, *17*, 6344.

(11) Holgado, M.; Garcia-Santamaria, F.; Blanco, A.; Ibisate, M.; Cintas, A.; Miguez, H.; Serna, C. J.; Molpeceres, C.; Requena, J.; Mifsud, A.et al *Langmuir* **1999**, *15*, 4701.

(12) Jiang, P.; Bertone, J. F.; Hwang, K. S.; Colvin, V. L. *Chem. Mater.* **1999**, *11*, 2132.

(13) Velev, O.; Lenhoff, A.; Kaler, E. *Science* **2000**, *287*, 2240.

(14) Fudouzi, H.; Xia, Y. N. *Langmuir* **2003**, *19*, 9653.

(15) Arsenault, A. C.; Puzzo, D. P.; Manners, I.; Ozin, G. A. *Nature Photonics* **2007**, *1*, 468.

(16) Asher, S. A.; Holtz, J.; Liu, L.; Wu, Z. J. *J. Am. Chem. Soc.* **1994**, *116*, 4997.

(17) Pan, G.; Kesavamoorthy, R.; Asher, S. *J. Am. Chem. Soc.* **1998**, *120*, 6525.

(18) Reese, C. E.; Guerrero, C. D.; Weissman, J. M.; Lee, K.; Asher, S. A. *Journal of Colloid and Interface Science* **2000**, *232*, 76.

(19) Ge, J.; He, L.; Goebl, J.; Yin, Y. *J. Am. Chem. Soc.* **2009**, *131*, 3484.

(20) Ge, J.; Yin, Y. *J. Mater. Chem.* **2008**, *18*, 5041.

(21) Ge, J.; Yin, Y. *Adv. Mater.* **2008**, *20*, 3485.

(22) Ge, J.; Hu, Y.; Zhang, T.; Huynh, T.; Yin, Y. *Langmuir* **2008**, *24*, 3671.

(23) Ge, J.; Hu, Y.; Yin, Y. *Angew. Chem. Int. Ed.* **2007**, *46*, 7428.

(24) Xu, X. L.; Friedman, G.; Humfeld, K. D.; Majetich, S. A.; Asher, S. A. *Chemistry of Materials* **2002**, *14*, 1249.

(25) Xu, X. L.; Majetich, S. A.; Asher, S. A. *Journal of the American Chemical Society* **2002**, *124*, 13864.

(26) He, L.; Hu, Y.; Kim, H.; Ge, J.; Kwon, S.; Yin, Y. *Nano Lett.* **2010**, *10*, 4708.

(27) Ge, J.; Goebl, J.; He, L.; Lu, Z.; Yin, Y. *Adv. Mater.* **2009**, *21*, 4259.

(28) Ge, J.; Lee, H.; He, L.; Kim, J.; Lu, Z.; Kim, H.; Goebl, J.; Kwon, S.; Yin, Y. *J. Am. Chem. Soc.* **2009**, *131*, 15687.

(29) Skjeltorp, A. T. *Physical Review Letters* **1983**, *51*, 2306.

(30) Clausen, S.; Helgesen, G.; Skjeltorp, A. T. *Physical Review E* **1998**, *58*, 4229.

(31) Erb, R. M.; Son, H. S.; Samanta, B.; Rotello, V. M.; Yellen, B. B. *Nature* **2009**, *457*, 999.

(32) Erb, R. M.; Yellen, B. B. *Journal of Applied Physics* **2008**, *103*.

(33) Helgessen, G.; Svasand, E.; Skjeltorp, A. T. *Journal of Physics-Condensed Matter* **2008**, *20*.

(34) Pieranski, P.; Clausen, S.; Helgesen, G.; Skjeltorp, A. T. *Physical Review Letters* **1996**, *77*, 1620.

(35) Ge, J. P.; Hu, Y. X.; Biasini, M.; Dong, C. L.; Guo, J. H.; Beyermann, W. P.; Yin, Y. D. *Chemistry-a European Journal* **2007**, *13*, 7153.

(36) Qiu, D.; Cosgrove, T.; Howe, A. M. *Macromolecular Chemistry and Physics* **2005**, *206*, 2233.

(37) Islam, M. F.; Lin, K. H.; Lacoste, D.; Lubensky, T. C.; Yodh, A. G. *Physical Review E* **2003**, *67*, 021402/1.

Chapter 6

Magnetic Assembly and Patterning of General Nanoscale Materials through Nonmagnetic Templates

6.1 Introduction

Interest in the self-assembly of colloidal objects has been driven by the fact that colloidal suspensions are ideal model systems to study fundamental problems in condensed matter physics at a length scale more experimentally accessible than the atomic scale.[1, 2] In addition, colloidal assembly has also attracted increasing interest as a general bottom-up method for producing functional materials and devices.[3-6] Of particular technological interest is the development of effective bottom-up self-assembly approaches for organizing colloidal building blocks into well-defined aggregates with controlled sizes, shapes, structures, and positions, for the fabrication of microstructured electric, optical and sensing devices.[7-9] A variety of template-assisted self-assembly methods have been utilized to direct the deposition of colloidal particles onto patterned surfaces, including physical confinement during the dewetting process[10-12], electrostatic adsorption on an oppositely charged patterned surface[13], as well as electrophoretic deposition of charged colloids on patterned microelectrode arrays[14]. However, the

precision of the structural and orientational control, the efficiency, general applicability, and scalability of these processes still need to be greatly improved before the wide practical usage of these methods is feasible.[15, 16] Moreover, many of these assembly processes are essentially irreversible and provide limited opportunities for further tuning of the electric, optical or mechanical properties of the assembled structures.

Magnetic assembly is regarded as a powerful tool for rapidly organizing nanoscale matter into complex structures.[17, 18] In particular, it has been demonstrated that a magnetic field can serve as an effective stimulus to rapidly tune the optical properties of colloidal photonic structures.[19-21] For example, we have recently developed magnetically responsive photonic systems through the instantaneous assembly of colloidal particles into photonic nanostructures guided by external magnetic fields.[22-26] In principle, magnetic manipulation of nanoscale objects can provide precise control over their local arrangement and properties if the external magnetic field can be modulated.[27] However, in practice, it is difficult to generate the well-controlled complex magnetic fields needed for assembling nanoscale objects. Multiple steps and sophisticated instruments have been used to pattern micromagnets on solid substrates,[28-31] adding significant challenges for device fabrication and integration. In this chapter, we demonstrate a general nonmagnetic-template-assisted magnetic self-assembly strategy that is capable of rapidly and reversibly organizing and positioning nanoscale objects

with micrometer scale precision.[32] The key is to use ferrofluids as media to induce magnetic interactions between general target objects and nonmagnetic template patterns. The nonmagnetic templates exposed to magnetized ferrofluid behave as "reverse micromagnets" in an external magnetic field owing to the difference in the magnetization between the templates and the surrounding ferrofluid. The spatial distribution of the magnetic field around the templates can then be modulated to induce a large field gradient locally even though the external magnetic field is uniform, making it possible to attract the nonmagnetic target objects which are dispersed in the same ferrofluid and have acquired net magnetic moments.[33]

6.2 Materials and Methods

Synthesis of ferrofluid: Magnetite (Fe_3O_4) nanocrystals with an average diameter of 11.5 nm were synthesized using a polyol procedure we reported previously. In a typical synthesis, a mixture of 4 mmol of polyacrylic acid (PAA, Mw 1800), 2 mmol of $FeCl_3$, and 15 mL of diethylene glycol (DEG) was heated to 220 °C in a nitrogen atmosphere with vigorous stirring. 4 mL of NaOH/DEG stock solution (2.5 mol/L) was then injected into the above solution which turned black immediately. After the temperature reached 220 °C again, 5 mL of $FeCl_3$ stock solution (0.4 mol/L) was added into the reaction mixture. The temperature dropped to around 200 °C. Another 3 mL of NaOH/DEG stock solution (2.5 mol/L) was then injected once the temperature returned to 220 °C. The resulting mixture was further heated for 10 min to yield 11.5 nm Fe_3O_4 nanocrystals. These colloids were first washed with a mixture of deionized (DI) water and ethanol several times to remove additional surfactant and salt, and finally dispersed in DI water. The volume fraction of Fe_3O_4 in the final ferrofluid was 5%.

Synthesis of polystyrene latex spheres: Monodisperse Polystyrene spheres with size of 166 nm were synthesized through an emulsion polymerization method. 50 mL of deionized water was degassed with Nitrogen for 30 min. 5 mL of styrene and 0.75 mL of methyl methacrylate were injected into the above DI water. 0.05 g p-styrene sulfonic acid sodium salt in 1 mL DI water was then added. The mixture solution was further

degassed with Nitrogen for 30 min and then heated to 70 °C. 0.5 g ammonium persulfate in 1 mL DI water was injected to initiate the polymerization. The reaction mixture was kept stirring at 70 °C for 12 h before cooled down to room temperature. The as-obtained polymer spheres were washed with DI water four times and dispersed in DI water. The volume fraction of polymer spheres stock solution was about 10%. The 188 nm and 210 nm latex spheres were synthesized using the same process with different amount of p-styrene sulfonic acid sodium salt (0.03 g for 188 nm and 0.02 g for 210 nm).

Synthesis of 1.5-μm sulfate functionalized mercapto-silica beads: Mercapto-silica (MPS) spheres were first prepared by using a one-pot procedure we reported previously. In a typical synthesis, MPS precursor in the amount of 1 mL was added to 1% NH_4OH aqueous solution (0.05 M) for a total volume of 30 mL and vigorously shaken for 1 min using an IKA MS3 minishaker at a speed of 2500 rpm. The resulting mixture was then incubated at room temperature for several hours. The products were collected via centrifugation and washed with ethanol several times. The MPS spheres dispersed in 25 mL of ethanol were reacted with 1 mL of H_2O_2 aqueous solution for 2 h. 1 mL of dilute sulfuric acid (1M) was added into the reaction mixture to obtain sulfate functionalized mercapto-silica microspheres. The final products were cleaned with DI water several times and dispersed in DI water. The volume fraction of the final stock solution was 5%.

Colloidal microspheres: 6.5-μm, 6.2-μm and 4.5-μm carboxylate functionalized polymer latex microspheres were obtained from Polymer tech. All these particles were cleaned with DI water twice and redispersed in DI water. The final volume fraction was 5%.

Pattern preparation. The master patterns were produced on silicon wafers by using standard photolithography processes. After treatment of the photoresist with a fluorinated silane, (tridecafluoro-1, 1, 2, 2, -tetrahydrooctyl) trichlorosilane, polydimethylsiloxane (PDMS) stamps were then made by casting and curing the prepolymer against the photoresist patterns. Final polymeric patterns are obtained by sandwiching a layer of liquid polyurethane prepolymer(NOA 81, Norland Products) between a clean glass slide and the PDMS stamp, followed by UV exposure to solidify the prepolymer and then removing the PDMS stamp.

Assembly and optical observation. Observation of the assembly was performed on a Zeiss AXIO Imager optical microscope operated in the dark-field mode. In a typical process, a 3 μL solution of ferrofluid and nonmagnetic colloidal particles mixed at desired volume fractions were deposited on the patterned substrate, and covered with an 18 mm x 18 mm glass coverslip to form a thin liquid film. A NdFeB magnet was placed beneath the sample stage and its position could be vertically changed to adjust the magnet-sample distance.

Simulation of magnetic fields. The 2D cross-sectional magnetic field distribution around different patterns was simulated using the COMSOL MUTLIPHYSICS software package. The volume susceptibility of the ferrofluid was set at 1.8. The volume susceptibility of the pattern was set at 1. The external magnetic field was set to be uniform and oriented in the vertical direction.

Characterization: The morphology and size distribution of the Fe_3O_4 nanocrystals and polystyrene spheres were characterized under a Tecnai T12 transmission electron microscope (TEM). Colloids dispersed in water at an appropriate concentration were cast onto a carbon-coated copper grid, followed by evaporation under vacuum at room temperature. The patterns were characterized using a Philips FEI XL30 scanning electron microscope (SEM) and a Keyence Laser Microscope. The drying process for the sample shown in Figure 2f and 2g was simply performed under ambient condition in the applied magnetic fields. The cover slides were then removed and the patterns with beads were observed directly by using SEM.

6.3 Patterned Assembly of Nonmagnetic Objects

To demonstrate this strategy, we first use topologically patterned polymer templates as an example to guide the assembly of colloidal spheres. **Figure 6.1a** shows the SEM image of a typical polyurethane pattern on a glass slide obtained through rapid UV-polymerization of an oligomer film molded against a pre-fabricated polydimethylsiloxane (PDMS) stamp. Consistent with the general advantages of soft lithography, the patterns can be generated within minutes without the need for any additional surface treatment and the stamps can be reused many times, making it possible to realize cost-effective large-scale production.[34] To visualize the "inverse micromagnet" effect, we simulated the two-dimensional magnetic field strength distribution around the patterns immersed in a ferrofluid when exposed to a uniform external magnetic field (**Figure 6.1b**). The nonmagnetic pattern induces an inverse magnetic field relative to the ferrofluid on the tops of the patterned features, where the strength of the local magnetic field is lower than that in the bulk ferrofluid. On the other hand, the magnetic field near the sides of the features is strengthened by the induced magnetic field. Consequently, a large magnetic field gradient is generated at the edge areas of the patterned bumps. Additionally, the nonmagnetic colloidal objects immersed in the ferrofluid can gain net magnetic moments through the well-known "magnetic hole"

mechanism.[35] The effective magnetic moment of a spherical nonmagnetic object in the magnetized ferrofluid is given by

$$\boldsymbol{m}_v = -V\,\chi_{eff}\boldsymbol{H} \tag{1}$$

where V is the volume of the nonmagnetic object, χ_{eff} is the effective volume susceptibility of the ferrofluid and H is the local magnetic field strength. The magnetostatic energy, or Zeeman energy, of the nonmagnetic object can be expressed by

$$\boldsymbol{E}_m = -\frac{\mu_0}{4\pi}\boldsymbol{m}_v \cdot \boldsymbol{H} = \frac{\mu_0 V\,\chi_{eff}}{4\pi}|\boldsymbol{H}|^2 \tag{2}$$

where μ_0 is the magnetic permeability of free space and $|H|$ is the local magnetic field norm. Hence, the modulation of the local magnetic field in the vicinity of the pattern creates an energy well to trap the nonmagnetic objects near the tops of the patterned features, where the magnetic field is at the minimum, to reduce the magnetostatic energy (Figure 1c). Besides the positioning of nonmagnetic objects on the top of the pattern, interactions between the particles, mainly electrostatic and magnetic dipole-dipole forces, will also induce secondary assembly above the pattern.[36] In the cases described here, the interparticle electrostatic force is always repulsive due to the like surface charges. The magnetic dipole-dipole interaction between two particles with the same dipole moment is directional in nature which can be expressed by

$$\boldsymbol{F}_d = \frac{3\mu_0(1-3\cos^2\alpha)}{4\pi d^4}|\boldsymbol{m}_v|^2\,\boldsymbol{r} \tag{3}$$

where α is the angle between the magnetic dipole and the line connecting the center of the two particles, d is the center-center distance and r is the unit vector connecting the centers of the two particles.[36] The dipole-dipole force is attractive along the magnetic field direction and repulsive in the direction perpendicular to the magnetic field. As discussed in detail later, the interparticle magnetic dipole-dipole attraction along the magnetic field direction can be balanced by the electrostatic repulsion to induce the organization of colloidal spheres into one-dimensional dynamic chain-like structures.

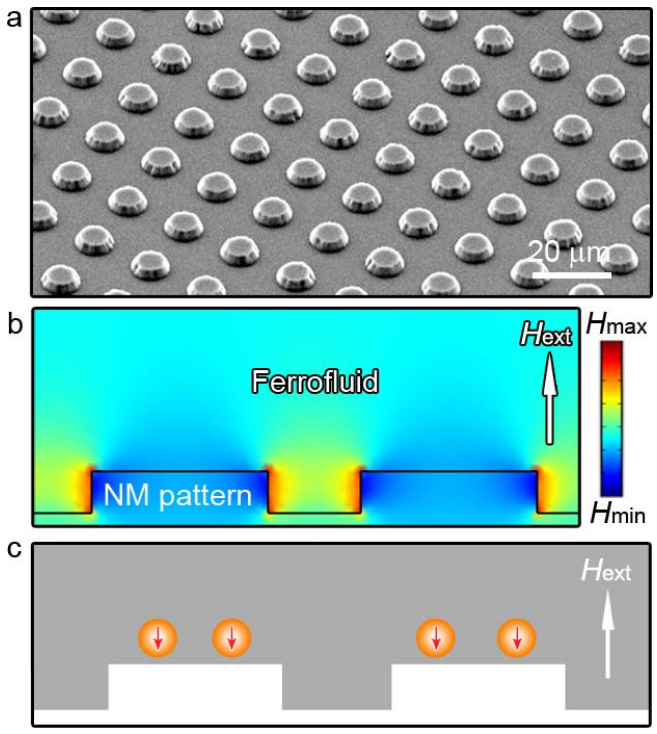

Figure 6.1. a) SEM image of a typical cone frustum type polyurethane pattern with the top diameter D_1 of 5.5 μm, the bottom diameter D_2 of 9.5 μm and the height h of 2.25 μm. b) Simulated cross-sectional magnetic field distribution around the nonmagnetic pattern immersed in a magnetized ferrofluid. c) Assembly scheme of nonmagnetic objects immersed in the ferrofluid on the nonmagnetic patterned surface. The arrows in the spheres indicate the direction of the magnetic moment. Reproduced with permission from Ref. 32 @ 2013 American Chemical Society.

Experimentally, we first demonstrate our assembly principle for the organization of colloidal microspheres with different diameters above patterned conical frustum structures with a top diameter D_1 of 5.5 μm, bottom diameter D_2 of 9.5 μm and height h of 2.25 μm (**Figure 6.2**). A polymer bead with diameter d of 6.5 μm is positioned above each frustum to form an ordered non-close-packed monolayer structure in the external magnetic field as the ratio of the particle diameter to the top diameter of the pattern d/D_1 is larger than 1 (**Figure 6.2a**). Due to the relatively large interparticle separation, assembly is dominated by the interaction between the templates and the spheres. However, the interparticle interaction cannot be ignored for larger particles. We occasionally observed the slight off-centering of spheres due to the strong magnetic and electrostatic repulsive force from a nearby larger sphere, such as the one with a diameter of 8.4 μm indicated by the arrow in **Figure 6.2a**. For smaller beads, colloidal clusters with different structures can be formed by controlling the concentration of particles and/or the d/D_1 value. Taking 4.5-μm beads for example, owing to the magnetic and electrostatic repulsive force between the particles when they are located above the same frustum, they tend to occupy as many platforms as possible at low concentrations (**Figure 6.2b**). Increasing the particle concentration leads to the formation of dimeric and trimeric clusters in the same magnetic field (**Figures 6.2c**, **6.2d**).

Compared to prior studies involving particle assembly in confined spaces, the magnetic route developed here allows additional control over the cluster size by tuning the concentration of the beads when other parameters are fixed.[11, 13] Interestingly, the assemblies confined above the relief patterns remain dynamic and we were often able to observe the replacement of component beads by others moving along the flow direction. As shown in Figure 2e, when an additional bead hit a trimeric cluster which had been positioned on the frustum, an unstable tetramer formed which quickly "ejected" another bead to return to the stable trimer configuration. As the size ratio between bead and pattern is further decreased, more beads can be deposited on top of each frustum. **Figures 6.2f** and **6.2g** show the cluster structures formed by magnetic assembly of 1.5-μm mercapto-silica (MPS) colloidal beads on the same frustum, followed by drying. It is clear that our magnetic assembly strategy is capable of rapidly assembling various micro-objects on topologically patterned surfaces without the need for complicated pretreatment to introduce special chemical, electric, or magnetic components to these objects to enable assembly.

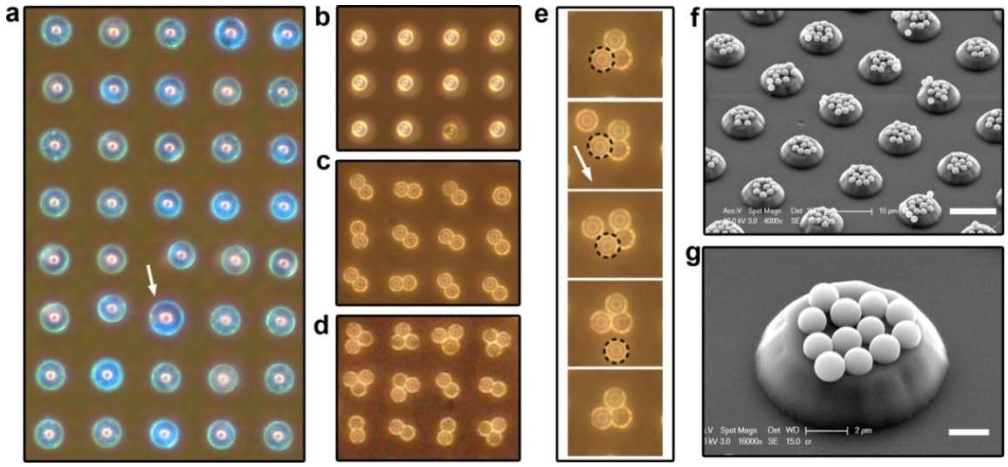

Figure 6.2. Assembly of microbeads above nonmagnetic relief patterns. a) Dark-field optical microscopy image showing monolayer structure with one bead occupying each template from an aqueous suspension of 6.5-μm nonmagnetic beads (1% volume fraction) and ferrofluid (2% volume fraction of Fe_3O_4 nanoparticles). The arrow shows the off-centering of beads around an 8.4-μm bead. b-d) Dark-field optical microscopy images showing different structures from an aqueous suspension of 4.5-μm nonmagnetic beads (0.5 % for **b**, 1% for **c**, 1.5% for **d** and **e**, volume fraction) and ferrofluid (2% volume fraction). e) Dynamic replacement of beads above the template along the flow direction (shown with the arrow). f-g) SEM images showing the structure obtained by magnetic assembly of 1.5-μm nonmagnetic beads (1% volume fraction) in the ferrofluid (2% volume fraction) after drying. The scale bars are 10 μm for **f** and 2 μm for **g**. All the images used the same pattern shown in **Figure 6.1a**. Reproduced with permission from Ref. 32 @ 2013 American Chemical Society.

As demonstrated above, the assembly behavior is determined by the local magnetic field distribution which is affected by several parameters including the feature size, shape, and aspect ratio of the patterns. To understand how these parameters contribute to the modulation of the magnetic field, we first simulate the two-dimensional magnetic field distribution around three typical trapezoid shaped patterns with the same height (**Figure 6.3**). Although a similar trend can be observed for all three patterns, in that the magnetic field is weakened on the top of the feature, the spatial distribution of the magnetic field and thereby the location of the energy wells is different. For quantitative comparison, we plot the magnetic field norm at different heights above the pattern (**Figures 6.3a-c**). For the pattern with the smallest diameter, there is only one apparent magnetic field minimum which is located at the center of each feature (**Figure 6.3a**). However, for the larger patterns, the magnetic field minimum splits into two symmetric points located near the edges of the feature at a height of 1 μm (**Figures 3b, 3c**). The location of the magnetic field minimum gradually moves towards the center and the depth of the energy well, or the contrast of magnetic field strength, decreases when moving away from the pattern surface. Under the simulated conditions, the magnetic field strength difference is less than 2% of the applied magnetic field at a position 8 μm high above the pattern surface. Therefore, the modulation of the magnetic field effectively occurs near the edges of the conical-frustum-shaped patterns. When the

feature is small (small D_1), the magnetic fields at the two edges interfere with each other such that the field minimum merges and appears in the center area. The transition for the magnetic field splitting occurs at a D_1 value of 9 μm if one examines the magnetic field distribution at positions 2 μm above the pattern surface. Since an initially free moving object dispersed in the ferrofluid would be trapped in the magnetic field minimums, modulation of the size and shape of the patterns allows one to control the location and assembly behavior of these objects. As shown in **Figures 6.3d-f**, the simulated magnetic field distribution can be experimentally confirmed by the placement of beads in the field minimums created above three patterns with different thicknesses. The beads are trapped above the center of the smallest pattern while they are trapped near the edge of the larger patterns.

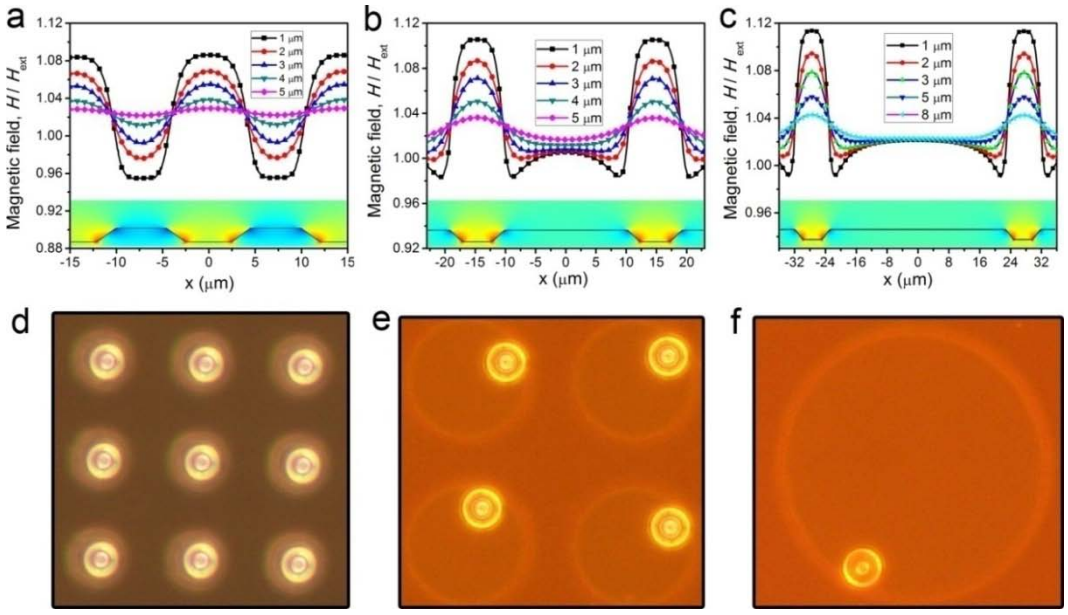

Figure 6.3. a-c) Simulated cross-section magnetic field distribution and plots of magnetic strengths at different heights around frustum-shaped relief patterns exposed to ferrofluids in a uniform vertical external magnetic field. The parameters for the patterns are: (**a**) top diameter D_1=5.5 μm, bottom diameter D_2=9.5 μm and height h=2.25 μm; **(b)** D_1=20.5 μm, D_2=24.5 μm and h=2.25 μm; (**c**) D_1=46 μm, D_2=50 μm and h=2.25 μm. d-f) Dark-field optical microscopy images showing magnetic trapping of nonmagnetic beads above relief patterns of various sizes. The beads are trapped at the center of the relatively small patterns (**d**), while they are positioned at the edge of the patterns (**e,f**) when the lateral dimension of the patterns increases. The diameters of beads are 4.5 μm in (**d**), and 6.2 μm in (**e**) and (**f**). Reproduced with permission from Ref. 32 @ 2013 American Chemical Society.

We have also studied the effect of the D_1/D_2 ratio of the frustum pattern on the assembly behavior (**Figure 6.4**). We found that at a fixed height, a single feature with a large D_1/D_2 value generates a deeper energy well at its top, so that the trapping effect is stronger from a thermodynamics point of view (**Figure 6.4c**). However, kinetically, the existence of the magnetic field maximum at the top edge of the same pattern may create an energy barrier for particles moving from the bottom area towards the top region. In contrast, the field distribution for the pattern with a small D_1/D_2 value drives more efficient repositioning of particles, particularly for lifting particles from the bottom area to the top surface of the pattern (see arrow in **Figure 6.4a**). For patterns with the same slope and aspect ratio, larger patterns modulate the magnetic field distribution over a greater range, leading to a more significant trapping effect (**Figures 6.4d, 6.4e**). For three cylindrical patterns, the smallest pattern (height = 3 μm) effectively modulates the field gradient within 8 μm from the top surface. On the other hand, the range of modulated magnetic field around the largest pattern (height = 9 μm) can reach as far as 24 μm. It is worth noting that the concentration of the ferrofluid and the strength of the applied magnetic field also play important roles in determining the relative depth of the energy wells. The direction of the external magnetic field is also critical, but in order to simplify the study we limit our discussion here to the vertical direction in all cases.

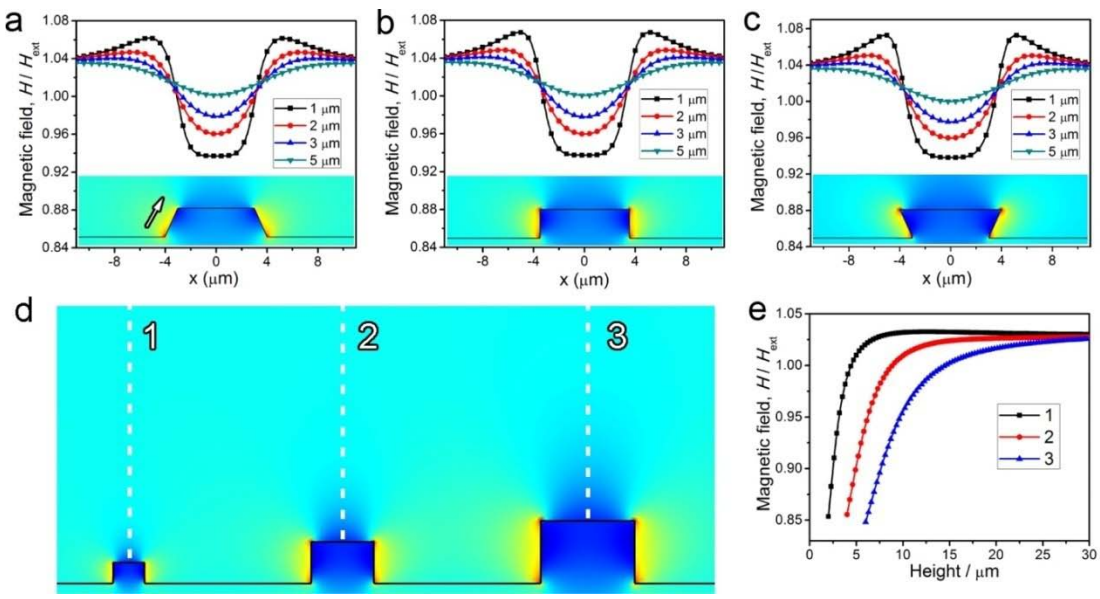

Figure 6.4. Effect of pattern shape and height. a-c) Simulated magnetic field distribution around differently shaped frustum patterns and the corresponding plots of magnetic field at different heights above the upper surfaces of the patterns. The arrow in (**a**) shows the field gradient near the pattern edge that drives the movement of beads from the bottom to the top surface. d) Simulated magnetic field distribution around different cylinder type patterns with the same aspect ratio (D_1=D_2= 3 μm, h=2 μm for the left pattern; D_1=D_2= 6 μm, h=4 μm for the middle pattern; D_1=D_2= 9 μm, h=6 μm for the right pattern). e) Plots showing the magnetic field strengths above the center of each pattern (dotted lines). The height is defined as the distance from the bottom surface. Reproduced with permission from Ref. 32 @ 2013 American Chemical Society.

Assembly of submicron beads under similar conditions leads to the formation of many one-dimensional chains, each containing a string of beads, in the magnetic field minimum created by the relief pattern. When uniform beads are used, 1D periodicity can be achieved, leading to strong optical diffraction if the periodicity is comparable to the wavelength of visible light.[33, 37] Improved from our previous systems for the assembly of photonic structures in bulk dispersions, it is now possible to confine the assembly of beads to particular positions through the relief patterns printed on the substrate, thus providing great opportunities for achieving high-resolution field-responsive color expression.[33] In **Figure 6.5**, we demonstrate the magnetic assembly of nonmagnetic polystyrene beads on the medium and large patterns. Similar to the assembly of microspheres, the submicrometer beads are preferentially trapped above the edges of the patterned features. The interparticle dipole-dipole attractive force, which is balanced by the electrostatic repulsion, induces chaining of the submicrometer beads with regular spacing along the direction of the magnetic field. Owing to the periodicity, the dynamic chains diffract visible light in a manner that can be described by Bragg's law

$$m\lambda = 2nd\sin\theta \quad (4)$$

where m is the diffraction order, λ is the wavelength of incident light, n is the effective refractive index, d is the lattice spacing, and θ is the glancing angle between the incident light and the chain norm.[38] By using latex particles with different diameters, different

color patterns can be obtained. Since the particle chains have only one translational order, switching between the assembled and disassembled states is instantaneous and fully reversible. Moreover, the assembled structures are very stable in a fixed magnetic field, suggesting great potential for field-responsive color display. Color patterns with other geometric shapes and arrangements can be produced simply by controlling the structural design of the relief patterns (**Figure 6.6**). By increasing the concentration of the latex particles, we can tune the assembled structures from 1D chains (**Figure 6.6a**) to many large 3D crystal domains (**Figure 6.6b**) with enhanced diffraction intensity, which is consistent with our earlier studies.[33] The localized assembly follows the nature of the relief structures printed in the substrate, as demonstrated in **Figures 6.6b-c** by the assembly of photonic structures above the original and inverse circular patterns. More complicated color patterns can be obtained by increasing the complexity in the substrates, as shown in an example in Figure **6.6d**, suggesting the great potential of this general assembly strategy for modulating structural color through the design of corresponding nonmagnetic patterns.

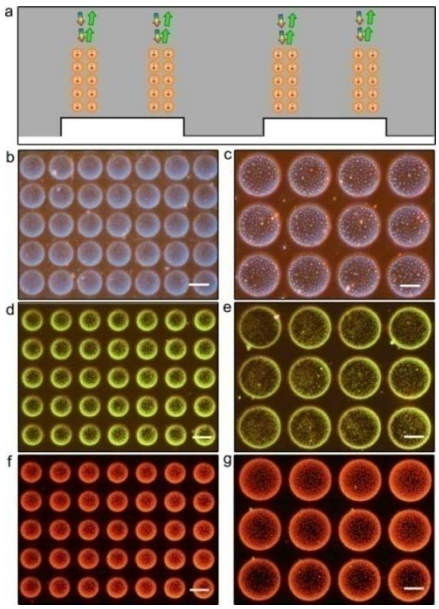

Figure 6.5. Assembly of colloidal beads into patterned photonic chains. a) Schematic illustration of the chaining of nonmagnetic beads above the edge area of the nonmagnetic patterns. The periodicity in the chains leads to optical diffraction so that they display structural colors. b-g) Various structural colored patterns formed by assembling different sized PS beads on circular relief patterns: (**b, c**) blue chains from 166-nm beads; (**d, e**) green chains from 188-nm beads; and (**f, g**) red chains from 210-nm beads. The volume fraction of PS beads is 1% and that of Fe_3O_4 nanoparticles 3%. A medium-sized frustum pattern (D_1 of 20.5 μm, D_2 of 24.5 μm and height h of 2.25 μm) was used for **b**, **d** and **f**. A large frustum pattern (D_1 of 46 μm, D_2 of 50 μm and height h of 2.25 μm) was used for **c**, **e** and **g**. The scale bars are 20 μm for all images. Reproduced with permission from Ref. 32 @ 2013 American Chemical Society.

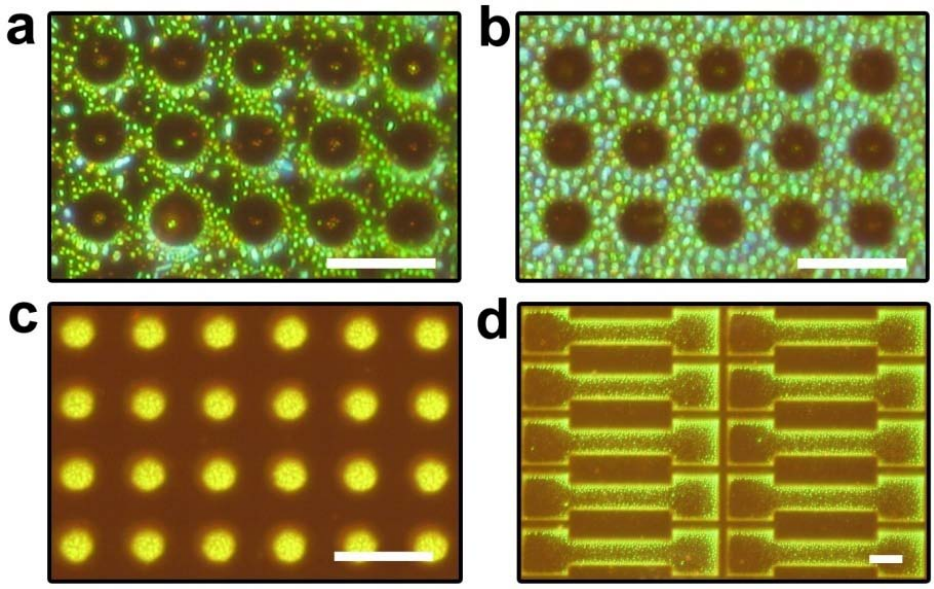

Figure 6.6. Structural Color Patterning by Nonmagnetic Templates. a-b) Photonic structures formed by assembling 188-nm nonmagnetic PS beads in a ferrofluid (2% volume fraction of Fe_3O_4 nanoparticles) above circular PDMS hole patterns: **(a)** 1D photonic chains when the volume fraction of PS beads is 1%; **(b)** 3D photonic crystal domains when the volume fraction of PS beads is 4%. c) 3D photonic structures assembled from 188-nm PS beads (volume fraction of 3%) above a circular relief pattern. d) More complex structural colored pattern formed by assembling PS beads on dumbbell-shaped templates. The scale bars are 20 μm for all images. Reproduced with permission from Ref. 32 @ 2013 American Chemical Society.

6.4 Patterned Assembly of Superparamagnetic Photonic Labyrinth Structures

To further demonstrate the universality of our nonmagnetic-template-assisted magnetic assembly strategy, we studied the patterned assembly of uniform superparamagnetic Fe_3O_4 colloidal nanocrystal clusters (CNCs) into photonic labyrinth structures.[39] The suspension of the Fe_3O_4 CNCs itself now serves as the "ferrofluid" and the modulation of local magnetic fields is essentially the same as in above case. As shown in **Figure 6.7b**, the magnetic field is strongest around the side of the pattern and weakest on the top. In addition, the influence of the nonmagnetic pattern decreases with increased distance in the perpendicular direction. Since the change of magnetic strength can in turn induce the change of CNC particle distribution, the Fe_3O_4 CNCs thus prefer to stay close to the side of nonmagnetic pattern (as illustrated in **Figure 6.7c**), which has been confirmed by both optical microscopy and SEM characterization. As shown in **Figure 6.7d**, a bright photonic labyrinth structure formed upon application of a strong magnetic field (~ 1500 G). Interestingly, the as-obtained labyrinth structure is substantially different from that obtained by using a flat substrate, in which long and linear labyrinth is the dominant morphology. Instead, short arc-shaped labyrinths are formed around the patterns, as shown in **Figure 6.7e**.

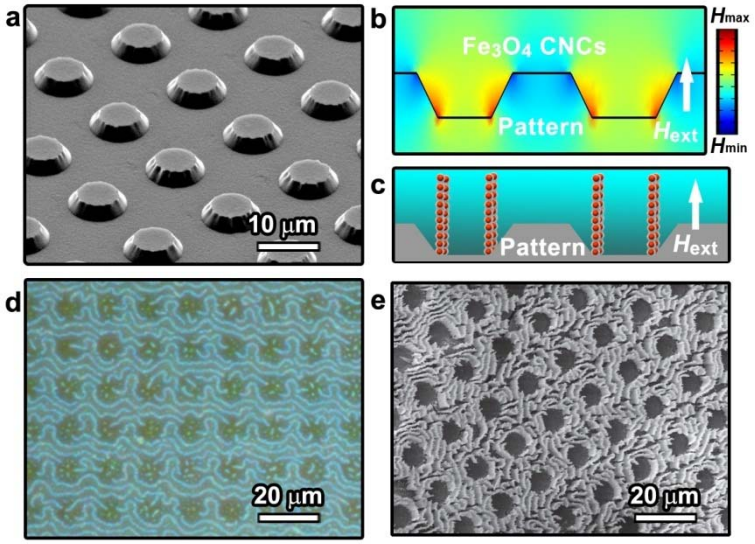

Figure 6.7. a) SEM image of a typical cone frustume polyurethane pattern with the top diameter D_1 of 5.5 μm, the bottom diameter D_2 of 9.5 μm, and the height h of 2.25 μm. b) Simulated cross-sectional magnetic field distribution around the nonmagnetic pattern exposed to a magnetized dispersion of CNCs. The color bar indicates the relative strength of the local magnetic field and applies for the whole article. c) Assembly scheme of Fe_3O_4@SiO_2 CNCs on the nonmagnetic patterned surface. The arrow in the scheme shows the direction of the magnetic moment. d) Optical microscopy image of patterned photonic labyrinth structures assembled from 20 mg/mL of Fe_3O_4@SiO_2 CNCs. e) The corresponding SEM image. Reproduced with permission from Ref. 38 @ 2013 American Chemical Society.

The requirements for the formation of a 2D labyrinth structure include a relatively high magnetic field strength and a high local volume fraction of colloidal magnetic particles. Since the introduction of a non-magnetic pattern can induce a local magnetic field gradient and thereby a particle concentration gradient, it can significantly lower the required magnetic field strength and volume fraction of magnetic particles in the bulk fluid. Without a patterned substrate, a 1500 G magnetic field is needed to induce the formation of a labyrinth structure (with final particle concentration ~ 20 mg/mL), while an 800 G magnetic field is sufficient to induce the labyrinth formation on the patterned substrate. When the concentration of Fe_3O_4 CNCs is low (with final concentration ~ 5 mg/mL), no labyrinth structure can be formed on flat substrate even under strong magnetic field (~ 2700 G) but this becomes possible when a patterned substrate is used for assembly. As shown in **Figures 6.8a** and **6.8b**, when the concentration of Fe_3O_4 CNCs is around 5 mg/mL, a single ring like structure can form around each pattern. As depicted in Figures **6.8c** and **6.8d**, when the concentration is increased to 15 mg/mL, the number density of labyrinth structures around the patterns is increased. Short labyrinth structures can occasionally be observed atop the patterns, as the sides have been fully occupied. When the final concentration of Fe_3O_4 CNCs is further increased to 28 mg/mL, as shown in **Figure 6.8e-f**, both the sides and the tops of the patterns are occupied by labyrinth structures.

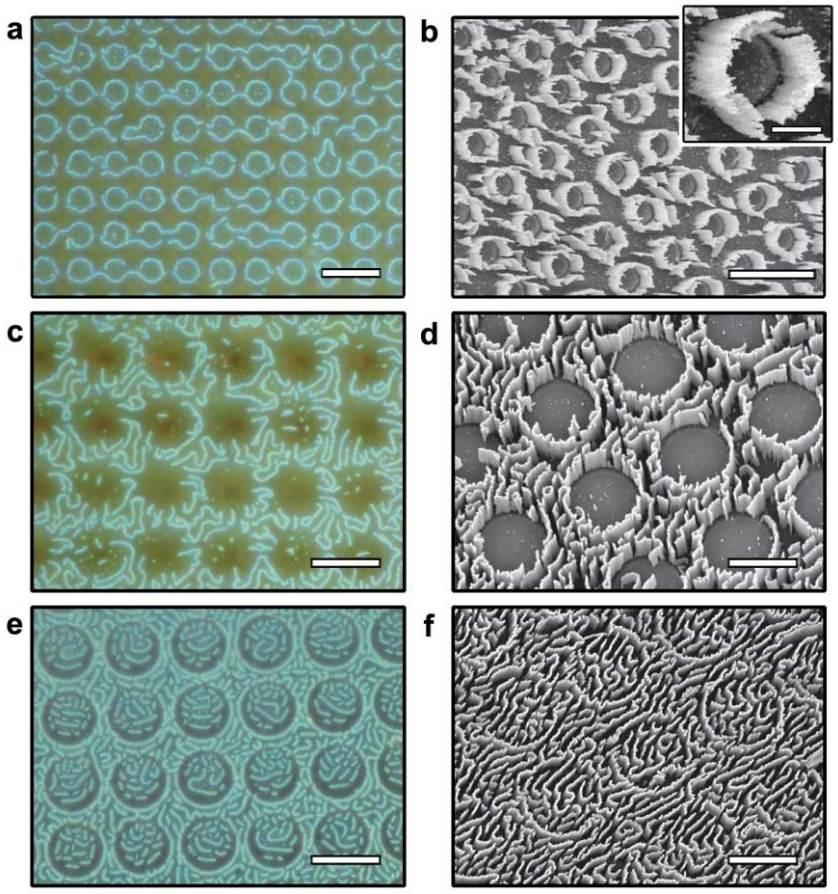

Figure 6.8. Dark-field optical microscopy and corresponding SEM images of patterned photonic labyrinth structures formed by assembling (a, b) 5 mg/mL of Fe_3O_4@SiO_2 CNCs against small sized patterns (D_2 = 9.5 μm with h = 2.25 μm); (c, d) 15 mg/mL of Fe_3O_4@SiO_2 CNCs against medium sized patterns (D_2 = 25 μm with h = 2.25 μm), and (e, f) 28 mg/mL of Fe_3O_4@SiO_2 CNCs against medium sized patterns. All scale bars are 25 μm, except for the inset (5 μm). Reproduced with permission from Ref. 38 @ 2013 American Chemical Society.

Since the local magnetic field distribution can be modulated by the presence of non-magnetic patterns, here we use square-shaped patterns as the model systems to precisely manipulate the 2D dynamic self-assembly by systematically tuning the sizes of the nonmagnetic features. The side lengths of the three patterns are 8 μm, 25 μm, and 50 μm, respectively. As shown in the simulated field distribution profile in **Figures 6.9a-c**, despite the fact that the field is significantly enhanced at the side of all the patterns, the extent of field attenuation on top of the patterns is different when the size of the pattern changes. For the smallest pattern with side length of 8 μm, the field strength at the pattern surface is greatly lower than that in the bulk solution (**Figure 6.9a**), so that particles do not tend to assemble on top of the patterns. As shown in **Figures 6.9d** and **6.9g**, when 20-mg/mL CNCs are assembled against the small patterns, photonic labyrinth structures can be observed everywhere on the substrate but the top area of the squares. When the side length of the squares is increased to 25 μm, the magnetic field only slightly attenuated at the central area of the pattern surface (**Figure 6.9b**), making it likely to form labyrinth structure on top of the patterns. As suggested in **Figures 6.9e** and 6.9**h**, the majority of labyrinth structures are formed around the patterns, while some short labyrinth structures can be observed on top of the patterns. In the case of 50-μm sized square patterns, the local magnetic field on the pattern surface is not influenced by the presence of pattern except for the area near the edges (**Figure 6.9c**), implying a high

likelihood of formation of labyrinth structures in the central area, which has been confirmed by the experimental results. As shown in **Figures 6.9f** and **6.9i**, labyrinth structures are obtained on both the top of patterns and in non-patterned areas. However, one can clearly notice a gap between the two regions, which is caused by the minimum magnetic field within the edges of the square patterns. Additionally, an interesting feature of the template-directed assembly is that the labyrinth structures tend to align themselves by surrounding the patterns, while the labyrinth structures atop the patterns are randomly oriented. By varying the shapes of the nonmagnetic patterns, many different types of 2D photonic labyrinths can be readily obtained. The above results clearly demonstrate the successful magnetic manipulation of the 2D superparamagnetic photonic labyrinth structures guided by the nonmagnetic templates.

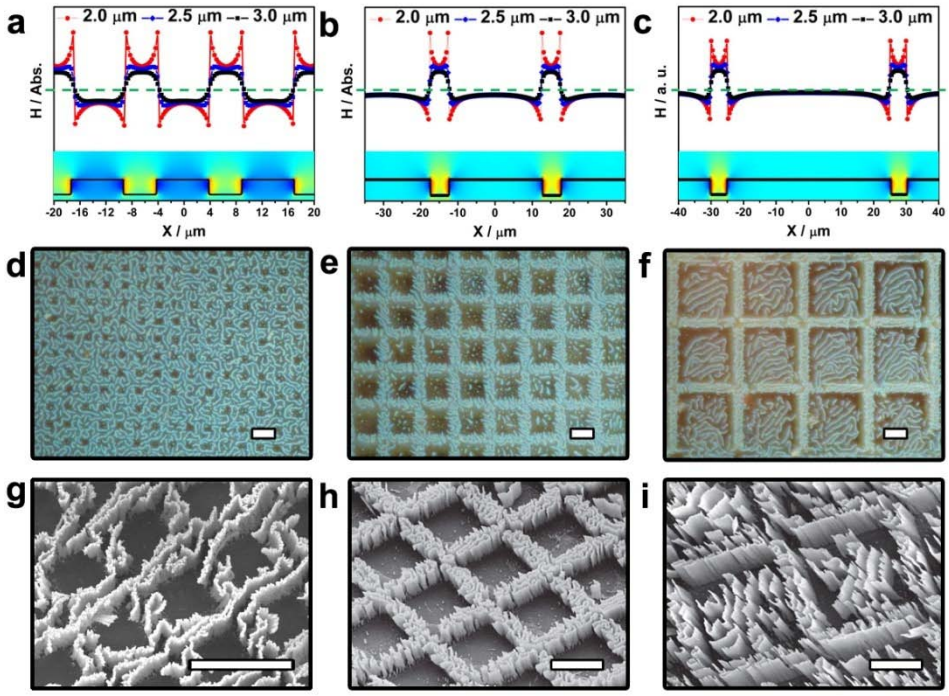

Figure 6.9. a-c) Simulated cross-sectional magnetic field distribution at different heights above three differently sized patterns when they are exposed to dispersions of Fe_3O_4@SiO_2 CNCs in a uniform vertical external magnetic field: (a) small pattern with side length of 8 μm; (b) medium pattern with side length of 25 μm; (c) large pattern with side length of 50 μm. The height *h* is 2.25 μm for all the patterns. d-f) Dark-field optical microscopy images of photonic labyrinths formed by assembling 20 mg/mL of Fe_3O_4@SiO_2 CNCs against the different sized patterns, and (g-i) corresponding SEM images. All scale bars are 20 μm. Reproduced with permission from Ref. 38 @ 2013 American Chemical Society.

6.5 Conclusion

In conclusion, we have developed a general yet effective approach for assembling and patterning colloidal structures with micron-scale resolution by taking advantage of the magnetic interactions between nonmagnetic objects when they are immersed in a magnetized ferrofluid. Owing to the difference in magnetization, the nonmagnetic templates exposed to ferrofluid behave as “reverse magnets” which modulates the spatial distribution of the magnetic fields and induce a large field gradient locally even in a uniform external magnetic field. We first demonstrated the application of this strategy for the patterned assembly of nonmagnetic colloidal particles into different structures. The efficient local magnetic field modulation has wide applications in the fabrication of novel devices, formation of complex structures and magnetic control of optical, electric or photonic properties. As an example, we also demonstrated the organization of submicrometer colloidal beads into patterned photonic structures, which can be directly used as a high resolution field-responsive color display. Finally, we demonstrated the universal application of this strategy for the patterned assembly of magnetic particles. As the nonmagnetic templates can be readily and rapidly fabricated at low lost, our method enhances the applicability and scalability of magnetic assembly routes for the fabrication of patterned functional structures from a large variety of nonmagnetic and magnetic nanoscale building blocks.

6.6 References

(1) Pusey, P. N.; van Megen, W. *Nature* **1986**, *320*, 340.

(2) Yethiraj, A.; van Blaaderen, A. *Nature* **2003**, *421*, 513.

(3) Kamenetzky, E. A.; Magliocco, L. G.; Panzer, H. P. *Science* **1994**, *263*, 207.

(4) Velev, O. D.; Lenhoff, A. M.; Kaler, E. W. *Science* **2000**, *287*, 2240.

(5) Xia, Y. N.; Gates, B.; Yin, Y. D.; Lu, Y. *Adv. Mater.* **2000**, *12*, 693.

(6) Talapin, D. V.; Shevchenko, E. V.; Bodnarchuk, M. I.; Ye, X. C.; Chen, J.; Murray, C. B. *Nature* **2009**, *461*, 964.

(7) Yin, Y.; Xia, Y. *Adv. Mater.* **2001**, *13*, 267.

(8) Dinsmore, A. D.; Hsu, M. F.; Nikolaides, M. G.; Marquez, M.; Bausch, A. R.; Weitz, D. A. *Science* **2002**, *298*, 1006.

(9) Yin, Y.; Lu, Y.; Gates, B.; Xia, Y. *J. Am. Chem. Soc.* **2001**, *123*, 8718.

(10) Xu, W.; Sims, C. E.; Allbritton, N. L. *Anal. Chem.* **2010**, *82*, 3161.

(11) Xia, Y.; Yin, Y.; Lu, Y.; McLellan, J. *Adv. Funct. Mater.* **2003**, *13*, 907.

(12) Yin, Y.; Xia, Y. *J. Am. Chem. Soc.* **2003**, *125*, 2048.

(13) Lee, I.; Zheng, H.; Rubner, M. F.; Hammond, P. T. *Adv. Mater.* **2002**, *14*, 572.

(14) Dziomkina, N. V.; Hempenius, M. A.; Vancso, G. J. *Adv. Mater.* **2005**, *17*, 237.

(15) Velev, O. D.; Gupta, S. *Adv. Mater.* **2009**, *21*, 1897.

(16) Li, F.; Josephson, D. P.; Stein, A. *Angew. Chem. Int. Ed.* **2010**, *50*, 360.

(17) Erb, R. M.; Son, H. S.; Samanta, B.; Rotello, V. M.; Yellen, B. B. *Nature* **2009**, *457*, 999.

(18) Zerrouki, D.; Baudry, J.; Pine, D.; Chaikin, P.; Bibette, J. *Nature* **2008**, *455*, 380.

(19) Xu, X. L.; Friedman, G.; Humfeld, K. D.; Majetich, S. A.; Asher, S. A. *Adv. Mater.* **2001**, *13*, 1681.

(20) Xu, X. L.; Majetich, S. A.; Asher, S. A. *J. Am. Chem. Soc.* **2002**, *124*, 13864.

(21) Ge, J. P.; Lee, H.; He, L.; Kim, J.; Lu, Z. D.; Kim, H.; Goebl, J.; Kwon, S.; Yin, Y. D. *J. Am. Chem. Soc.* **2009**, *131*, 15687.

(22) Ge, J. P.; Hu, Y. X.; Yin, Y. D. *Angew. Chem. Int. Ed.* **2007**, *46*, 7428.

(23) Ge, J. P.; He, L.; Goebl, J.; Yin, Y. D. *J. Am. Chem. Soc.* **2009**, *131*, 3484.

(24) Ge, J.; Hu, Y.; Zhang, T.; Huynh, T.; Yin, Y. *Langmuir* **2008**, *24*, 3671.

(25) Ge, J.; Yin, Y. *Adv. Mater.* **2008**, *20*, 3485.

(26) He, L.; Hu, Y.; Han, X.; Lu, Y.; Lu, Z.; Yin, Y. *Langmuir* **2011**, *27*, 13444.

(27) Mirica, K. A.; Ilievski, F.; Ellerbee, A. K.; Shevkoplyas, S. S.; Whitesides, G. M. *Adv. Mater.* **2011**, *23*, 4134.

(28) Yellen, B.; Friedman, G.; Feinerman, A. *J. Appl. Phys.* **2003**, *93*, 7331.

(29) Helseth, L. E.; Wen, H. Z.; Hansen, R. W.; Johansen, T. H.; Heinig, P.; Fischer, T. M. *Langmuir* **2004**, *20*, 7323.

(30) Yellen, B. B.; Friedman, G. *Langmuir* **2004**, *20*, 2553.

(31) Yellen, B. B.; Hovorka, O.; Friedman, G. *Proc. Natl. Acad. Sci. USA* **2005**, *102*, 8860.

(32) He, L.; Wang, M.; Zhang, Q.; Lu, Y.; Yin, Y. *Nano Lett.* **2013**, *13*, 264.

(33) He, L.; Hu, Y.; Kim, H.; Ge, J.; Kwon, S.; Yin, Y. *Nano Lett.* **2010**, *10*, 4708.

(34) Xia, Y. N.; Whitesides, G. M. *Angewandte Chemie-International Edition* **1998**, *37*, 551.

(35) Skjeltorp, A. T. *Phys. Rev. Lett.* **1983**, *51*, 2306.

(36) Ge, J.; He, L.; Hu, Y.; Yin, Y. *Nanoscale* **2010**, *3*, 177.

(37) Ge, J.; Yin, Y. *Angew. Chem. Int. Ed.* **2011**, *50*, 1492.

(38) Leal Calderon, F.; Stora, T.; Mondain Monval, O.; Poulin, P.; Bibette, J. *Phys. Rev. Lett.* **1994**, *72*, 2959.

(39) Zhang, Q.; Janner, M.; He, L.; Wang, M.; Hu, Y.; Lu, Y.; Yin, Y. *Nano Lett.* **2013**, *13*, 1770.

Chapter 7

Conclusion and Outlook

7.1 Conclusion of This Dissertation

Over several decades, there are immediate practical interests in the development of smart materials, which have one or more properties that can be significantly changed in a controlled fashion by external stimuli, such as temperature, stress, moisture, electric or magnetic fields. Responsive photonic bandgap materials, or more commonly known as responsive photonic crystals, which can remotely change their structural colors in response to the external stimuli, have important applications in areas such as color displays, biological and chemical sensors, inks and paints, or many optically active components.[1] Compared with conventional optical lithography methods based on top-down strategy, colloidal assembly are technologically favorable due to mild processing conditions, low cost, ease manipulation in three dimensions and potential for scale-up.[2, 3] It is also more convenient to modify the building blocks before or after the formation of crystal structures to enable responsiveness to a given stimulus.

Despite the development of different types of colloidal responsive photonic systems, wide use of these systems in practical applications is hampered by low fabrication

efficiency, limited tunability of the band gap (with peak position changes typically in the range of tens of nanometers), a slow response to the external stimuli (typically several minutes to a few hours), and difficulty of integration into existing photonic systems. To broaden the tuning range of diffraction color, the external stimulus must be able to induce large changes in either the refractive index of the components, or the symmetries, lattice parameters or orientations of the ordered arrays. New mechanisms need to be established to also significantly enhance the response rate of the active components to the external stimuli in order to offer dynamic optical modulation that can meet the demand of practical applications.

Through magnetic assembly route, we attempted to develop new types of responsive photonic nanostructures with improved fabrication efficiency, rapid response, and wide tunability of the band gap.[4-8] We have demonstrated the rapid assembly of superparamagnetic colloidal particles into various photonic nanostructures, from 1D chains to 2D labyrinths and 3D colloidal crystals.[9, 10] We have also demonstrated that an external magnetic field can be used as an effective stimulus to manipulate the photonic properties of the self-assembled nanostructures by affecting the lattice constant, the orientation, or the crystal structures.[8, 11] The magnetically responsive photonic system provides a new platform for various chromatic applications.[12-18]

To further exploit the magnetic assembly strategy, we studied the assembly behavior

of superparamagnetic Fe_3O_4@SiO_2 colloids in complex magnetic fields and demonstrated that a horizontal magnetic field sandwiched between two vertical fields would allow one to change the orientation of the particle chains, producing a high contrast in color patterns.[19] Our study not only demonstrates the great potential of magnetically responsive photonic structures in the visual graphic applications such as signage and security documents but also points out the potential challenge in pattern stability when the particle assemblies are subjected to complex magnetic fields that often involve large field gradients.

Experimental demonstration of the rich phase diagram in the suspensions of magnetically dipolar spheres is highly desired to verify the theoretical predictions and fabricate new types of colloidal superstructures. In the second stage, we demonstrate magnetically induced phase transitions of superparamagnetic particle suspensions from colloidal fluids to 1D dipolar chain structures, 2D hexagonal sheets, and finally 3D structures.[9, 10] Our studies clearly demonstrate that the suspensions of superparamagnetic colloids are not only suitable model systems for study the fundamental aspects of colloidal assembly but also can be used to fabricate various types of colloidal photonic nanostructures.

Thanks to the correlation between the photonic response and the interparticle distance, we also demonstrate that the use of magnetically responsive photonic

assemblies for studying fundamental problems about colloidal interactions. As an example, we take advantage of the optical response of the core-shell magnetic colloids in magnetic fields to study the thickness of solvation layers formed when the colloidal silica surface is covered by different solvents.[20] By selectively screening the electrostatic force, the neighboring particles interact with each other through the repulsion resulting from the overlap of solvation layers, which balances the magnetically induced attraction and forms ordered assemblies. The thickness of solvation layer can be then estimated by using Bragg's law. A relationship between the hydrogen-bonding ability of the solvents and the thickness of solvation layer on Fe_3O_4@SiO_2 colloidal surface has been identified, which is consistent with the prior understanding of a hydrogen-bonding origin of the solvation force. It is believed this magneto-photonic method represents a simple yet very effective tool for studying many types of short-range colloidal interactions including not only the solvation forces between various surfaces but also the steric effects which are fundamentally critical to chemistry, biochemistry and pharmacology.

As there are many more choices for nonmagnetic colloidal particles with uniform size and optimal refractive index, it would be advantageous to extend this magnetic assembly strategy to nonmagnetic particles to allow their rapid assembly into large-area photonic crystals with high quality. Conventionally, magnetic assembly of nonmagnetic materials is achieved by modifying these building blocks with magnetic materials, which

apparently limits the choices of materials and the applicability of the processes. In our work, we demonstrated the use of nanocrystal-based ferrofluids to direct the assembly of nonmagnetic colloidal particles into photonic crystal structures.[21] The process is general, efficient, convenient, and scalable and thus represents a new and practical platform for the fabrication of colloidal crystal-based photonic devices.

In principle, magnetic manipulation of nanoscale objects can provide precise control over their local arrangement and properties if the external magnetic field can be modulated. However, the ordered assembly is typically achieved by using magnetic micro-patterns, for which the downside is that they require advanced micro-fabrication techniques to produce, adding significant challenges for device fabrication and integration. Based on our improved understanding of magnetic assembly, we have developed a general strategy that allows convenient magnetically-driven assembly of general objects in defined locations with high spatial resolution.[22] The process involves immersing a polymer relief pattern in a uniformly magnetized ferrofluid, which modulates the local magnetic fields around the pattern. Nonmagnetic target objects dispersed in the same ferrofluid can then be magnetically assembled at positions defined by the polymer pattern. We also demonstrated the universal application of this strategy for the patterned assembly of magnetic particles. As the nonmagnetic polymer patterns can be conveniently fabricated at low cost through photolithography and soft-lithography

processes, our method provides a general yet very effective means to assemble a wide range of nonmagnetic objects with controlled spatial distribution, paving the way towards patterning functional microstructures.

7.2 Outlook and Future Work.

With the development of nanotechnology, people will be able to design and control the magnetic fields more precisely and rapidly through a computer. With the ability of pixel-level manipulation of local magnetic fields in parallel, the magnetically responsive photonic system can widely used in high-resolution field-responsive color display. Through the creation of bi-stability of the system so that an energy input is only needed for color changing, it is possible to realize energy-saving reflective color display, which can replace the current black-white versions of E-ink based kindles . Many applications will be developed, including but not limited to active color display, structural color printing, anti-counterfeiting, security, camouflage, and information storage.

Future work will be focused on the optimization of the assembly efficiency, response rate, optical tuning range and the quality of the photonic nanostructures. The study of 2D responsive structures remains a challenge, but may lead to many interesting results. Another important direction is the miniaturization of the responsive system to the micrometer scale, which would allow pixel-level control of photonic properties in parallel towards real display applications.

7.3 References

(1) Ge, J; Yin, Y. *Angew. Chem. Int. Ed.* **2011**, *50*, 1492.

(2) Li, F.; Josephson, D. P.; Stein, A. *Angew. Chem. Int. Ed.* **2011**, *50*, 360.

(3) Ozin, G. A.; Hou, K.; Lotsch, B. V.; Cademartiri, L.; Puzzo, D. P.; Scotognella, F.; Ghadimi, A.; Thomson, J. *Mater. Today* **2009**, *12*, 12.

(4) Ge, J.; He, L.; Goebl, J.; Yin, Y. *J. Am. Chem. Soc.* **2009**, *131*, 3484.

(5) Ge, J.; He, L.; Hu, Y.; Yin, Y. *Nanoscale* **2011**, *3*, 177.

(6) Hu, Y.; He, L.; Yin, Y. *Angew. Chem. Int. Ed.* **2011**, *50*, 3747.

(7) Hu, Y.; He, L.; Yin, Y. *Small* **2012**, *8*, 3795.

(8) He, L.; Wang, M.; Ge, J.; Yin, Y. *Acc. Chem. Res.* **2012**, *45*, 1431.

(9) He, L.; Malik, V.; Wang, M.; Hu, Y.; Anson, F.; Yin, Y. *Nanoscale* **2012**, *4*, 4438.

(10) Malik, V.; Petukhov, A. V.; He, L.; Yin, Y.; Schmidt, M. *Langmuir* **2012**, *28*, 14777.

(11) He, L.; Yin, Y. *Proceedings of the SPIE - The International Society for Optical Engineering* **2011**, *8031*.

(12) Ge, J.; Goebl, J.; He, L.; Lu, Z.; Yin, Y. *Adv. Mater.* **2009**, *21*, 4259.

(13) Ge, J.; Lee, H.; He, L.; Kim, J.; Lu, Z.; Kim, H.; Goebl, J.; Kwon, S.; Yin, Y. *J. Am. Chem. Soc.* **2009**, *131*, 15687.

(14) Kim, J.; Song, Y.; He, L.; Kim, H.; Lee, H.; Park, W.; Yin, Y.; Kwon, S. *Small* **2011**,

7, 1163.

(15) Kim, J.; He, L.; Song, Y.; Yin, Y.; Kwon, S. *Chem. Commun.* **2012**, *48*, 6091.

(16) Wang, M.; He, L.; Hu, Y.; Yin, Y. *J. Mater. Chem. C* **2013**.

(17) Wang, M.; He, L.; Yin, Y. *Mater. Today* **2013**, *16*, 110.

(18) Zhang, Q.; Janner, M.; He, L.; Wang, M.; Hu, Y.; Lu, Y.; Yin, Y. *Nano Lett.* **2013**, *13*, 1770.

(19) He, L.; Hu, Y.; Han, X.; Lu, Y.; Lu, Z.; Yin, Y. *Langmuir* **2011**, *27*, 13444.

(20) He, L.; Hu, Y.; Wang, M.; Yin, Y. *ACS Nano* **2012**, *6*, 4196.

(21) He, L.; Hu, Y.; Kim, H.; Ge, J.; Kwon, S.; Yin, Y. *Nano Lett.* **2010**, *10*, 4708.

(22) He, L.; Wang, M.; Zhang, Q.; Lu, Y.; Yin, Y. *Nano Lett.* **2013**, *13*, 264.